Indoor Solar Lamp

Simulating Interior Radiant Energy for the Design and Prototyping of an Indoor PV Lamp

Maarten Verkou

Indoor Solar Lamp

Simulating Interior Radiant Energy for the Design and Prototyping of an Indoor PV Lamp

by

Maarten Hendrik Verkou

in partial fulfilment of the
requirements for the degree of

Master of Science
in Sustainable Energy Technology

at the Delft University of Technology,
to be defended publicly on Friday September 20, 2019 at 09:00 AM.

Photovoltaic Materials and Devices
Delft University of Technology,
the Netherlands

Abstract

Solar photovoltaic cells are destined to become an important contributor in the renewable energy sector, also for small electrical systems inside buildings. They can be used to mobilise the electrical infrastructure, by providing an independent energy source for medium-consumption products, like decorative lighting. This thesis shows all aspects of designing and building an interior, solar powered lamp. First, the ideal position for indoor light harvesting has been investigated extensively, by recreating two typical Dutch rooms with 3D modelling software Blender. The light simulation tool RADIANCE was then used to compute the irradiance at various spots in the room, considering three standard sky types. Weather data from the KNMI was used to classify the sky conditions for every hour during two weeks in November, and the results were compared with pyranometer measurements, showing an error of 20% on a daily basis, and 5% over a five day period. The same simulation method was applied to predict the PV energy yield of four common solar cell technologies for a full year, for multiple room orientations and positions on a wall. Based on these results, three concepts were designed, corresponding to three specific room positions with different indoor light characteristics. Ultimately, one concept was chosen to be build as a prototype, with tailor-made, foil-to-foil laminated PV module, consisting of laser cut SunPower interdigitated back contact (IBC) cell technology. At standard test conditions, the measured short-circuit current was 2.37 A, with an open-circuit voltage of 21.5 V and a maximum power point of 35.9 W_p, resulting in an efficiency of 20.3%. Furthermore, a charge controller with maximum power point tracking algorithm was used to charge a 12 V polymer lithium-ion battery pack. The combination of pyroelectric infrared (PIR) motion sensor detector and a light sensor module assures a conservative use of a 2.4 W strip of light emitting diodes (LED).

Keywords — Indoor photovoltaics (IPV), interior light simulation, RADIANCE, Blender, PV module design, prototyping, SunPower IBC technology, laser cutting, integrated sensors

Acknowledgements

I would like to express my very great appreciation to Hesan Ziar, my daily supervisor, for guiding me, hearing me out, and keep me confident I was heading in the right direction with the thesis. Whenever I was a bit troubled with poor results before Thursdays, Hesan would calm me down. Secondly, I want to thank my main supervisor prof. dr. Miro Zeman for initialising the idea for the project, and finding time to keep contact once every so often. To my second supervisor, dr. Olindo Isabella, I would like to thank you for the guidance at an early stage and throughout the thesis. The cluster meetings and other meetings to discuss progress were very useful and I enjoyed working together. Assistance provided by process engineer of the PVMD group, Martijn Tijssen, was greatly appreciated during the design process of the frame of the module. The same holds for Arturo during circuit building I also wish to acknowledge the help provided by dr. Marc Korevaar from Kipp&Zonen when some issues were coming up with a data logger. For anyone still reading, I would like to thank you for showing sincere interest in this topic and this work. I hope you enjoy reading and wish you well.

Maarten Verkou
Delft, September 2019

Contents

List of Figures

List of Tables

Chapter 1

Introduction

The sun as a renewable energy source is on its way to lead the energy transition to more sustainable electricity production [1]. Vast solar farms are boosting out of the ground onto wide fields all across the world, producing megawatts of electrical power with all kind of photovoltaic (PV) technologies. The slim and lightweight build of solar panels make it especially practical to put it on rooftops inclined towards the sun, making PV systems already the perfect choice for small stand-alone systems used by households and in the future also for smart cities [2]. The next territory PV can demarcate are wireless consumer products, fitting perfectly inside the green, intelligent buildings of the future.

Look into any modern living room and you will find that almost every electrical device is cable connected, apart from some low power consumption devices, like the remote control. In this area, photovoltaic cells have already found a home over 40 years ago, for example in the famous solar pocket calculators [3]. For high power consumption devices, like televisions, the electrical infrastructure inside a building dictates the furnishing of the room. This can restrict the organisation of medium power consumption devices, like decorative lamps, inside the room. The development of PV cell efficiency opens a door to make such devices cable free. To make a long story short:

there is a gaining potential for cable-free, solar-powered products,
inside ordinary households of the future

A lamp is a perfect example, because its location depends highly on the desires of the user. Furthermore, if you ever tried to move a desk light across an overflowing desk, you understand there is a willingness-to-pay for a similar cable-free option. You might nowadays see rechargeable batteries being used for such devices. These already reduce greenhouse gas emissions otherwise needed for the production and transport of new single-use batteries [4]. Using photovoltaic cells to charge a rechargeable battery, will take away the constant requirement to recharge it.

The subclass of using photovoltaics cells in the low irradiance indoor conditions has fittingly be given the abbreviation IPV (indoor photovoltaics) and pioneers started working on this topic already some 15 years ago [5],[6]. Also, indoor light conditions have already been explored widely from the nineties onwards to explore indoor climate comfort and energy savings [7] or and even in 1930 for the analysis of health issue from ultra violet radiation [8]. Nevertheless, the investigation to harvest the microwatts of power is limited and no standard indoor lighting conditions exist, similar to the AM1.5G spectrum [9], to compare the performance of solar cell technologies.

1.1 Aim and method

The goal of this project is to design and prototype a cable-free, easy-to-install solar powered lamp for interior spaces. The product has to be aesthetically pleasing as well as functional for the environment in which it is designed. The target group for the product are ordinary Dutch households, so research will be done there on the availability of radiant energy. This will then be used to determine the required shape and size of the solar module to produce the desired power for a light emitting diode (LED) light source.

Firstly, an assessment needs to be made on the potential of indoor light. It would be too extensive to quantify the amount of light for a lot of rooms throughout the country, so it is chosen to investigate only two rooms, namely a household living room and a university office room. The room and its surroundings are accurately reproduced in the open source 3D modelling program Blender. The irradiance along every surface can then be calculated with the help of RADIANCE, a light simulation tool that uses a backwards ray-tracing algorithm. Some fast simulations will show the most interesting parts of the investigated rooms, which will be valuable information for the initial phase of the research.

Secondly, measurements are done at a specific position close to the main room window with a pyranometer, to find the incident irradiance. The simulation can then also compute the irradiance at the same position and the results can be compared. For large deviations, the cause will be investigated and the detail of the simulation can be increased until the overall simulation satisfies the desired outcome. It should be kept in mind that increasing detail will generally increase the computation time, which can become significant over larger simulations.

Thirdly, with a suitable simulation method and 3D model for the two rooms, the same procedure can be used to simulate the indoor light at different global orientations of the room and different positions and orientations of the sensor plane inside the room. This can be done for the full year, to make a prediction of the mean daily solar insolation of each month. Then, the conversion efficiency of multiple PV technologies in low irradiance conditions needs to be taken into account to find the best performing cell technology to use in the module.

Finally, the newly gained insights on the performance of different PV cell technologies for different room characteristics, will be the foundation of three concept design, corresponding to three unique indoor light conditions. Only one concept will be developed more extensively and this leads to the production of a prototype that can be tested in the exact room and position for which it is designed.

1.2 Main research questions

Three main research questions have been formed to cover the important aspects of the thesis. The first one is about the research phase and the other two are about the outcome, the second one is about the translation of research to design and the last one is about the prototyping.

1. For a general household and office room in the Netherlands, what is the ideal position for an indoor PV installation?
2. How should the design of a indoor PV led lamp look at the specified location, considering shape, size and PV technology used?
3. What are the challenges that come with the design and prototyping of a real indoor PV LED device?

1.3 Sub research questions

Each part can be further investigated with sub questions. Four questions support the first main question, one for the second question and one sub question for the third main question.

1.1 Which simulation software is best suited to quantify the amount of radiation indoors?

1.2 What amount of detail should be employed in the simulation to minimise computational effort, whilst maintaining sufficient accuracy?

1.3 Can the weather conditions be matched in the simulations?

1.4 How can a yearly prediction on the energy PV yield be carried out?

2.1 What are the influences of position and orientation of a solar module under indoor light conditions?

3.1 What components are more likely to fail and how long can it be guaranteed to work?

1.4 Scientific and practical relevance

The thesis will provide insights and recommendations for future work on indoor PV technology applications. The research on the available radiant energy will provide a method that is suitable for any light simulation that focuses on the irradiance inside buildings. Emphasis has been laid on reducing the computational effort, whilst maintaining sufficient accuracy. So it will be useful for any researcher that has problems with the time it takes to perform extensive simulations. Furthermore, the building of an aesthetically pleasing prototype will require some playing around with state-of-the-art solar cells. This can open up some new possibilities on the integration of solar cells in everyday objects.

More specifically, a practical relevance can be found in the process of cutting SunPower interdigitated back contact (IBC) cells. In total 50 cells were laser cut in 3 parts, therefore, valuable experience is gained in that aspect.

1.5 Outline of the report

Chapter 2 will include a state-of-the-art analysis, consisting of three parts, namely a scientific review, a software review and a market review. Next, Chapter 3 shows all the important setup required to do accurate, but quick simulations. Chapter 4 will validate the simulation results with real-life measurements and Chapter 5 will show the reader how the models were eventually used to predict the PV energy yield for varying room characteristics. Chapter 6 will then describe the design of the first prototype, after selecting one of three created concepts. The research will conclude with Chapter 7, where the research questions will be answered and future work will put on the table. For a more detailed outline it is recommended to take a quick look at all the chapter title pages, which includes a diagram showing the relation of the content per chapter.

Chapter 2

State-of-the-Art of Indoor PV

Before starting directly with designing an indoor solar lamp, first some effort has to be made to find the best location for such a device. Research has to be done to find the latest and most acknowledged literature on this topic. The purpose of this chapter is to show the reader the most important literature on the topic of indoor PV systems. Even for those not interested in further research in this thesis will find some usable information and references here, for their investigation for indoor solar products.

Most scientific literature was used to investigate the current state of research on methods to determine the available energy indoors. Some reports were also used to gather information on which software was best to use for this project. For the design part, sources were mainly used to get an understanding of the market of products that have a similar use as the prototype that will be designed for this purpose. With this in mind, it makes sense to name the first part the 'scientific review' and the second part 'software review' and the final part 'market review'. An overview of the three parts is given in Figure 2.1 with the most important literature linked to each part of the review. The listed references are the must-reads for anyone that wants to proceed on this research topic.

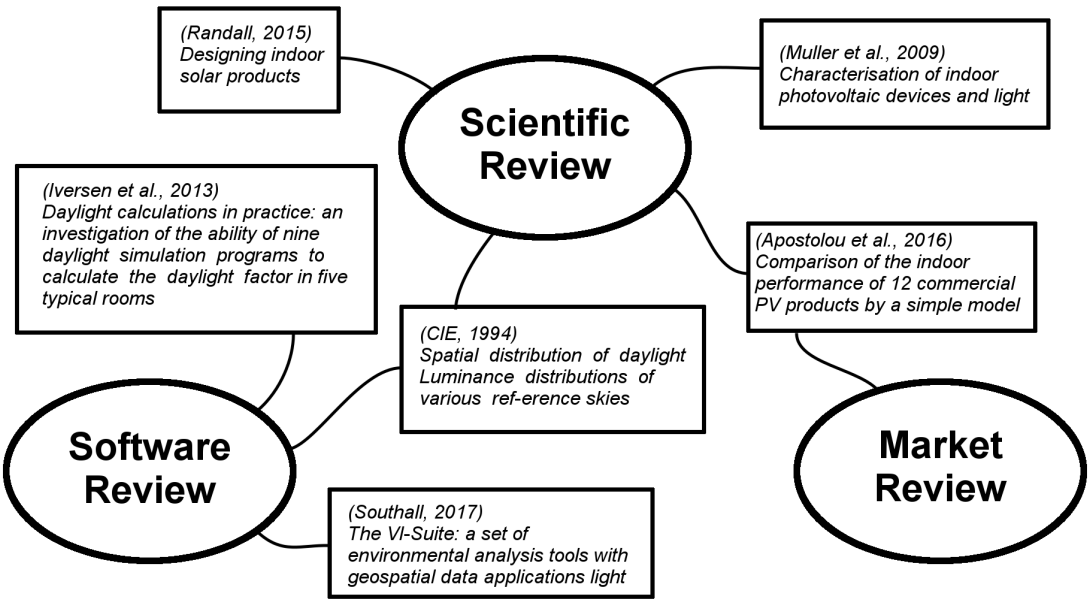

Figure 2.1: Map of the three parts of the literature review in this thesis. The connections show how each reference was connected to each part. Some form a bridge between two parts.

2.1 Scientific review

For those reading to get familiar with the use of solar cells indoors must have come across the name of Julian Randall. Almost no other researchers in this topic fail to mention his work. It comes at no surprise that the most complete source is his book 'Designing Indoor Solar Products' from 2005 [10]. The book starts to explore ambient light as an available energy source for low-consumption indoor applications. Articles, like Vullers et al. [11] show that ambient light is competitive with other micro-energy sources, as displayed in Figure 2.2.

Source	Source power	Harvested power
Ambient light		
Indoor	0.1 mW/cm^2	10 μW/cm^2
Outdoor	100 mW/cm^2	10 mW/cm^2
Vibration/motion		
Human	0.5 m @ 1 Hz 1 m/s^2 @ 50 Hz	4 μW/cm^2
Industrial	1 m @ 5 Hz 10 m/s^2 @ 1 kHz	100 μW/cm^2
Thermal energy		
Human	20 mW/cm^2	30 μW/cm^2
Industrial	100 mW/cm^2	1–10 mW/cm^2
RF		
Cell phone	0.3 μW/cm^2	0.1 μW/cm^2

Figure 2.2: Table with potential harvested power of common available micro sources, taken from [11].

The majority of Randall's book is dedicated to factors that influences the available energy resources found indoors and sizing a solar product accordingly. The chapters are filled with numerous of detailed variables that can change the incident light; from site obstacles to wall and glass properties to window furnishing. The book helps to give an overview of all the things that should be considered in the design process, but the influence of all the factors cannot simply be combined to give a general image of how much radiant energy can be expected indoors over a complete year. It is mentioned that computer simulations are attractive to use for this scenario. However, Randall claims that simulation software minimises exact laws of physics, in order to maximise computational speed. But now 14 years later, computer simulations have taken over a large part of research, courtesy of the ever increasing computational power. Also in this thesis, the available energy will be estimated with computer simulations, but still, careful attention needs to be put towards the accuracy.

2.1.1 Indoor light conditions

The amount and type of light required in a room is very specific to the use of this room. For an ordinary household room the desired illuminance is between the 150 and 200 lux [12]. During the day, a large portion of this light can come from outside, even on overcast days. So artificial light is only really required during the night, when everybody comes home from work. In office buildings, the most productive working environment requires much higher light levels up to 500 lux. These rooms also tend to have less window area, meaning artificial light is turned on almost the whole working day, until everybody goes home. Some study was required to find the availability of these two types of light sources.

Artificial light

One useful figure for getting an insight in the availability of artificial light can be seen in Figure 2.3. It shows that the irradiance on the wall directly beside the lighting receives an irradiance between 1 and 1.5 W/m^2 at a height of close to 1.5 meters from the floor. Go higher and the irradiance reduces to less than 0.5 W/m^2. It should be noted that these measurements were done in a classroom, so a lot of artificial light is required. This means that in ordinary household rooms the available light can be expected to be even lower.

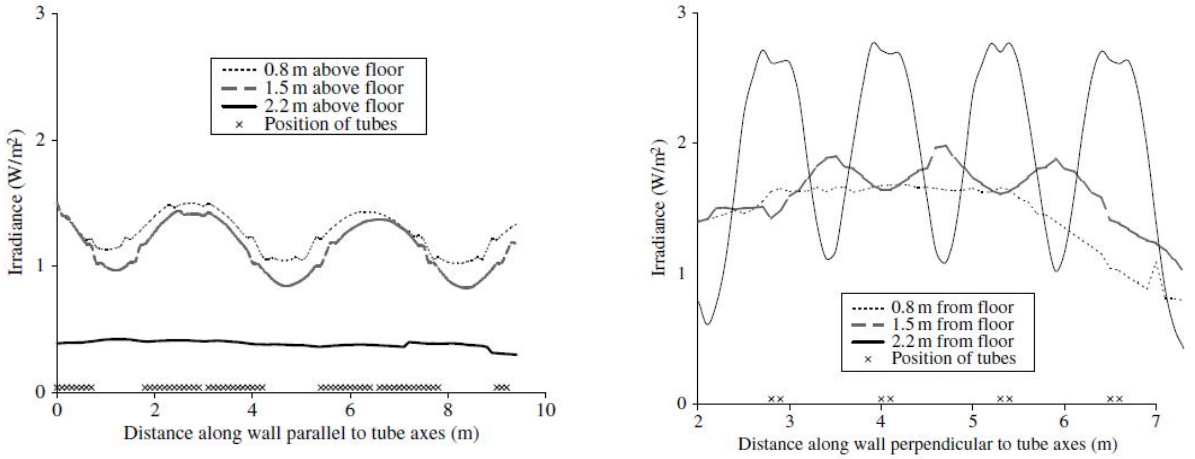

Figure 2.3: Irradiance on a wall at different heights from the floor. The wall is directly beside the fluorescent lamps. In the figure, the string of crosses show the location of the tubes with the corresponding irradiance levels on the vertical axes at that distance along the wall [10].

Sunlight

A study [13] from 2016 came from the Faculty of Industrial Design Engineering at the Delft University of Technology. Apostolou et al. compared twelve commercial PV products with a simple model to estimate the performance of solar cells as a function of the distance from light sources. This was very useful as it showed how poor solar cells actually perform in low-irradiance and that maybe even different cell technologies can outperform crystalline silicon. With measurements along a wall from multiple distances from the window they could produce the graph from Figure 2.4. The report fails to mention exact sensor placement and orientation and weather conditions, meaning the values cannot be used for proper analysis. But because the measurements were done at the same university, it does give a good estimation of indoor irradiance levels near a window.

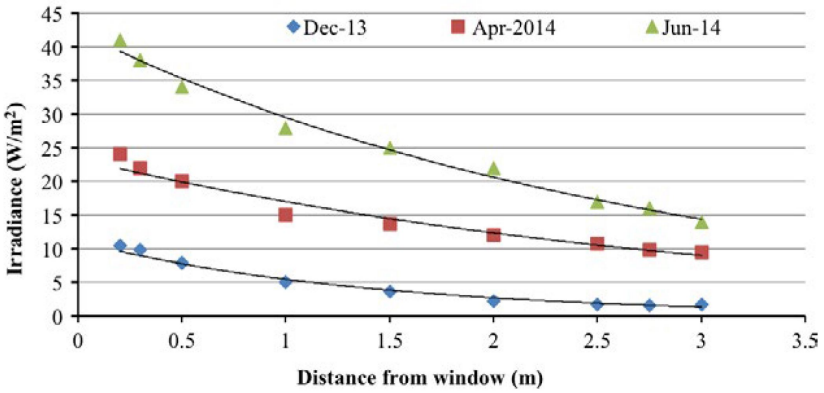

Figure 2.4: Irradiance levels at certain distance from the window in an office in Delft, for three dates [13].

2.1.2 Indoor light simulation

There are a number of algorithms developed to render realistic light in three-dimensional scenes. Most programs available nowadays are a buildup of previous work on ray-tracing and other light and energy transfer [14], but only the last decades have commonly accessible computers been good enough to perform the calculations in a time that is worth the while of researchers around. Here, the working principle of two such algorithms will be briefly explained.

Radiosity
Radiosity is an algorithm based on the principle of heat transfer. All surfaces are divided into smaller patches, and for each of these patches the view factor between them is computed, as can be seen in Figure 2.5a The total illumination is then calculated by adding the contribution of all surrounding patches and light sources [15]. This method is simple and computationally friendly, allowing for fast rendering [15]. However, the calculations can become more complex when scenes have an increasing number of objects and meshes with unconventional geometries, leading to slower and inaccurate simulations. The manner in which the geometries are broken down into patches can fasten up the process for these kind of scenes [16]. Also, problems can arise with daylight scenes with a lot of direct light [15].

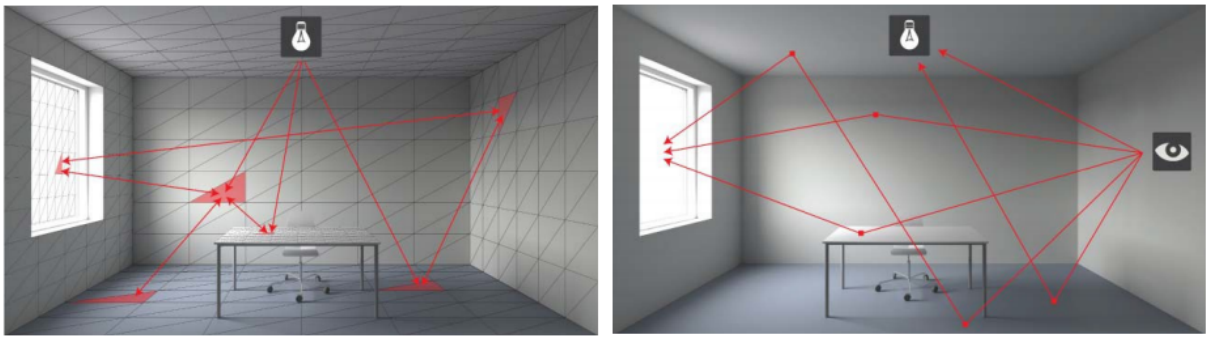

(a) Radiosity algorithm **(b)** Backwards ray-tracing

Figure 2.5: The working principle of the radiosity and backwards ray-tracing algorithm, taken from [15].

Ray-tracing
With this method, a large number of rays are emitted into the scene. Based on the collective number of rays received onto a sensor surface, the illuminance is determined only for this investigated plane. Both, forward and backwards ray-tracing are used in the light simulation industry. With forward ray-tracing the rays follow the same path light would naturally take from the light sources to the objects. This method is not very effective in scenes where the investigated surface is not in the direct view of the light sources, because most rays will never find the sensor surface [17]. Backwards ray-tracing is thus often the preferred option. As indicated with the eye in Figure 2.5b, rays are shot from the sensor in all directions and the contribution of each ray is taken into account in determining the final irradiance on the sensor surface. Programs aiming to perform photo-realistic rendering often chose a hybrid approach of multiple techniques, which try to compromise speed and accuracy [17].

3D model details
An article that comes closest to the work in this thesis is from Müller et al. [18]. Here, a simulation method for indoor irradiance using ray tracing programs Radiance and DAYSIM is presented to characterise typical values of irradiance. They consider the influence of latitude of the location and distance from the window along different axes. Also the artificial light and a simple user presence model is added to the simulation. The simulations were compared with measurements from multiple locations across the room, and the initial findings suggest an accordance of 10%. Using higher and lower detailed models of the room, it is found that only main objects are required in a room, especially for areas orientated towards the direct light. At the start of the project, this was a valuable finding as it meant not to much detail had to be spend to investigate influences from details such as simple room furniture.

Simulation settings
Other aspects to save computational effort, can be the interval of calculation points and accuracy of the simulation. For long simulations an hourly interval is often used, as cloud cover and other disturbances such as shade, will average out over the course of a month or so. But for daily simulations, and especially for indoor climates which are highly vulnerable for shading, a higher resolution might be required to get meaningful values of the incident irradiance. The number of rays used to calculate irradiance in ray-tracing determines the accuracy and indeed the time it takes to calculate the incident irradiance. Simply setting this to highest accuracy leads to computation times of several hours, this could hamper the progress of the research and generally is bad practice. For these two settings no exact literature was found about the best options, so this gap lead to the research part of this thesis.

2.1.3 PV cell efficiency for low irradiation

In standard test conditions (STC), conventional crystalline silicon outperforms all other single-junction thin-films technologies and emerging PV, bar GaAs cells. However, the conditions found indoors will not even come close to the 1000 W/m^2 standard used to evaluate performance of solar cells. Furthermore, in these low-irradiance conditions, there exists a whole different pecking order among the different cell technologies. For example, a paper of Afsar et al. [19], shows that under 1 W/m^2, amorphous silicon has a power conversion efficiency that is an order of magnitude greater than that of crystalline silicon.

Multiple efforts to standardise the method to evaluate the performance of photovoltaic cells indoors have been found. In most case, the intensity of a fluorescent or LED light source is ranged somewhere between 1-100 W/m^2, and some conventional and new solar cell technologies are tested and compared [19],[20],[21]. A more useful contribution came again from Julian Randall, who proposed back in 2003 a phenomenological model that relates the solar cell characteristics to a realistic solar cell efficiency in low-intensity light [5]. This research has also been copied to his book from two years later [10]. From Randall's measurements, it was shown that the overall trend of the efficiency is constant down to 200 W/m^2 and a straight line on a logarithmic scale in the range 1-100 W/m^2. A relation is formulated based on two solar cell parameters a and b that determine the logarithmic equation as

$$\eta(\%) = a \ln(G) + b \tag{2.1}$$

where G is the irradiance in (W/m^2), the parameters are defined as

$$a = \mathrm{FF}\alpha_f \frac{kT}{q} \tag{2.2}$$

and

$$b = \mathrm{FF}\alpha_f \frac{kT}{q} \left[\ln \alpha_f + \ln \beta_f + \frac{E_g}{kT} \right] \tag{2.3}$$

where α_f and β_f are constants, FF is the fill factor, kT/q is the thermal voltage and E_g is the band gap energy. Further details on the derivation of this formula can be found in Appendix C. Figure 2.6 shows the model on top of the measurement results of some cell technologies.

The ratio a/b is inversely related to the band gap and in general the lowest a/b ratio is recommended for IPV design. Appendix C shows the a and b values of the investigated samples, and generally it can be seen that thin film technologies as amorphous silicon and CdTe have a low a/b ratio. The fact that these types of solar cells perform well in low intensity light is echoed by more PV scientists [13],[20]. Even organic PV and dye-sensitised solar cells show good performance in low intensity indoor light compared to crystalline silicon [21].

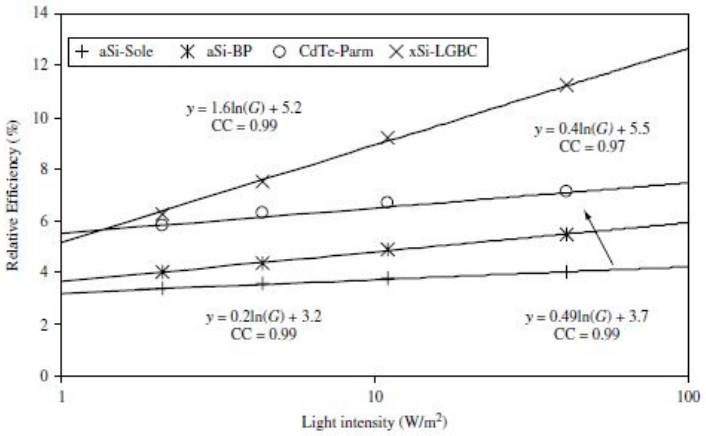

Figure 2.6: Curve fit of Randall's measurements for four solar cell samples [10]. The equations next to the curves are in the form of Equation 2.1 and CC stands for the linear correlation factor.

2.2 Software review

There are a number of different light simulation programs. A study from the Danish Building Research Institute from the Aalborg University in Copenhage [15] investigated and compared the performance of nine such programs. Three well-known programs are DIALux, Relux and Radiance. From a survey [22] with 182 respondents it was found that DIALux is used by 40%, Relux by 14% and Radiance by 12%. However, it can be seen from the graph in Figure 2.7 that most researchers tend to use Radiance.

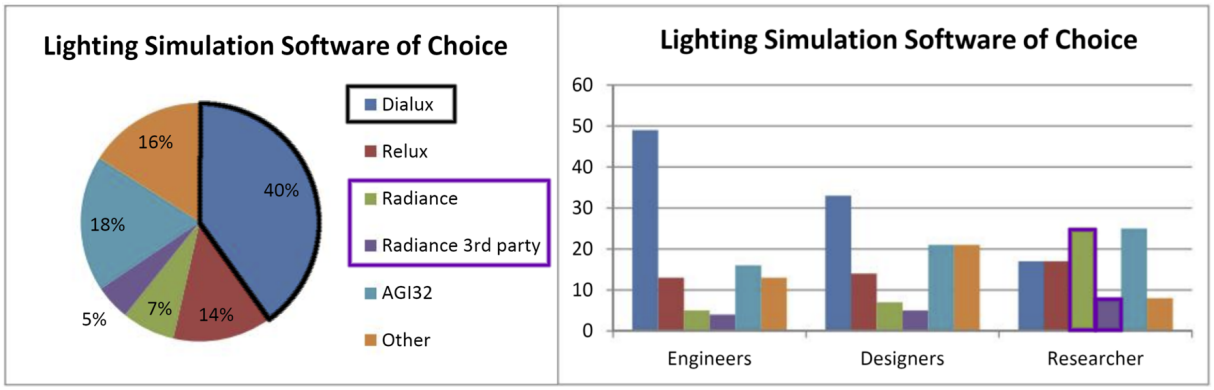

Figure 2.7: Software chosen by engineers, designers and researchers, taken from [22].

Based on these findings, it was chosen to further investigate the possibilities of both DIALux and Radiance for this thesis. Both were installed and a simple model of an office at the Faculty of Electrical Engineering, Mathematics & Computer Science (see Figure 2.9a) was created in both programs with similar lighting conditions. The general working principles of both were investigated and knowledge was gained about the use of and limitations of each program. This part will only contain a brief introduction too both software programs.

2.2.1 DIALux

DIALux (`www.dial.de`) is a very user friendly light simulation program, created to make lighting design in buildings accessible for everyone. It requires no extra installation of an so-called add-on, sufficient tutorials exist to let the user quickly create a simple scene and perform simulations. It follows standard metrics and easy import options, so that artificial light, for example, can be directly imported if manufacturers provide the standard luminaire files. It uses a radiosity

algorithm, which is based on calculating the view factor between all surfaces. To increase the accuracy, all the relevant surfaces are subdivided into small meshes. This limits the use of DIALux to simple models with mostly flat surfaces.[15] Also, DIALux is performing less accurate in day lighting situations [15],[22]. In DIALux a light scene has to be manually selected. Not a lot of options exist in this settings, and not a lot of information is provided online about the exact settings used. They only provide that daylight simulation calculations are based on standard sky intensity models from the CIE 110-1994 publication [23][24]. It consists of 16 standard skies and DIALex allows for only three sky options. The output of the simulation in DIALux provides a so-called false colour map (see Figure 2.8b) in luminous flux, with unit lux. Also, there is no simple option to simulate a whole year and only whole hours can be selected, nothing in between. There is the option to calculate the power density from lamps during a certain instance.

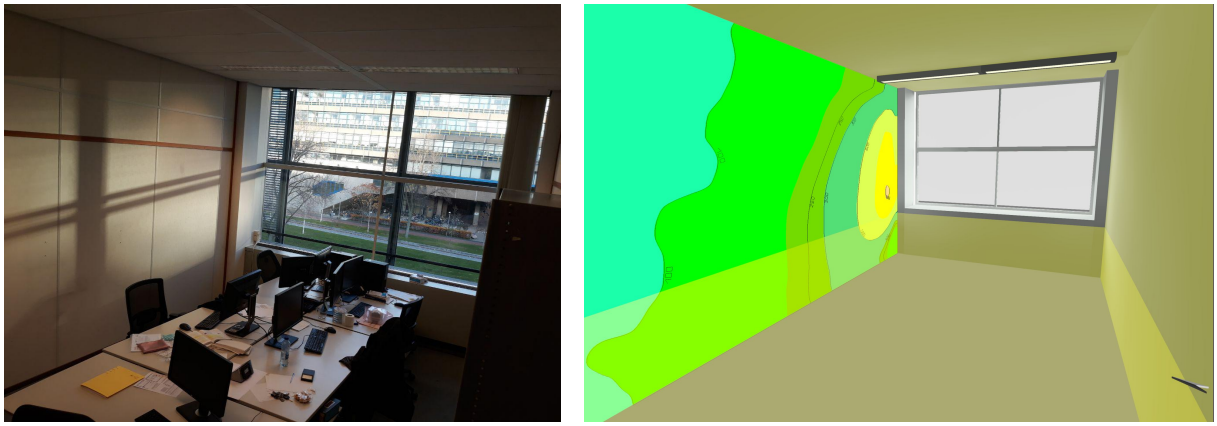

(a) An interior photograph of a university office room. **(b)** University office room reproduced in DIALux.

Figure 2.8: An interior photograph of a office room of the Faculty of Electrical Engineering, Mathematics & Computer Science at Delft University of Technology against the same room reproduced in DIALux and with illuminance calculations.

2.2.2 RADIANCE and Blender 3D

The lighting software tool RADIANCE (`https://www.radiance-online.org`) is very established among researchers and was developed by Greg Ward at the Lawrence Berkeley Laboratory in the early 90's. The program uses text files to specify the geometry and material types, which can be created by hand or using a CAD program. The software will then calculate the irradiance on specified sensor planes using backwards ray tracing. The lack of general interface makes it uneasy to use and it is thus preferred to use another program for the input and visualisation. Blender (`www.blender.org`) is an open source 3D application for which the VI-suite add-on is made to aid the visualisation of RADIANCE [25]. Blender uses meshed based modelling, which allows more complex setting to be made more easily. From the created scene in Blender, a number of text files are created that the radiance software uses to perform the simulations. Accurate results can be gathered in situations where daylight has a large influence due to to possibility to add photon mapping [15],[22]. However, the VI-suite add-on (currently version 0.4) is still limited and has some operational limitations. A lack of complements makes it hard to play with values like for the materials.

Also, the design of the IPV product can be recreated more easily in Blender. It can then be placed in the existing scene to calculate if the irradiance is the same on the PV cells in the design compared to the predicted values. In Radiance, for each ray the radiance is divided into Red, Green and Blue (RGB) based on the visible colour. They note that RADIANCE is obviously less precise, but "this disadvantage is outweighed by the fact that colour data from materials are much more frequently available as colour metric values than as detailed spectral curves". It

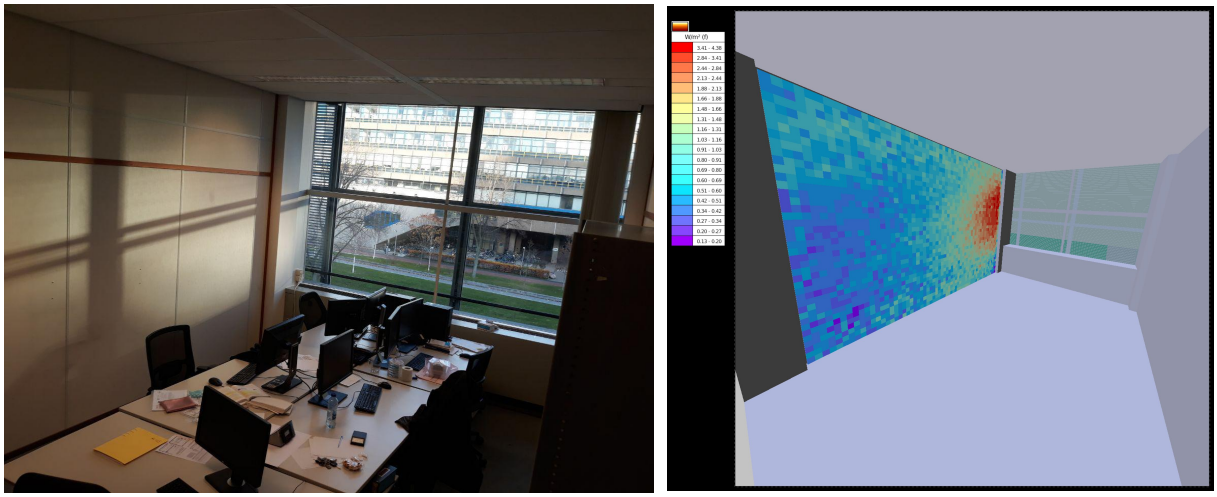

(a) An interior photograph of a university office room.

(b) Office room in 3D Blender with RADIANCE.

Figure 2.9: Comparison of model room with real room photograph. Also, with irradiance profile on the walls.

is important to understand that this information comes from a tutorial on their website, but it comes from 1997, so this argument might be invalid with the current software. They also mention that spectral effects are limited since colours commonly used in buildings are not very saturated. So it is important to include this in the calculations later [26],[27].

2.2.3 Comparison of software

Having worked a lot with Blender 3D before the start of this project and never with DIALux, it became clear that even with the experience of the former, DIALux would be much more easier to work with. It is easy to quickly produce nice looking lux-maps and see how light propagates through a room. However, the lack of simulation options would make the process of creating a yearly simulation very time consuming as every simulated hour would have to be entered by hand. So as most researchers already found out, Radiance is the desired option that allows for customised simulations. It requires an extra program to put in the data and obtain easy usable results, and options as Grasshopper and DAYSIM exist and are used successfully in older literature. But with the experience from previous years and the availability to change the code of the open-source add-on used to make custom simulations, Blender is picked.

2.3 Market Review

Most wireless products, like remote controls, still rely on alkaline batteries that have to be replaced every once in a while. The production and shipment of these single-use batteries are the majority of their contribution to greenhouse gas emissions [4]. For products that use more energy, it is better to use rechargeable batteries, like the common lithium-ion found in smartphones. But these battery types are still maturing and are associated with high costs. Photovoltaic cells can help to reduce the costs and durability of a product by reducing the need of a large rechargeable battery. In the Netherlands, small PV devices have already invaded the market of outdoor garden design to light up garden paths and barn doorsteps when night falls. But older examples of small PV cells on pocket calculators show the potential already for 20 years in low-consumption indoor devices. Both of these kind of products have been investigated or even acquired to properly access the state-of-the-art.

2.3.1 Low-consumption PV products

The research of Apostolou et al. [13] shows the performance of 12 commercial PV products in irradiance levels of approximately 10 W/m^2. The efficiency ranges between 2 and 10%, meaning that for the small panels used on these products, the available power is in the order of miliwatts. This is enough for the low-consumption products investigated in the article, such as a remote-control or a mini-desktop lamp. From the 12 investigated products, six had monocrystalline silicon cell technology, four had polycrystalline and only two were made from amorphous thin-film silicon. The measured power conversion efficiency was between the 2% and 10%. There was no obvious best performing cell technology at the investigated irradiance. However, at standard test conditions, the polycrystalline silicon cells easily outperforms the others. This means that in the low irradiance conditions, even amorphous silicon becomes competitive with the crystalline technologies, as was already obtained from literature in the previous sections.

Figure 2.10: Images of some low-consumption PV products used in the research of Apostolou et al. [13].

,

2.3.2 (Outdoor) Solar LED Lamps

The advantages of having a cable-free, stand-alone lamp has already been widely explored for outdoor purposes. As can be seen in Figure 2.11, their is a wide variety of solar lamp products available in the Dutch market. Also, it is not uncommon to find solar lamps like these in the backyard of everyday people. For the purpose of product investigation in the design phase, these products have been bought for further examination of the working.

The high potential of 100 mW/cm^2 of sunlight outdoors [11], makes these small devices surprisingly powerful, meaning they can even be used if sun conditions are not ideal, for instance due to partial shading. The 'Raven wandlamp' (b) has been placed tested on a wall outdoors and was facing south. It can be said that after half a year it still works perfectly and switches

on its lights every night when someone passes by the motion detector. However, when placed in persistent poor conditions the performance deteriorates. The other four devices were placed face up on a table in a room with a main window facing east, and they all stopped working within a week, except four some of the 'RVS LED Buitenlamp' (e). Only by placing them near the window, could the internal battery keep itself charged to occasionally give light on demand. Leaving the lights on overnight would always mean they could not be used the following day.

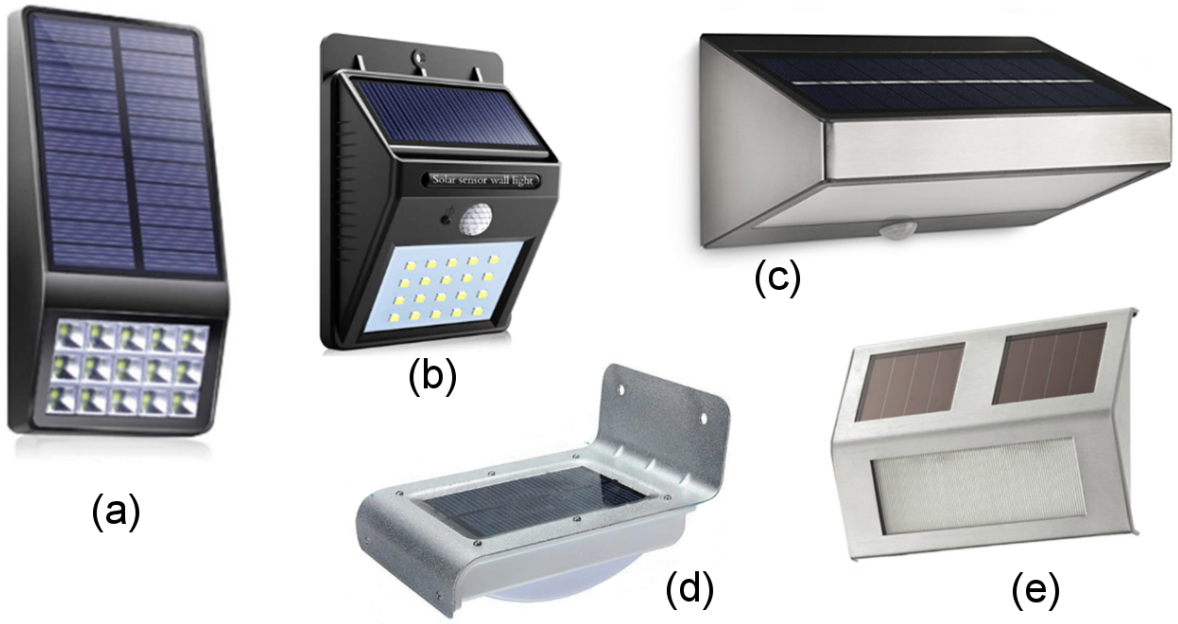

Figure 2.11: Images of some outdoor solar lamps that were closely investigated: (a) SensaHome solar lamp, (b) Raven wandlamp, (c) Philips myGarden Greenhouse, (d) Quintech Tuinverlichting, (e) Mascot RVS LED Buitenlamp.

From online reviews it was also found that the general opinion was, that everybody was happy using the lamp straight out of the box, as they finally had a light in the back of there garden or next to there doorstep. But often, customers would come back on the review page to complain that the device stopped working after a month or so. The suspicion is that people are not aware about the light requirements of the lamps and simply place it at the desired location without considering the need for (direct) sunlight. Indeed, only the 'Philips myGarden Greenhouse' had an user manual, but only one simple figure vaguely indicated that the device should be rotated towards the south, for highest performance and could even stop working when it was facing south. So it is understandable were not using the solar lamp properly, resulting in the poor performance.

Looking inside the products

The products were opened up to peek inside the working principles of these products. It was found that most products are compact and have a small module consisting of 11 cut mono- or multicrystalline silicon solar cells connected in series, to achieve a combined voltage slightly above the system voltage of 5 VDC. In all investigated products a 3.7 V lithium-ion battery is charged using a small micro controller, which can then power one or a few LEDs with a combined power below 1 W. Some products also had a good functioning motion detector and light sensor.

Chapter 3

Indoor Light Simulation Using RADIANCE

From the investigation in the state-of-the-art, it became clear that computing the overall irradiance on a tilted plane inside a room can get very complex, especially if multiple rooms and orientations are to be investigated. The best option is to make use of light simulation tools such as RADIANCE. Due to reasons explained in Section 2.2.3, Blender 3D was chosen as the supporting modelling software for RADIANCE. All objects that need to be considered to calculate the incident irradiance form the scene. It needs to be determined which level of detail in the scene works well for these simulations and a consistent method will have to be formed.

The purpose of this chapter is to show all the important settings and details required to reproduce an accurate but also quick simulation setup. The details to recreate the scenes used in this thesis are described in Section 3.1. Next, Section 3.2 holds the simulation setup used to create some general simulations with different standard sky types and light sources. The information came from user manuals, as well as reports from previous work. A lot of simulations were run to check and adjust some of the settings and in 3.3 the results are used to find the ideal interval of calculation points and accuracy of the simulation. The outcome is an indoor simulation method that proposes the settings to create three graphs, corresponding to three standard weather types for one full day. Figure 3.1 shows a visualisation of the performed steps to get to this outcome.

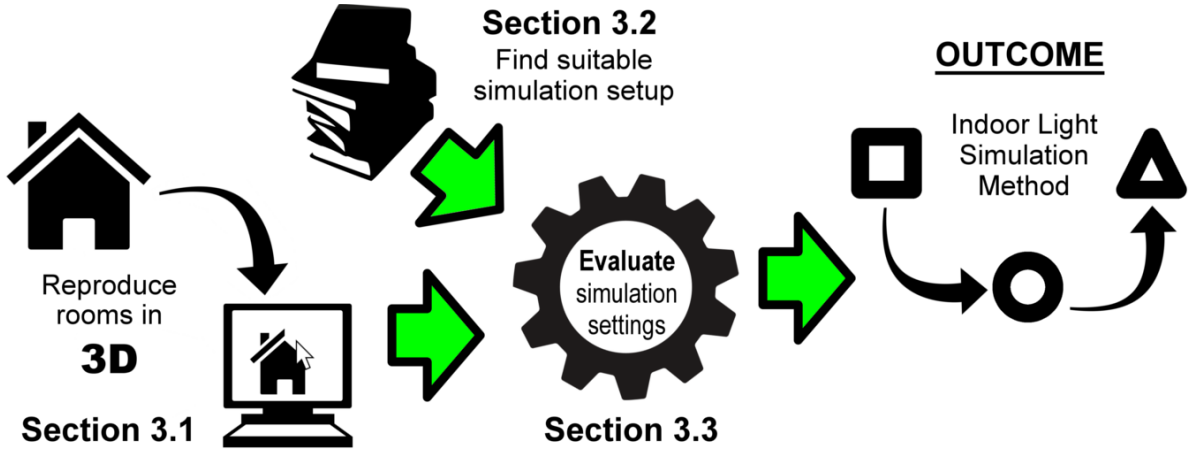

Figure 3.1: Visual representation of the content of Chapter 3. The section numbers can be found near the corresponding icons. The green arrows show the relation between the sections and outcome.

3.1 Scene details of two investigated rooms

For this project two ordinary scenes are chosen to rebuild in Blender 3D and perform calculations with RADIANCE. Room 1 will be a living room in a common Dutch household in the south of Delft. Room 2 will be an office room at the University of Delft. This part will describe the main characteristics of the rooms and how they were translated to a three-dimensional model.

3.1.1 Main room specifications

This section contains a proper introduction to the two investigated rooms. The main dimensions rooms will be obtained from tape measurements with centimetre accuracy. All these relevant dimensions can be seen in Appendix A. The geometry and location of buildings, and other shade-casting objects in the nearby environment, were obtained from satellite images from Google Maps.

Household Living Room
The first room, the household living room, will from now be referred as household for simplicity. It is a single-floor, terraced house in the south of Delft, with multiple other houses and trees around it in the neighbourhood. This means that there are multiple shade-casting objects needed to be considered from outside. The south facing short side is 5.2 meters wide and has the main window of 1.9 meters height and 2.3 meters width. The window of regular double glazing is divided in two parts by a wooden frame and for most days the blinds are down. Furthermore, the room has grey laminate flooring and white wallpaper inside, which means the walls are rough but have noticeable specular reflection. The objects in the room share the same tint of colours as the walls and not much furniture and room decoration is present, which will simplify the simulations. During a normal working day, nobody will be in the room, so no artificial lights will be turned on in the room during daylight conditions. The satellite image below (Figure 3.2) has been used to get the orientation of the room within a few degrees of accuracy.

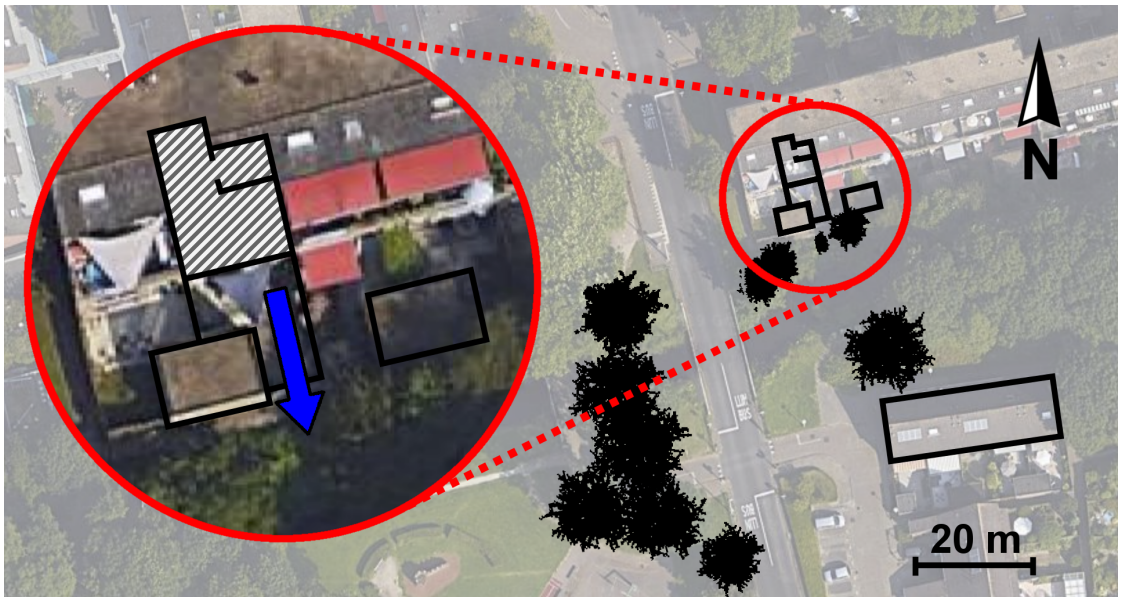

Figure 3.2: A satellite image from Google Maps 2019 of the close surroundings of the household room. The important walls are marked by the black lines, and also the most influential trees have been marked black on the map. The floor of the investigated living room has been given a striped pattern and the direction of the main window has been emphasised by the blue arrow.

The big blue arrow shows the normal of the main window in the room. It has been estimated that the main window faces 167 degrees clockwise from the north, which means it is close to facing south.

University Office Room

The office room, which is located on the second floor of the EWI faculty at the University of Delft, will from now be referred to as office. Because the room is located almost 10 meters above the ground, there is less influence from nearby shading object like trees. There is however a big faculty across the campus which needs to be accounted for. The room is 3.9 meters wide and the main single glass window fills the complete width, 80 centimetres above the floor. But directly outside this window is another single glass window completely filling the view. Blinds are available, but are normally opened up in the morning. Adjacent rooms however, do have the blinds down, which will limit the light coming in on certain short times of the day. On the other side of the room, 6.6 meters from the main window, there are three single glass windows 2.2 meters from the floor filling the whole width. These windows lead to the hallway and not a lot of direct light can enter from this side of the building. The walls on each long side of the room are made from old white drywall sharing similar properties as the walls used in the household room. The floor is a grey carpet and the room is filled almost completely by five desks with computers and chairs. Further attributes are only on the side far from the main window. Again, it could be estimated that the main window is facing 67 degrees clockwise from the north, which is equivalent to east-northeast. This means the sun comes mainly into the building in the morning, resulting in the artificial lights being turned on for most of the days, as people are always working in the office. This will be considered in the simulation of the total irradiance.

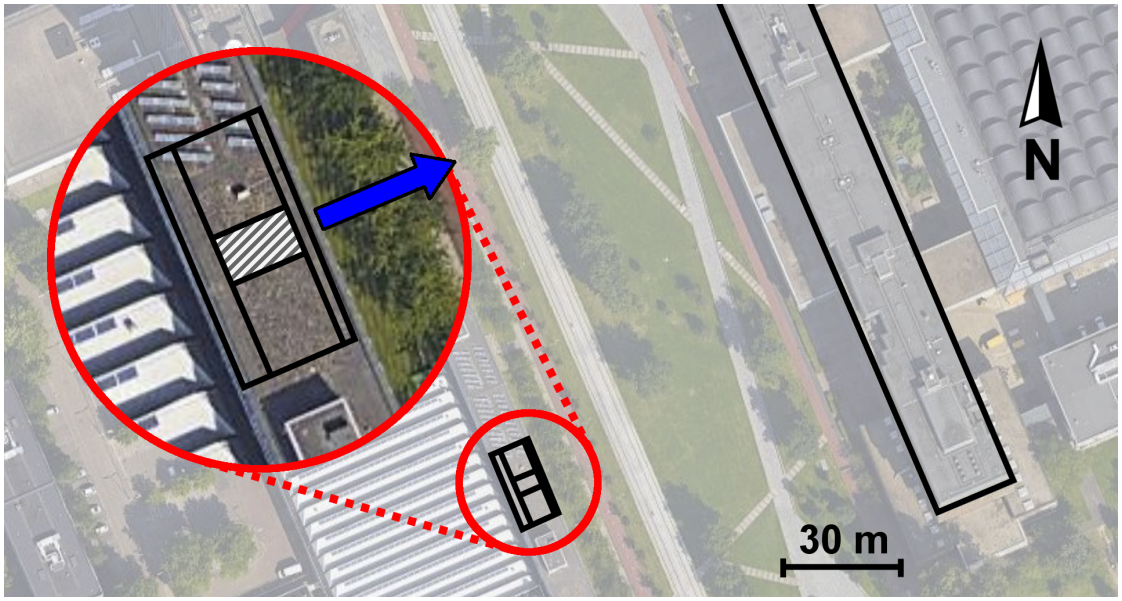

Figure 3.3: A satellite image from Google Maps 2019 of the close surroundings of the office room. The important walls are marked by the black lines. The red circle shows an enlargement of a part of the building of interest. The floor of the specific office room (LB02.480) has been given a striped pattern and the direction of the main window has been emphasised by the blue arrow.

3.1.2 Simple simulation to find locations of interest

Before starting to create detailed 3D models, it is advised to first run basic simulations, without much scene details, to check which areas in the room are interesting and which areas can be ignored. In this case an interesting area is one that receives the highest irradiance on average, but as an example, an area with a very constant input of energy could be interesting for other cases. To be more specific, in this thesis, the focus is on high irradiation on a wall near a window. The initial requirements (See Section 6.1) state that the device should be able to work during most of the year, so for these simulations, an average sky (partly cloudy) is used. Sensor planes

are placed on the walls, floor and ceiling and the simulation is run at three different times, namely the morning (9 AM), noon (1 PM) and afternoon (5 PM). For this particular simulation, the sensor planes had a size of 25x25 cm. Smaller sensor planes give a higher resolution image at the costs of computational effort. The accuracy setting of the simulation was set to medium, the meaning of this will be explained in detail in Section 3.2. Each simulation took approximately 15 minutes, which resulted in more then accurate enough images to get an idea of the irradiance profile along the walls. The results of the simple simulation can be seen in Figure 3.4 for the household and office room.

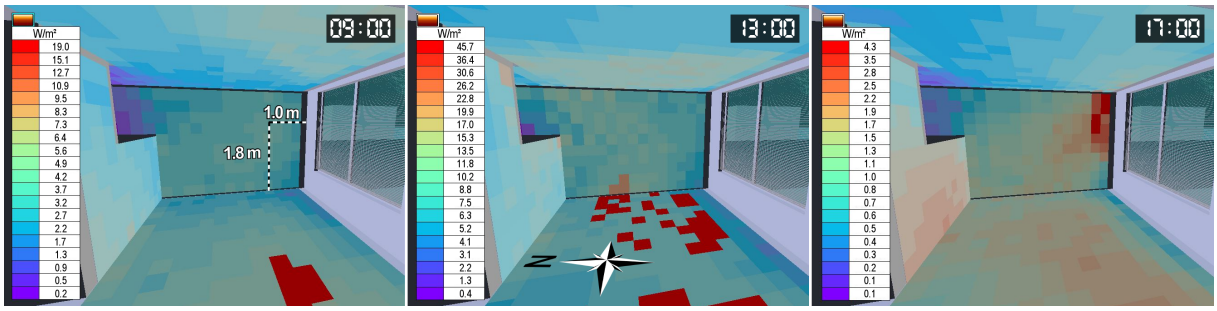

(a) Irradiance profile for the household room.

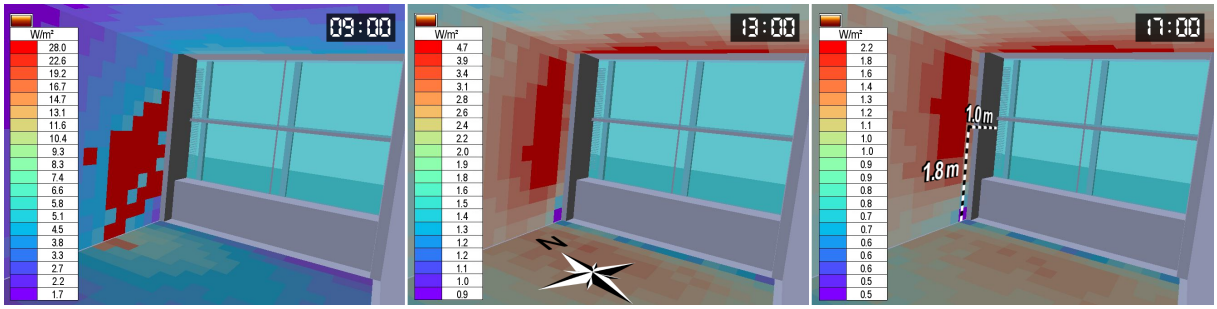

(b) Irradiance profile for the office room.

Figure 3.4: The colour map with values for the incident irradiance for all relevant surface areas in the morning (left), at noon (middle) and in the afternoon (right). The middle images shows a compass to see the global orientation of the room. The black and white rulers beside the window show the chosen pyranometer location of 1.0 meter from the window and 1.8 meter from the floor. Note, the colour map values are on a logarithmic scale.

The most important finding is that the area of highest radiation for both cases is close beside the window. This area also receives uniform irradiance over large enough area for a PV device. The main difference between the two rooms is the time of the peak irradiance, which is highly dependent on the orientation of the room. For the office, the sun shines on the wall in the morning, for the household, this is just after noon. The floor and wall also receive noticeably more light close to the window. This is fairly obvious, but the images show how immediate the drop off is deeper into the room. Furthermore, in most rooms the floor is often filled with objects like tables and closets, meaning that high-up on the wall is also in that area a more suitable location. So from these quick simulations early in the research it was already determined that the wall beside the window is the main area of interest. The exact position of the sensor location was set to 1.8 m from the floor and 1.0 m from the window on the wall that receives the most direct sunlight.

3.1.3 Reproducing rooms in 3D models

As mentioned before in Section 2.1.2, research [18] has shown that only main geometry and objects are required for simulation models, especially when the investigated areas are in the direction to a source of direct light. In this case, the location of interest is somewhere where sunlight plays a significant role in the energy yield of the system, so to decrease computational

effort, only the main geometry and objects that directly influence the sunlight have been modelled. It should be noted that the computed irradiance can be 5% higher compared to higher detailed models [18], because there are not as many objects in the view of the sensor that block or absorb light.

Geometry and objects

Important objects from outside the room are the ones that cause shade into the room or block a significant portion of the sky view. A simple look out of the window is a reasonable attempt to see which objects would influence the incoming irradiance. But for more complex scenarios, with trees and buildings, a more trial-and-error approach can be used to see which objects play a role and which can be neglected. Quick simulations where run with increasing number of outside objects to check if the influence of nearby objects where significant enough. All final objects used can be seen in the top views from Figures 3.2 and 3.3. The location and sizes of each of these objects was pinpointed by using photographs from exact known positions and using this as a background to draw the 3D models. In this case, the position of a pyranometer (See Section 4.1), was used. Its location was already determined in the previous subsection, as one that is likely to receive a high and uniform irradiance profile. The results of the models in Blender 3D compared with the real-life photographs, can be seen in Figures 3.5a and 3.5b for both rooms.

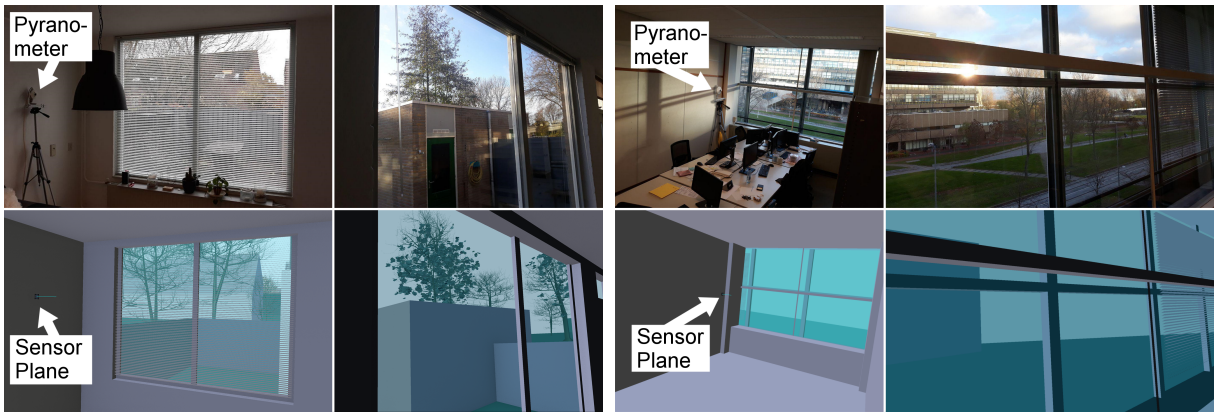

(a) Household living room. **(b)** University office room.

Figure 3.5: The recreated 3d models of the household room (a) and the office room (b). The top row shows the real rooms, the bottom the reproduced rooms in 3D. In both (a) and (b), the left side shows an overview of the room with the pyranometer, which is also created in Blender 3D and denoted by "Sensor Plane". The right side of the image shows the view from the pyranometer location, in the direction of the main window.

Materials

In RADIANCE, opaque materials are defined by three general parameters. One is for the colour the material reflects. Another for the roughness of the surface, which determines how much the light reflects like a mirror or diffuse. Then, their is also a parameter for how much of the light is reflected compared to the incoming light. RADIANCE calls this the specularity or specular reflection. A number of different material presets can be selected [28] for different type of materials, like glass or metals. But for most general opaque materials, the "plastic" preset is used. In this work the specularity and roughness of the walls, ceiling and floor with the help of [29], which shows renders of materials for a lot of different values of the roughness and specularity. In this way, it can be visually compared with your own material to find values in the right order of magnitude.

3.2 Simulation settings

Now that the scenes are set in a three-dimensional environment, the simulation settings need to be fine-tuned to suit the real-life conditions found at the investigated rooms, whilst minimising the computational effort required for accurate results. A more detailed look in the working of principles of the light simulation software RADIANCE is needed.

3.2.1 RADIANCE input

As mentioned in Section 2.2.2, Dr Ryan Southall has created an add-on to provide the data required for the RADIANCE simulation. Blender uses a node setup to display the relations between input, transformations and output of data and files it uses for the simulation. This nodal representation can be seen in Figure 3.6

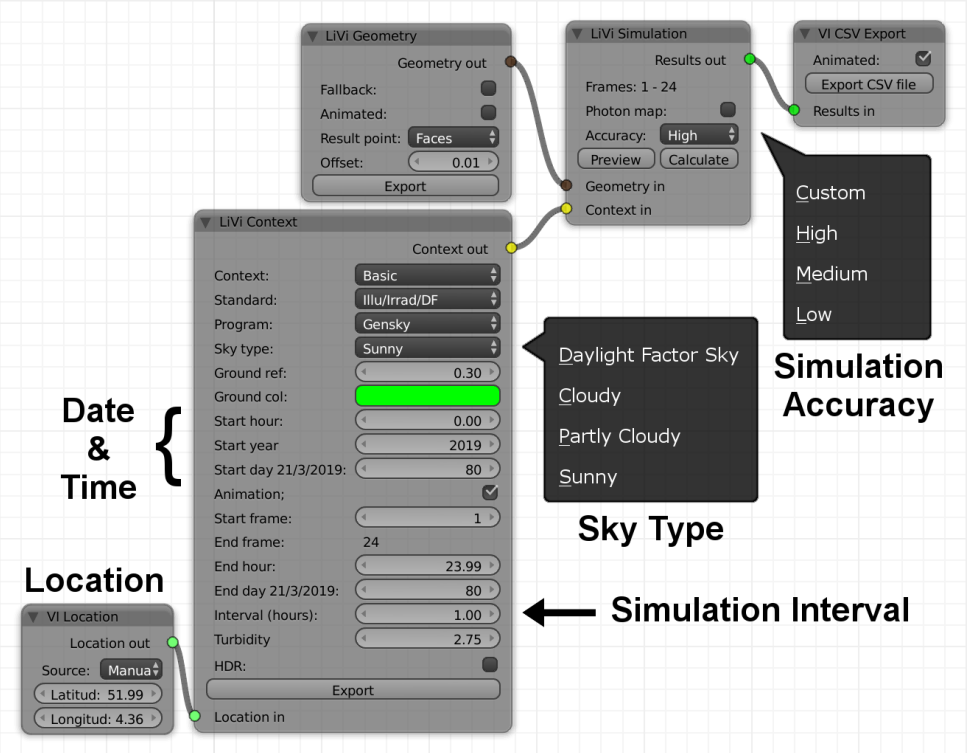

Figure 3.6: Node representation for simulation settings in Blender. This is the default setup used for the RADIANCE lighting simulation process. Each grey block represents a different part needed to create text files that are processed by RADIANCE. The sky type and accuracy settings show an exploited view of the available options. Also, some text is added to highlight the most important options for the simulations.

The main blocks used in this setup will now be explained below. It should be said that no detailed information could be found on each of the settings. Only by hovering on the parameters, a few words of information was given in the Blender add-on. For most of the settings the exact nature and influence was deducted from looking through the source code of the settings, which can be found by clicking with the right mouse button on the setting and select "Edit Source".

VI Location
The block "VI Location" is used for setting the latitude and longitude. Alternatively, the source can be an EWP file. The block has to be connected to the "LiVi Context" block.

LiVi Geometry
The "LiVi Geometry" block is used to export a text file which defines all the important faces defined in the 3D model. For some complex sensor plane geometries, the position of the sensor might not be calculated as expected. In this case, the "result point" option should be set from "Faces" to "Vertices", to use the vertices directly to determine the position. The "Offset" option determines the offset between the sensor plane and the actual calculation position, which should be just in front of the geometry to prevent blocking. In this case the default value of 0.01 leads to an offset of 2.6 mm. The "Fallback" option can be used to enforce simple geometry creation and "Animated" should be selected if the position of some objects is set to change during the simulation, both were not used in the simulations here.

LiVi Context
This block defines all the other simulation settings. There are three context options; "Basic", as is used in the simulations here, "Compliance", which can be selected to use a predefined compliance analysis, and "CBDM", which stands for climate based daylight modelling. For "Basic" context the "Standard" can be set to either "Glare" or "Illu/rad/DF". The later is used here because the irradiance needs to be calculated. Multiple sky creation models can be selected under "Program". The "Gensky" option makes use of the three standard CIE "Sky types", in this case "Sunny", "Partly Cloudy" and "Cloudy". More details about this model will be given in further sections. Another model program that can be used is "Gendalit", which makes use of the well-known Perez model [30], which defines the sky illuminance with two parameters. Epsilon is used as the sky clearness factor and Delta defines the sky brightness.

The ground colour and reflectively are left at their default settings green ([R,G,B] = [0,1,0]) and 0.30, respectively, because in these scenes there is a floor plane covering the ground anyways. The start and end hours are used to set the time in UTC, and the interval can be set from one minute to any value below 24 hours. The sky turbidity can also be set here, between one and five.

LiVi Simulation
In this block the accuracy of the simulation can be set on "Low", "Medium" or "High". Each step will use more rays to try and calculate the irradiance falling on the sensor plane. This will obviously come at higher computational effort. Note, there is also an option to use "Custom" accuracy, however, this option was not working in the current version of the vi-suite add-on. The "Photon map" option allows for a second calculation process in which forward ray-tracing is used together with the already carried out backwards ray-tracing.

3.2.2 Solar position and intensity

The solar position is determined in the VI-suite add-on from Blender 3D, based on the location, date and time. Figure 3.7 shows the household room scene with the sun just before noon at a day in spring.

In the program, the sun is displayed as a point light source at a certain location in the 3D scene, which makes the user able to obtain the azimuth and altitude angles. The book from Smets et al. [31] was used to verify if the position of the sun was correct and as expected at a certain time. Let us take somewhere in Delft in the morning of the first day of spring, 20 March in the year 2018 at 09:00 AM. The latitude is 52.00 and the longitude 4.37 degrees. Considering the timezone of +1, we can calculate 19.20 degrees and 116.56 degrees for the altitude and azimuth, respectively. Filling in the same input in Blender we find an altitude of 18.51 degrees and an azimuth of 116.89 degrees. A third online source like [32] can be taken as another reference. The same input lead to an altitude and azimuth of 19.24 and 116.72 degrees. So it looks like the position of the sun is calculated in a slightly different way for the Blender Add-on. To be certain, another point can be taken, like 10 July 2018, at 14:00. For this date and the time, the hand-calculated solar position was 60.10 and 185.63 degrees for the altitude and azimuth.

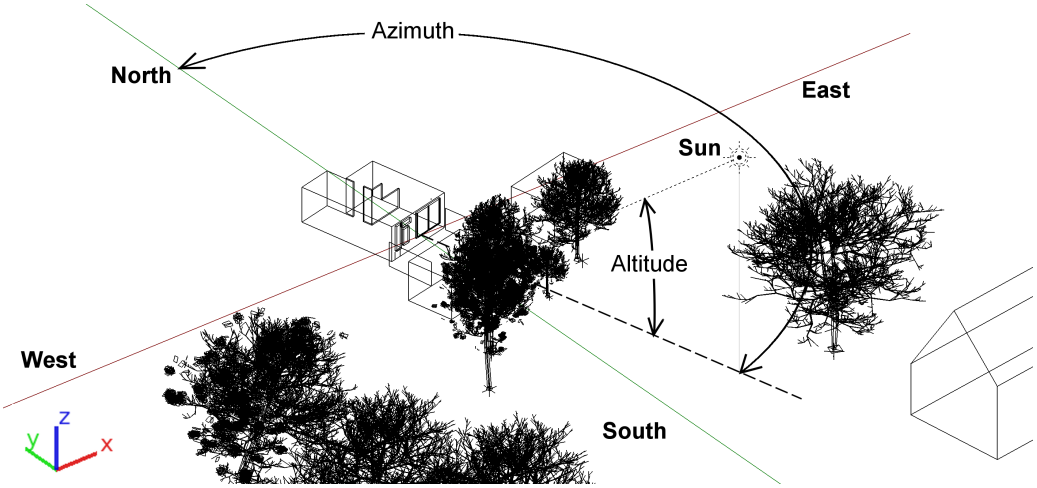

Figure 3.7: The household room scene with the position of the sun. It can be seen how the solar azimuth and altitude are defined.

The online source provided similar values again. This time the values calculated in Blender were closer with 60.14 and 185.80. The exact formulas and calculations can be seen in Appendix B. So it can be concluded that the position of the sun was calculated with a slight uncertainty for different dates during a year, but because the small misalignment, this will not be taken into account for future calculations.

The intensity of the sun was set implicitly by RADIANCE. A simple simulation was made with a single plane facing the sun to calculate the direct normal irradiance. For a clear summer day, June 21 2016, at 12:00 hr UTC, the calculated irradiance was 782 W/m^2. This value is as expected for the chosen location of Delft in the Netherlands. For a complete overcast day it was 112 W/m^2. There was no sun in this simulation, but for comparison reasons the same angle of incidence as in the previous sunny calculation was used. The partly cloudy, or intermediate, sky had an irradiance of 204 W/m^2.

3.2.3 Sky illuminance and cloud cover

At the start of this thesis DIALux was used as an alternative light simulation tool. As explained in Section 2.2.3, this programs was found not suitable, but already a lot of insight was gained in the simulation method. In particular the model used to simulate the sky illuminance was investigated and it was found out that the skies were generated following the CIE 110-1994 standards [24],[33]. From the 15 predefined standard skies, DIALux uses three skies called "Clear sky", "Overcast sky" and "Average sky", which allows for a quick selection with apparent differences. Only with the overcast sky, no direct sunlight is modelled in the scene. The average sky is in between overcast and clear and is developed from a long period of measurements [23] based on the work from Nakamura in 1985 [34]. There are no more options, so the skies cannot be adjusted perfectly to suit the real-life conditions, unless the sky is perfectly clear or overcast.

As mentioned earlier, in RADIANCE, multiple sky models can be used. The "Gensky" model uses the same principles as in DIALux with the CIE standard sky types [29]. This means the initial results from DIALux could be compared directly with those from RADIANCE. The "Gendaylit" model uses the well-known Perez model [30], which is characterised by three parameters epsilon, delta and zenith angle of the sun. With epsilon the sky clearness can be adjusted. For epsilon=1 the sky is fully overcast and the sky is clear for epsilon>6. The delta parameter stands for the sky brightness and can be considered as the opacity or thickness of the clouds [27]. Close to zero stands for dark clouds and 0.5 for very bright ones. It was found that it can get very complicated to convert the visible information for a real sky to epsilon and delta for a modelled sky for a whole day. Also, at the time, no useful literature was found to convert the

three standard skies used in DIALux and the "Gensky" model to the parameters from the Perez model, so for this reason the CIE standard sky model was used for the remainder of this thesis. This did make the comparison between real and modelled scene more difficult, as will be shown in later sections and so for future work it might be better to work with the Perez model instead.

Three standard skies
The three standard skies in the Blender 3D add-on used for RADIANCE are called "Sunny", "Cloudy" and "Partly Cloudy", similar to the "Clear sky", "Overcast sky" and "Average sky" from DIALux. The turbidity factor of the sky is the only other parameter that can be changed. Literature was found that compared real-life conditions with the standard skies from the CIE 110-1994 publication. In the article of Darula and Kittler [35], a site in Slovakia is chosen to show that the standard skies represent a realistic method to model daylight. In a more recent article from Li et al. [36] four approaches are suggested to help classify skies according to the standards. As most of the similar literature, they help you to classify a real sky to any of the 15 proposed standards skies from the CIE 110-1994 publication. But in this case, only three standard skies are used, meaning that, besides for completely clear and overcast, the modelled sky will hardly ever match a certain real-life skies. So some effort needs to be put for the comparison of real skies to modelled skies and this is further explained in Section 4.3.

3.3 Simulation results and discussion

With most simulation settings now fixed, their are two parameters in particular that need to be fine-tuned to create the best accurate, yet quick, simulation. The simulation step size and accuracy will be adjusted for different scenes and conditions to find what values are optimal in each situation. It should be noted that at this point, the irradiance values are unimportant. Thee values are used only to get an idea of the influence of changing settings.

3.3.1 Simulation time interval

The chosen step size of the simulation directly influences the computation time of the simulation. For the most accurate results a smaller step size is preferred, but it would obviously also take the most computational effort. The smallest possible step size is one minute and for the purpose of finding a suitable step size, also an interval of 10 minutes and 1 hour were investigated. This was done for all three cloud cover types (sunny, partly cloudy, and Cloudy) and also for both scenes (Household and Office). The accuracy for this plot type was set to low accuracy to save computational effort and no high accuracy is needed for this part, as it is solely used to justify later settings.

As can be seen in the tables, the computation time drastically decreases for the bigger intervals, but also the calculated energy yield goes down as critical high resolution data is lost at times when the sun comes and shines into the room. This is especially true for parts with a lot of sunlight as can be seen for the sunny simulation results, but not so much for cloudy scenarios. This has to due with the fluctuation of irradiance and can be explained easily by looking at the corresponding graph in Figure 3.8.

The results of the 1 minute interval simulation in the plot shows a spike each time the sun penetrates through to the sensor plane. The 10 minute interval plot and the 1 hour interval plot can follow the graph nicely until around 13:00 hr. There, the irradiance suddenly jumps to a high value of 140 W/m^2 and fluctuates between low and high for approximately 20 minutes, due to shading of a tree and eventually a building. The 10 minute interval does intersect with a high value at first, but is low for the next data point. The 1 hour interval does not have an intersection with a high value data point and thus continues without ever detecting the sudden

(a) The household simulation results.

Simulation Interval	Computation Time	Energy Yield (Wh/m^2)					
		Sunny		*Partly*		*Cloudy*	
1 minute	14 - 16 minutes	135.7	100%	28.0	100%	5.9	100%
10 minutes	2 minutes	124.9	92%	26.3	94%	5.8	98%
1 hour	15 seconds	47.9	35%	13.7	49%	5.5	93%

(b) The office simulation results.

Simulation Interval	Computation Time	Energy Yield (Wh/m^2)					
		Sunny		*Partly*		*Cloudy*	
1 minute	5 - 10 minutes	59.1	100%	13.9	100%	4.6	100%
10 minutes	1.5 minutes	54.3	92%	12.2	88%	4.7	102%
1 hour	15 seconds	27.5	47%	8.1	58%	4.8	104%

Table 3.1: Results from the simulation at low accuracy for three different intervals. The values for each sky type are given in Wh/m^2 and the percentages on the right of the show the value relative to the ideal high accuracy simulation. It can be seen that the choice of interval influences bright sunny simulations more than dark cloudy simulations.

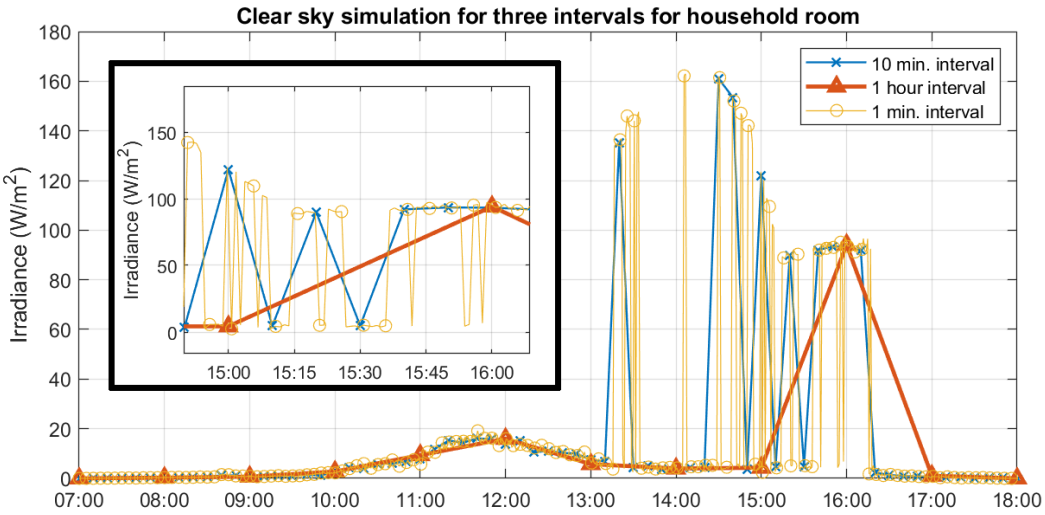

Figure 3.8: Results from a sunny sky simulation for three different time intervals. The date of the simulation is 22-11-2018 and the accuracy is set to low. A closeup is provided for the range between 3 PM and 4 PM. It can be seen that the choice of accuracy can influence the results in an unpredictable manner.

increase in irradiance. This example clearly shows the loss in data, and indeed why the total radiant energy is lower at longer intervals, but does not tell the whole story. Looking at the graph between 15 PM and 17 PM, one can see how it might be possible that the longer interval plots over estimate the irradiance at certain times. The 1 hr interval plot intersects with a high value of the 1 minute plot at 16 PM and goes linearly back to zero one hour later. But closer to reality, the sun is already blocked before 16:30 hr, meaning the graph falsely assumes higher values. The same is true for the 10 minute interval plot, but here it is less significant. A similar approach can be used to explain the relatively low change in calculated energy yield for cloudy conditions. The plot in Figure 3.9 shows the results of a cloudy day simulation for the 1 hour and 1 minute interval.

It can be seen that the 1 m interval plot holds a lot of unnecessary data because the 1 h plot can follow it hour by hour, because direct sunlight is not used in the simulation. Only at 14:00 hr does the 1 h plot intersect at a low value of disturbances in the 1 m plot, leading to a slightly lower overall radiant energy.

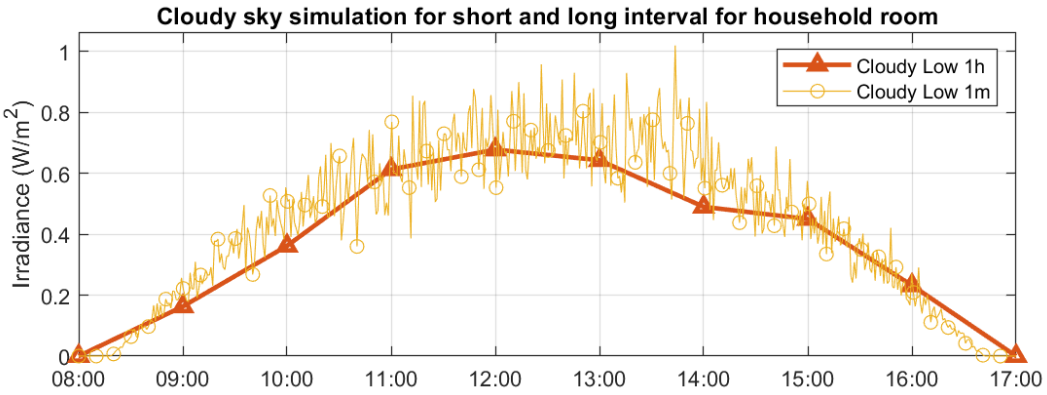

Figure 3.9: Results from a cloudy sky simulation for two different time intervals. The date of the simulation is 22-11-2018 and the accuracy is set to low. The plot shows that no short interval is needed for scenes without sun light.

3.3.2 Simulation accuracy

A higher simulation accuracy in backwards ray-tracing software, like used in RADIANCE, means more rays are send from the sensor plane to to try and find a light source. This will take longer but is preferred for simulations that require the certainty of finding the contribution of each light source in the scene. To find a suitable accuracy for the two scenarios, simulations were done for the three options for the accuracy, namely: "Low", "Medium" and "High". This was again done for all three cloud cover types (Sunny, Partly Cloudy, and Cloudy). The interval was constant throughout all nine simulations at 10 minutes, to get a reasonable high resolution of data, whilst reducing computational time compared to the 1 minute interval case.

(a) The household simulation results

Simulation Accuracy	**Computation Time**	**Daily solar insolation (Wh/m^2)**					
		Sunny		*Partly*		*Cloudy*	
High	8 - 14 minutes	161.4	100%	45.3	100%	15.9	100%
Medium	2 minutes	140.3	87%	33.3	74%	10.8	68%
Low	1.5 minutes	124.9	77%	26.3	58%	5.8	36%

(b) The office simulation results

Simulation Accuracy	**Computation Time**	**Daily solar insolation (Wh/m^2)**					
		Sunny		*Partly*		*Cloudy*	
High	15 - 20 minutes	60.1	100%	25.0	100%	10.4	100%
Medium	1.5 - 2 minutes	55.1	92%	13.9	56%	6.3	61%
Low	1 - 1.5 minutes	54.3	90%	12.2	49%	4.7	45%

Table 3.2: Results from the simulation at an interval of 10 minutes for three different accuracies. The values for each sky type are given in Wh/m^2 and the percentages on the right of the show the value relative to the ideal high accuracy simulation. It can be seen that simulations with clouds require a higher accuracy setting than scenes with a lot of sunlight.

It can be seen from the tables that for cloudier conditions the influence of different accuracy options becomes greater. For the household simulation results, it can be seen that there is not much difference overall between the low and medium accuracy simulations. This effect can be put down to the manner in which ray-tracing simulations operate. In backwards ray-tracing, if after a few bounces from walls and objects the ray hits a source, the incident irradiance is calculated by multiplying the irradiance send out from the source with the specular reflection of the material on each surface it reflects from. Each ray has a certain amount of radiance in W/m^{2}sr. The total incident irradiance can then be found by summing all contributions from

each ray that was send out. So by using a higher accuracy, more rays are added and resulting in a higher irradiance. If the scene has bright light sources that are easy to trace, so either directly or with one bounce, then fewer rays are needed to get an accurate estimating of the incident ray.

The simulations with a cloudy sky does not have a high intensity light source such as the sun in the scene, so in these scenes the influence can be seen very easily when looking at the graphs of different accuracies in Figure 3.10.

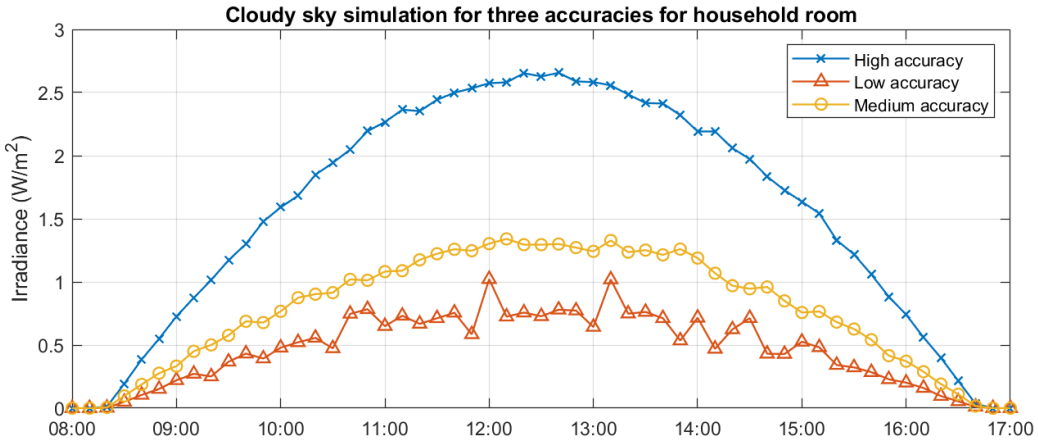

Figure 3.10: Results from a cloudy sky simulation for three different simulation accuracies. The simulation date is 22-11-2018 and the interval is set to 10 minutes. The influence of simulation accuracy in a scene without much light can be clearly seen.

Taking the sunny sky simulation from Figure 3.11, it can be seen that for times when the irradiance is relatively low, such as between 10:00 hr and 11:00 hr, the difference between the graphs of the three accuracies is still large. But when the sun is directly in view of the sensor, such as between 14:00 hr and 15:00 hr, the values of the incident irradiance are very similar. This clearly shows the difference response of accuracy in high and low intensity light scenes.

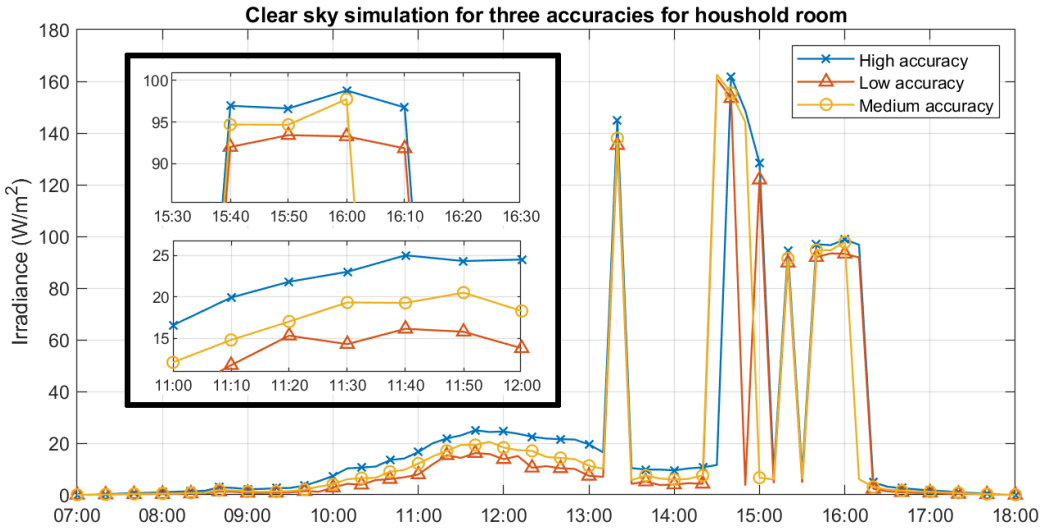

Figure 3.11: Results from a sunny sky simulation for three different simulation accuracies. The date of the simulation is 22-11-2018 and an interval of 10 minutes. Inside the black square are two zoomed in plots of the same curves. It can be seen that the relative difference is greater when the irradiance is lower, and vice versa.

3.4 Conclusions and recommendations

In this chapter, two rooms in Delft were recreated with the 3D modelling software program Blender. The validated lighting simulation tool RADIANCE was used to perform indoor light simulations for some relevant areas in the modelled rooms. The ideal settings in this simulation method were verified to be suitable to produce three different simulations, corresponding to three standard weather types, of a full day with a computation time of 20 minutes.

3.4.1 Room furniture is not required in 3D model

The first room was a household living room with main window facing almost south and the second one a university office room facing east-northeast. The rooms and its important surroundings were modelled with a measuring tape and satellite images. From the literature review it was already found out that not much detailed room furniture was needed for accurate simulations. However, this can mean that estimates are 5% higher compared to more detailed models, which contain objects that absorb light.

3.4.2 Using RADIANCE comes with difficulties

An additional user-made code (add-on) was needed to translate the 3D model in Blender to the required input data for the RADIANCE calculations. This so-called VI-suite add-on is still work in progress, so there are some minor bugs and difficulties limiting the use. To resolve these issues, some experience is required with Blender beforehand. Other, more conventional, options to use RADIANCE are DAYSIM with Rhinoceros or Ecotect. Furthermore, the RADIANCE tool uses backwards ray-tracing, which is known to be a slow computation method. So it is best practise to do quick, low accuracy simulations, to check if changing the settings has the desired outcome.

3.4.3 The standard sky model is comprehensible, but difficult to work with

Different models can be used to simulate the light coming from the sky. In this work, the CIE 110-1994 standard skies were used to define the sky distribution in favour of the Perez model, because DIALux, the other light simulation tool used in this work, also uses this same method. This means comparison between the two programs could be done directly. Another advantage is that the three standard sky types allows for an easy and quick comparison with real-life skies. It was found out later that, the Perez model is perhaps more accurate to work with when comparing modelled skies to real skies, because it has two parameters to accurately define the sky clearness and brightness.

3.4.4 The cleaner the sky, the shorter the time interval

For different sky types, different settings are needed to provide an accurate, but also quick simulation. When the sky is clear, the irradiance can drop quickly due to shading of nearby objects, so in these conditions a short time interval of one minute is needed between data points. This is only necessary if daily data is compared, because over longer time spans the over- and underestimations in the model would be filtered out. For complete overcast conditions, a one hour interval is sufficient because the sky illuminance only changes slightly during a day. For partly cloudy conditions, a ten minute interval is recommended as a good option in between clear and overcast.

3.4.5 Less light requires a higher accuracy

It was also found that the computation accuracy can be adapted for each situation to provide the quickest computation, whilst maintaining sufficient accuracy in the results. It can be concluded that bright conditions do not need high accuracy computation to get a value close to reality. So sunny conditions only need a low accuracy setting. Cloudy conditions on the other hand need a high accuracy simulation, due to the lack of light in the scene. A medium to high accuracy is recommended for partly cloudy situations depending on the scene.

Chapter 4

Comparison of Simulations with Reality

The previous chapter established a clear simulation setup for two common rooms in Delft. Now, it is important to check if this simulation produces a reliable output, by comparing them with the measurements. The most interesting time for the measurements is the winter period, where the energy yield of PV systems is typically low. The most difficult and important aspect will be to properly judge the weather conditions at the time of the measurements as they have to be reproduced as close in the simulation.

The purpose of this chapter is to validate the simulation results with real-life measurements. This will be done by setting up a pyranometer in the rooms that were recreated for the simulation. The experimental setup is explained in Section 4.1 and the results of the measurements are shown and discussed in Section 4.2. Section 4.3 explains very carefully how the weather data is used to merge simulations together and get an irradiance curve of each day. Section 4.4 includes the comparison made between real-life and the simulation. The simulation is assumed to be valid if the values match the measured values with an accuracy of 10%. Finally, conclusions and recommendations are summarised in the last sections. Figure 4.1 shows an overview of the content.

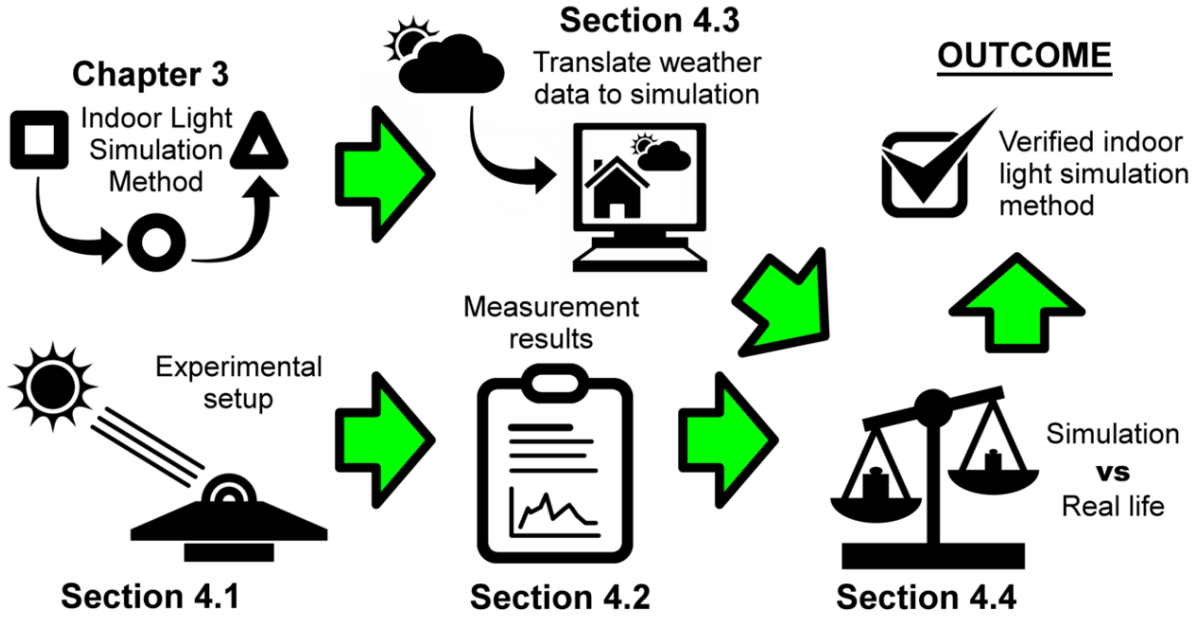

Figure 4.1: Visual representation of the content of Chapter 4. The section numbers can be found near the corresponding icons. The green arrows show the relation between the sections and outcome.

4.1 Experimental setup for indoor irradiance measurements

Similar to the research of [18], a pyranometer sensor was used to get the irradiance on a spot in the room, which is expected to have a substantial energy yield over other positions in the room. This spot was found as explained in Section 3.1.2 and is determined to be 1.8 meters from the floor and 1.0 meters from the window on the wall that receives more sun during the day. When standing in the room, facing the window, this was on the left-hand wall for both rooms. To make sure the pyranometer was at the right position a tripod stand was used, as can be seen in Figure 4.2.

(a) Experimental setup. **(b)** Equipment.

Figure 4.2: Experimental setup of the pyranometer placed on a tripod camera stand with adjustable tilt mechanism. A CMP3 pyranometer (top) [37] and an adjustable tilt mounting kit (bottom) [38]

4.1.1 CMP3 Pyranometer and adjustable tilt mount

The chosen pyranometer is the CMP3 pyranometer from Kipp&Zonen [37], because its sensor range is in the correct spectral range. The lighting simulation tool RADIANCE, calculates the irradiance for each single ray inW/m^2sr by using RGB colours, meaning that the visible irradiance is calculated. After that a constant factor is used to estimate the full irradiance value for the whole spectrum [26]. So to compare with this value, a pyranometer is needed that has a long range, and the CMP3 pyranometer is very suitable for this, because it has a spectral range from 300 to 2800 nm. An adjustable tilt, see Figure 4.2 mount was used to quickly and accurately adjust the angle of the pyranometer towards or from the window. This component was from the same suppliers as the pyranometer to ensure a safe and correct connection.

4.1.2 Position, orientation and time of the measurements

With the adjustable height of the stand and the possibility to adjust the tilt with the mounting kit, almost all orientations and positions could be quickly investigated in the room. But as discussed earlier (Section 3.1.2) the main focus was at a height of 1.0 meter from the window and 1.8 meter height from the floor. Before the start of the measurements it was already found out that the highest yield would be there, so no extensive measurements were done on all points across the room. Only two days were chosen to do the measurements. One cloudy day in the office room and one sunny day in the household room.

To properly investigate the influence of angle and position the measurements were done in stable light conditions around noon. Also, during the measurements no direct sunlight was falling on the sensor. This was done to prevent the optimal angle from being dependent only on the small time during a day that direct sunlight falls onto the investigated area.

Position
The height of the pyranometer was adjusted over multiple heights between 0.75 m and 1.8 m above the floor, this was done because any area outside these values was defined as not desirable for an IPV product. Also from the early simulations it showed that not much light falls outside of this area, because the window is also often between these two heights. The measurements were done 1 meter from the window. The position along the wall was changed in steps of 50 cm, from 0.5 m until the end of the wall. For the office room this meant the last measurement was done at 5.5 meter from the window, and for the household room it could only be done for 3.5 meters. All measurements were done at a height of 1.8 m.

Orientation
With adjustable tilt mounting the angle along the horizontal axis could be changed easily. The camera mount also allowed for rotation along the vertical axis, which made it possible to test a number of orientations. The angle influence was tasted at a height of 1.8 m, at 1 and 3 meters from the wall. The angle was set between 0 and 90 degrees towards the window with steps of 15 degrees.

4.2 Measurement results and discussion

The pyranometer is able to calculate the average for any given interval. The output file then gives the time of the measurement followed by the maximum, minimum and mean value. The values of the pyranometer at every measurement point are rounded to integers. So at low values this means the values are more unreliable. Also in some cases the data-logger recorded impossible high values, indicating an error lasting sometimes up to 8 minutes. These values were excluded from the file. For short interval errors and only when the irradiance values before and after the measurements were constant, the faulty values were replaced by the last true measurement value.

4.2.1 Pyranometer at specific position

The main pyranometer measurements were done during the winter period in the Netherlands. Normally, a more average month would be preferred for measurements, to give a more representative picture. However, the winter period can be assumed to be the worst-case scenario for indoor PV products, such as the one from this thesis, or any PV system in general. Not only are there a lot of cloudy days in this period, but also the sun is less hours above the horizon. So it is important to have an accurate simulation for this period and that is why the focus of comparing the model with real-life is based on this time of the year.

Household measurements
The graph in Figure 4.3 shows the pyranometer measurements during five days at the end of November. It can be seen that the irradiance values are much lower than can be expected outdoors. For most days, the irradiance at noon is comfortably lower than 10 W/m^2. On average, the measured daily solar insolation is approximately 40 Wh/m^2. During a normal winter day in the Netherlands, the solar insolation level on the ground is around the 780 Wh/m^2. This is a difference of almost a factor 20, which is a lot even considering the measurements were done one a vertical wall instead of horizontally.

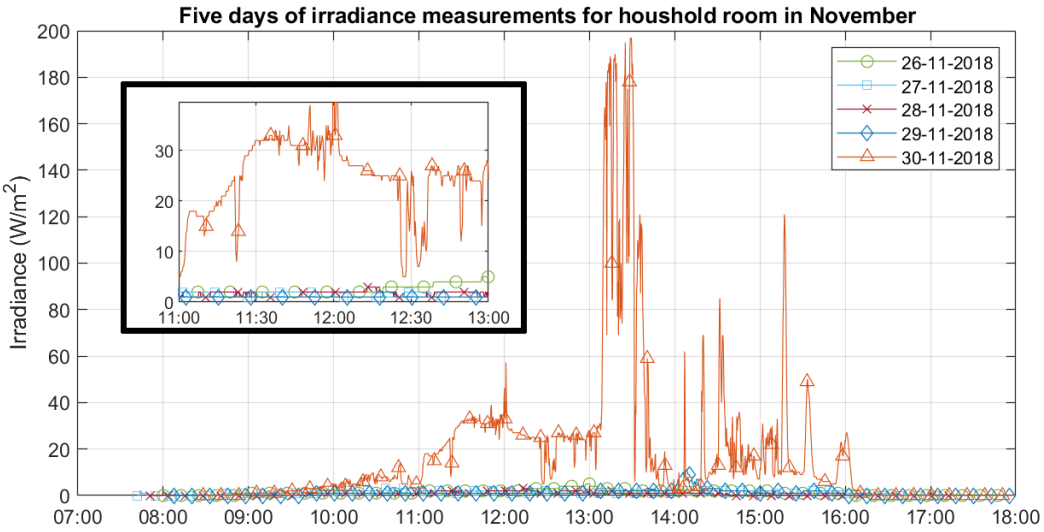

Figure 4.3: Results of pyranometer measurements for household week in November. The black square shows a zoomed in section around noon.

From the figure it can be concluded that only the 30$^{\text{th}}$ of November was a sunny day, because it is the only day with high peaks over 20 W/m^2. The rest of the days had a cloudy sky, resulting in a constant low irradiance of approximately 5 W/m^2. From the sunny day measurement, it shows that the sun fully enters the region close to the pyranometer between 13:00 hr and 13:45 hr. This is because of the south facing orientation of the main window. After that it is blocked by a nearby building and trees and only later in the afternoon does the sun come back in the building after 15:00 hr.

Office measurements

The figure below shows the pyranometer measurements from the office room. It can be seen that

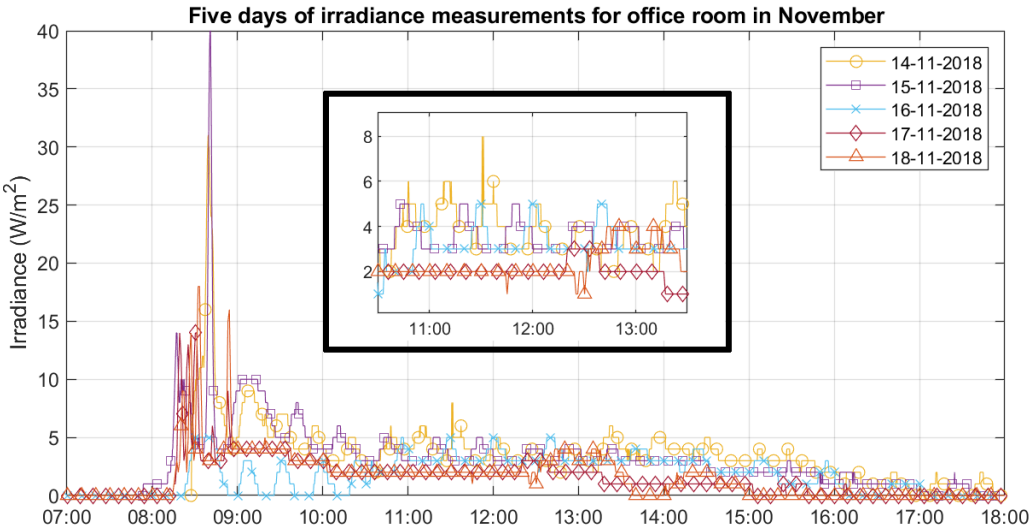

Figure 4.4: Results of pyranometer measurements for office week in November. The black square shows a zoomed in section around noon.

the irradiance values are much lower than the values found in the household. Only at a few days

in the morning did the sun enter in the morning hour between 8:15 hr and 9:00 hr. The rest of the day only reflected sunlight can enter the room, due to the east facing main window. After the morning, the irradiance gradually decreases. It should be noted that during most days, the lights in the room were on from 8:30 hr up until 18:00 hr.

4.2.2 Pyranometer at various positions in the room

It was found that changing the height did not change the irradiance significantly. More noticeable are the results from changing the distance along the wall can be seen in Figure 4.5.

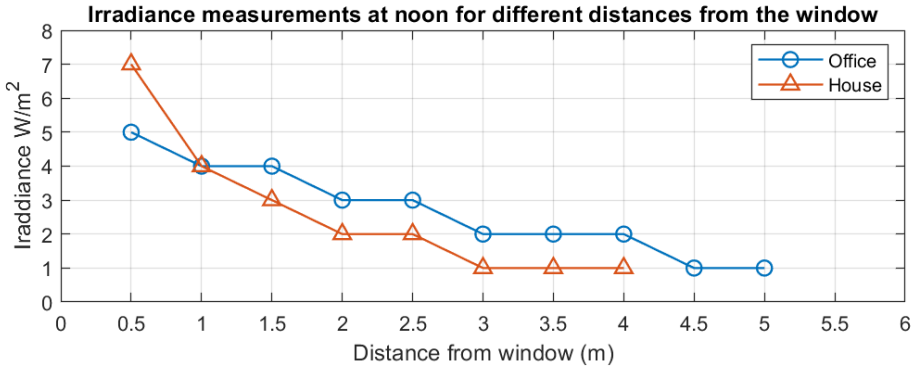

Figure 4.5: Results of pyranometer measurements in the house and office. The pyranometer was kept at an height of 1.8 m, but the distance from the wall was changed between 0.5 and 5 meters. The office measurements were done between 13:00 hr and 14:00 hr with largely clear sky and a few clouds. The household measurements were done at a fully overcast day between 13:45 hr and 14:30 hr.

The two graphs should not be compared with each other as they were measured at different days with different weather conditions. More important is the change from close to far from the window. Being only one meter from the window will give you values two to three times as high as two meters further. This means that it is very worthwhile to find a suitable design able to be placed close to the window.

4.2.3 Pyranometer at various orientations

The gathered measurements from rotating the pyranometer along its horizontal and vertical axis gave expected results. Rotating the device more towards the window will obviously increase the incident irradiance. The difference in irradiance from rotation along any axis was small and slightly inconsistent, meaning that showing the results in plots will only distract the reader from the obvious. The most important finding was that a combination of rotation along both axis could double the irradiance falling on the sensor. So if possible, the design should be able to turn towards the window in most cases.

4.3 Method to recreate simulations corresponding to weather data

This part explains how the simulations, as described in the previous chapter, are used to get a simulation in the same conditions as experienced during measurements. More specifically, if the sky was overcast for one hour and then partly cloudy the next, this should also hold for the simulation to get an accurate representation of the day.

4.3.1 Three base simulations

To start, simulations have to be made from the same period as the measurements. Because the position of the sun changes every day, the most accurate method would be to have simulations for all days. But this would take a lot of time to compute, and differences are relatively small, so it is better to pick a day in the middle of the investigated period. In this case the 21st November was taken as a suitable date as it is right in the middle of the two weeks of measurements. As a result, only 6 simulations of a full day have to be performed, instead of 42. For this date, three simulations were done as proposed in Chapter 3, namely (1) sunny sky, 1 minute interval and low accuracy, (2) partly cloudy sky, 10 minute interval and medium accuracy, (3) cloudy sky, 1 hour interval and high accuracy.

Household simulation
The graph in Figure 4.6 shows the three base simulations of the 21st of November. Comparing this figure to Figure 4.3, does already reveal that the irradiance values of the simulation are in the right order compared to the measurements. The difference between the sunny, partly cloudy

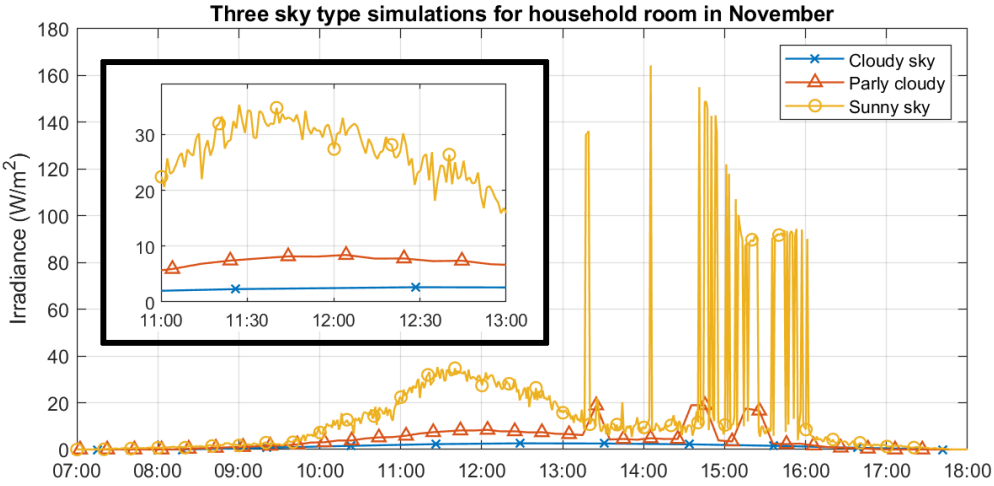

Figure 4.6: Three base simulations for household living room. Each of the three sky conditions can be found in the graph.Also, the black square shows a zoomed in section around noon.

and cloudy sky simulation is clearly noticeable. Only for the sunny sky simulation does the full intensity of the sun hit the sensor plane. It does so in a on/off manner, because of nearby blocking objects and also the blinds play prevent the sun from hitting the sensor at its full intensity continuously.

Office simulation
The graph in Figure 4.7 shows the three base simulations of the 21st of November. Again, the figure can directly be compared with the measurements from Figure 4.4. In this simulation, the difference between the three sky type simulations is only clearly noticeable at the start of the day when the sun comes in the room. There are not a lot of shading objects in the view from the window and blinds were not simulated for this room. This resulted in a more continuously irradiance in sunlight between 08:30 hr and 09:00 hr. After this it can be seen that there is not as much difference between the three simulations, compared to the household room. This is because only reflected sunlight can enter the room after the morning.

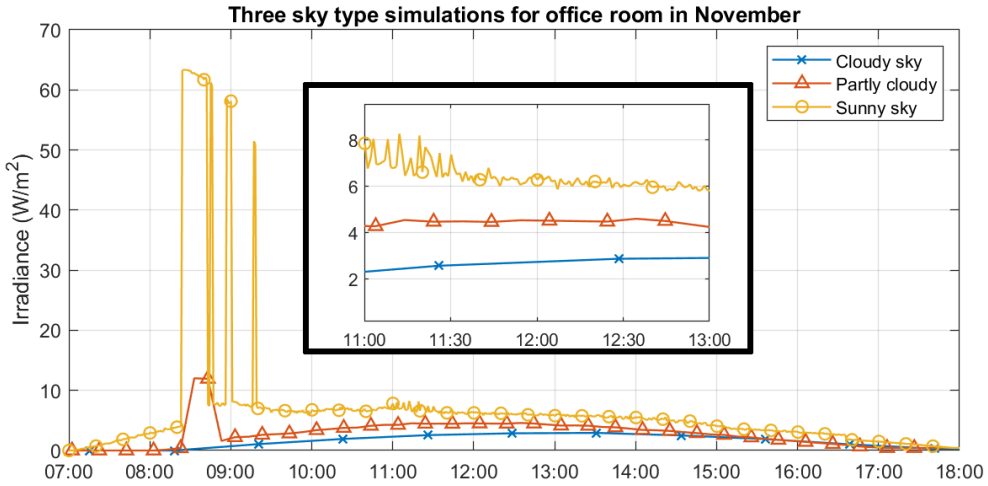

Figure 4.7: Three base simulations for university office room. Each of the three sky conditions can be found in the graph. Also, the black square shows a zoomed in section around noon.

4.3.2 Using the weather data

Weather data was taken from measured days, by selecting three weather station around the investigated location. For Delft this is Rotterdam, Hoek van Holland and Voorschoten. The data of each station was extracted for each hour and the average of was taken to get an estimated value for Delft. Further information on the used weather data is given below.

Cloud cover in oktas
The KNMI determines the degree of cloud cover in oktas at the end of every hour [39]. This can be a value from 0 to 8, where 0 means the sky is completely clear and 8 means the sky is completely covered in clouds. A value of four means the sky view was covered with clouds for 50%. A value of 9 can also be used in case the visibility is so poor that no measurement of the cloud cover could be taken. This is for instance the case when heavy rain or snowfall disturbs the visibility.

Sun time in hours
The time that direct sun rays were measured in one hour is summed in parts of 0.1 hours. This means that when the value is 10, the sun was unobstructed during the full hour. A value of two means the sun was visible for 0.2 hours or roughly 12 minutes in the corresponding hour.

Rain time in hours
The amount of hours any form of precipitation was detected was counted in the same manner as the sun time. This means that 10 means the rain has fallen for the whole hour and zero means no rain has fallen. This value is suitable to check if dark rain clouds were above Delft at the time of measurements.

4.3.3 Sky type determination criteria

With the weather data of the correct date, a consistent approach needs to be found to use it to decide which of the three base scenarios needs to be used for each hour of the day.

Clear sky or overcast for the whole day
To start, it is determined if the whole day was either sunny or overcast. To do this the average cloud cover in oktas and total sun hours were used from the time of sun rise to sun fall. If the

mean cloud cover was smaller or equal than 1.0 okta and the hours of direct sun was higher than 5.0 hours, then the day was considered to be fully clear and the corresponding base simulation could be used to calculate the irradiance over the whole day. If the mean cloud cover was higher than 7.0 okta and without any sun hours, then the whole day was considered as overcast. In these cases a full base simulation of a corresponding weather type could be taken, which saves some computational effort.

Partly cloudy day
If the day had even a bit of partly cloudy situation, every hour between sun rise and fall of that day was examined in more detail for specific weather data. The exact cloud cover, sun time and solar intensity were used to scale the simulations to suit the current weather conditions. It was decided that if the cloud cover was less than 4.0 okta and the sun had shown for at least half an hour during that hour, the sky was still considered sunny. This is also when the sun has shown itself for more than 8 hours, even with a cloud cover of 7.0 or less okta. When the cloud cover was higher than 7 okta and the sun was visible for 2 or less hours, then the sky for that hour is close to full overcast. In any other case, the current hour is said to be partly cloudy.

4.3.4 Further adjustments

Some final adjustments were added to the results of the simulation to account for extra factors not mentioned previously.

Increase factor for using low accuracy simulations
In order to speed up simulations, a lower accuracy simulation was carried out for higher illuminated scenes. This was the partly cloudy and sunny conditions in this work. As explained in the previous chapter, this decision should not influence the results much for the high peeks in irradiance, but are still of influence in the parts of lower irradiance. To compensate for this a non-linear increase factor was created to adjust the values from the low accuracy simulation to the high accuracy simulation.

Decrease irradiance during dark rain clouds
For the hours in which a lot of precipitation fell down, an extra decreasing factor was added to account for the lessened irradiance in the darker clouds. The exact influence of these clouds is hard to just as no focus was put on this topic at the time. For future work it might be interested to keep up with measurements and know the exact time of heavy clouds to see the decrease in sky illumination.

4.4 Comparison of measurements with simulation

From the method as described in the sections above, the results will be presented here and compared with the real-life measurements from before. The table below shows all significant values from every investigated date. Note that in this case five days were selected for each room, this was done because for the office room some days had incomplete data and for the household room to keep consistency. Appendix D.3 can be used to try and find the exact reason for large deviations in the results here. It can be seen that for most days the simulation is able to get a yield close to the measurements. But for some days the deviations can get big. This can be due to many factors. For instance, the weather data was taken from weather stations that were kilometres away. So a cloud or gap in the cloud for the same matter could change lead to a significant misconception of the data.

(a) The household room comparison results

Date	Average cloud cover [okta]	Total sun time [hrs]	Total rain time [hrs]	Daily solar insolation [Wh/m^2]		
				Measurements	*Simulations*	*Deviation*
26-Nov	8.0	00:04	00:56	12.6	15.0	119%
27-Nov	7.8	00:06	00:00	11.9	14.9	126%
28-Nov	8.0	00:00	04:35	6.2	7.5	121%
29-Nov	8.0	00:16	06:24	11.0	15.0	136%
30-Nov	5.0	04:38	00:00	168.8	153.6	91%
Mean	**7.4 okta**	**01:00 hrs**	**02:23 hrs**	**42.1 Wh/m^2**	**41.2 Wh/m^2**	**98%**

(b) The office room comparison results

Date	Average cloud cover [okta]	Total sun time [hrs]	Total rain time [hrs]	Daily solar insolation [Wh/m^2]		
				Measurements	*Simulations*	*Deviation*
14-Nov	8.0	07:28	00:00	35.2	15.5	44%
15-Nov	0.3	07:23	00:00	33.7	37.4	111%
16-Nov	8.2	00:14	00:00	19.8	18.3	92%
17-Nov	0	07:26	00:00	16.8	37.4	223%
18-Nov	4.3	06:39	00:00	17.6	20.9	119%
Mean	**4.2 okta**	**05:50 hrs**	**00:00 hrs**	**24.6 Wh/m^2**	**25.9 Wh/m^2**	**105%**

Table 4.1: Results of the simulations are compared with the measurements for both rooms. For each of the November days in 2018, the important weather conditions are shown on the left-hand side of the table. On the far right, the percentage deviation of the simulation from the measurement is given.

Looking more closely at the days with the biggest deviation, it becomes clear that the issue might be in the weather data. For instance for the office room, at 14 November, the cloud cover is 8 okta, even though the sun was visible the whole day. The results from the measurements also suggest that the day was sunny, but due to the high okta value, the simulation is underestimating the irradiance. The 17$^{\text{th}}$ of November was a very sunny day, when looking at the weather data, so the simulation treats it like this. But in reality there were partial clouds at Delft and the received irradiance was low. Except for those two days there is an accordance within 20% of the other days. The last row shows the mean of all columns. It shows that on average the simulated solar insolation deviates not more than 5% for both rooms. The mean from all the daily irradiance values was also calculated and the resulting plots can be seen in the figures below. It can be seen that for both figures, the simulation plot matches the curve for the smoother section of the measurement curve,such as between 11:00 and 13:00 hr. But

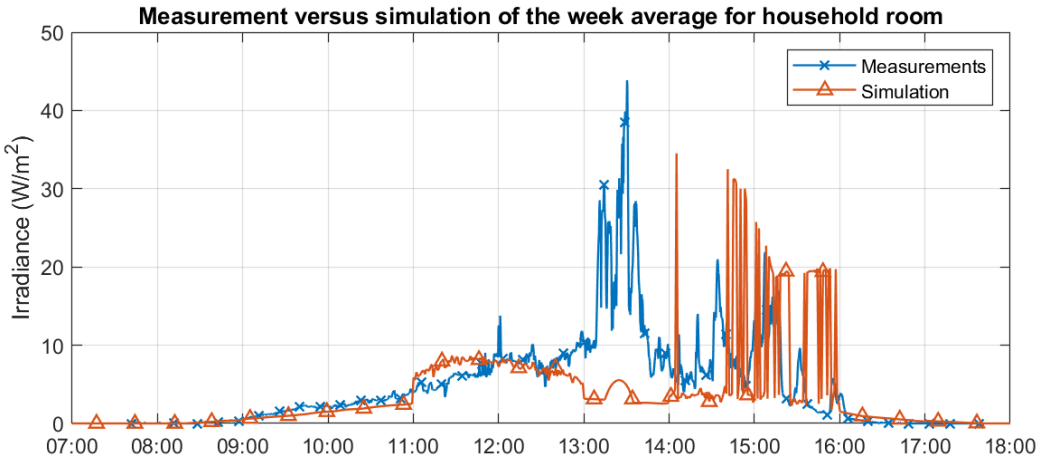

Figure 4.8: Household comparison simulation and measurement averages from a week in November. The big deviation between 13:00 and 14:00 hr is a direct result of an inaccuracy in the simulations. As can be seen in Figure 4.6

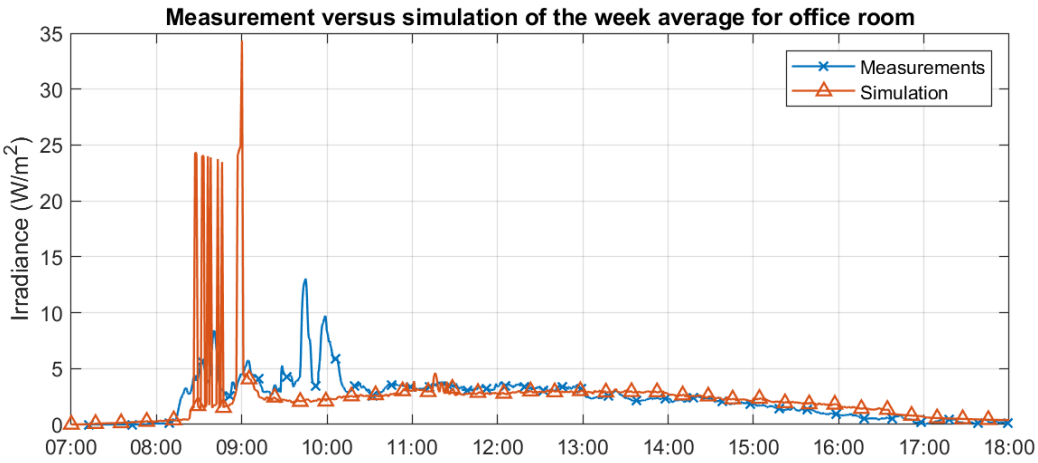

Figure 4.9: Office comparison simulation and measurement averages from a week in November

for the spiky regions with high irradiance, the simulation compares not very accurately with the reality. It would obviously be impossible to exactly match each spike in irradiance, due to the many unpredictabilities such as clouds. For the household room, there is a large deviation near noon, between 13:00 and 14:00 hr. Looking at the base simulation plot from Figure 4.6, it can be seen that the problem is in the simulation. For some reason the sun is blocked and not falling onto the sensor. This could be solved by a small change in the 3D model or maybe when another day is chosen as the base simulation. But for now, it clearly shows how this method is not very suitable when direct sunlight contributes to the incident irradiance.

The office simulation is a very good simulation for most of the day. Only in the first few hours, when the sun falls directly on the sensor, are there a lot of fluctuations. For the rest of the day the irradiance is more stable, and only reflected light comes into the room. This proves that the simulation is very good for indoor light simulation, where the direct sun is not playing a big role.

4.5 Conclusions and recommendations

In this chapter it has been verified that, on average, the simulations produce an accurate estimation of the actual indoor irradiance values. Measurements were done with a pyranometer at the same position in the household and office room as in the simulations. For proper comparison with the measurements, weather data was used for every hour in the simulation to determine the sky conditions. The results in Figures 4.8 and 4.9 show the averages of the measurements and simulations over a five day period for the household and office room, respectively. For certain hours of the day there were large deviations, but over the full week, there is only an inaccuracy of 5% between measurements and simulations.

4.5.1 The pyranometer measurements were focused on November

The pyranometer was placed on a camera tripod with adjustable mount to make sure the measurement position could be set easily and accurately to the same position as in the 3D models of the simulations. Data was gathered for one week during November in both the household and office room. More measurements were done spread over the year, but only the November data was analysed intensively, because it is the most important period to have an accurate simulation for. More specifically, being the worst-case period for almost any PV system, if a indoor PV product works in the winter, it should also work at any other time during the year. Apart from

the continuous daily measurements, the pyranometer was also placed at various positions and orientations in the rooms.

4.5.2 The irradiance indoors rarely exceeds 20 W/m^2

For the studied case, the average solar insolation on a wall, one meter from a south facing window is 42 Wh/m^2 in the winter months. The peak irradiance on a sunny day around noon gets up to 180 W/m^2, lasting only half an hour, before being blocked by nearby objects and walls. For the east facing office, the peak irradiance was not higher than 40 W/m^2, occurring in the first hour of the morning. For the rest of the day, the irradiance is below 20 W/m^2, even in the ideal clear sky conditions. During overcast conditions, the irradiance is always lower than 5 W/m^2. This is in accordance with values found in literature.

4.5.3 The pyranometer accuracy is questionable at low irradiance values

The values of the pyranometer are rounded to an integer, meaning that at low irradiance values the accuracy of the sensor becomes questionable. For instance, the irradiance coming from the artificial lighting was not enough to be noticed by a horizontally orientated pyranometer when it was dark outside, but did sometimes influence measurements during the day when being switched on or off. From this it could be said that the contribution of the artificial lights is likely to be close to 0.5 W/m^2. This means that, for the studied cases, even in cloudy winter conditions the contribution of artificial light is less than 10%. But due to the inaccuracy the contribution could also be even twice as low.

4.5.4 Use sun, clouds and precipitations data to determine sky illuminance settings

Three base simulations were created corresponding to the three standard sky types: sunny sky, cloudy sky and partly cloudy sky. A day in the middle of the analysed period was taken as a basis for the irradiance calculations for all other days. With weather data from KNMI stations, sun hours and cloud cover were used to determine the sky illumination settings. Further adjustments to increase or decrease the irradiance were applied in some situations, for instance to account for heavy rainy days.

4.5.5 In direct sunlight, the irradiance values become unpredictable

The method provided good results in parts where the direct sun does not play a significant role. This means it is a good comparison for most hours of the day, except for the short time when direct sunlight through the window is falls exactly on the sensor. Only at this time, small misalignment from nearby objects can result in big deviations in received irradiance. Only over a longer period are these uncertainties likely to cancel each other out, due to the changing solar position in the sky on a daily basis.

4.5.6 A one day simulation has an accuracy of 20%

Overall the simulation method provides a good accordance with the measurements. A deviation of around 20% was found for the two investigated rooms on a daily basis. Over a five day period, these deviation cancel each other out and the average deviation was less than 5% for both rooms. For some abnormal days, the weather data did not give a proper indication of the actual weather conditions for that day at the measurement locations, leading to simulated values being twice

as high or low as measured values. This could be because the data comes from nearby weather stations, instead of the actual location, inducing a time difference between the data and actual weather conditions. Factors such as wind could also contribute to this phenomena.

Chapter 5

Prediction of Yearly Energy Yield and Best PV cell technology

In the previous chapter it was shown that the simulations compare well with the measurements in the household and university office room. This means that the model can now be used to extend the simulations over longer periods of time. This will reveal valuable information about the expected PV energy yield for each month for the two studied rooms. After that, it is essential to apply the model to rooms with various characteristics to get a complete picture of the working regions of the indoor PV system. This can be done by using the already build 3D models of the two rooms, and change one parameter at the time to see the result of the adjustment. Simplifications need to be added to the explained the method to decrease the computation time, so that the solar insolation and PV yield can be determined for as much various situations as possible. The PV energy yield will have to be calculated to end with conclusions on the best PV cell technology.

The purpose of this chapter is to show the reader how the models were used to extrapolate the simulation over a full year to predict the energy yield of four different solar cell technologies for varying room characteristics. The method to get to the average daily insolation for each month is described in Section 5.1. Also, a more simplified approach was used to calculate the expected yield at different room characteristics in Section 5.2. The results are combined and discussed in Section 5.3 and the outcome is a map of where which technology performs best based on room orientation and position in the room. Figure 5.1 shows an overview of the content.

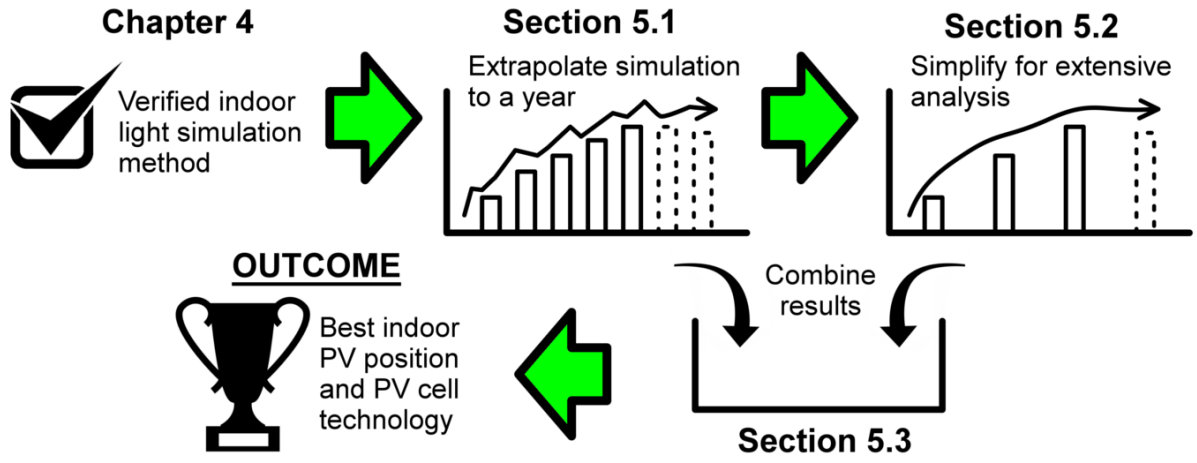

Figure 5.1: Visual representation of the content of Chapter 5. The section numbers can be found near the corresponding icons. The green arrows show the relation between the sections and outcome.

5.1 Method to predict daily PV energy yield

This section describes how the simulations were used to get a irradiance curve of every day in the year. The main steps and assumptions are in the subsections below. The outcome will be a propositions for doing simulations, as well as further calculations with the results from the simulations.

5.1.1 Hourly irradiance calculations

In this step, the irradiance in W/m^2 at every hour of the year is calculated based on weather data using the same method as described in Section 4.3. So again, three base simulations are computed of a complete day with the three sky types: clear sky, overcast and partly cloudy. Next, the weather data is consulted to decide on every hour which sky type is the most representative and some scaling factors may later be applied. The outcome is a hourly irradiance curve over the full year and integration will give the daily solar insolation in Wh/m^2.

Simulation of only one day in each month
Because of the high amount of simulations, the simulation is performed for only one day in the month and adjacent days use the closest base simulation as a reference. So in this case, the 21^{st} of each month is taken, meaning that the closer the day is to the 21^{st}, the more accurate the simulation is. Figure 5.2 shows the simulation of two months, in order to check how much this simplification influences the results.

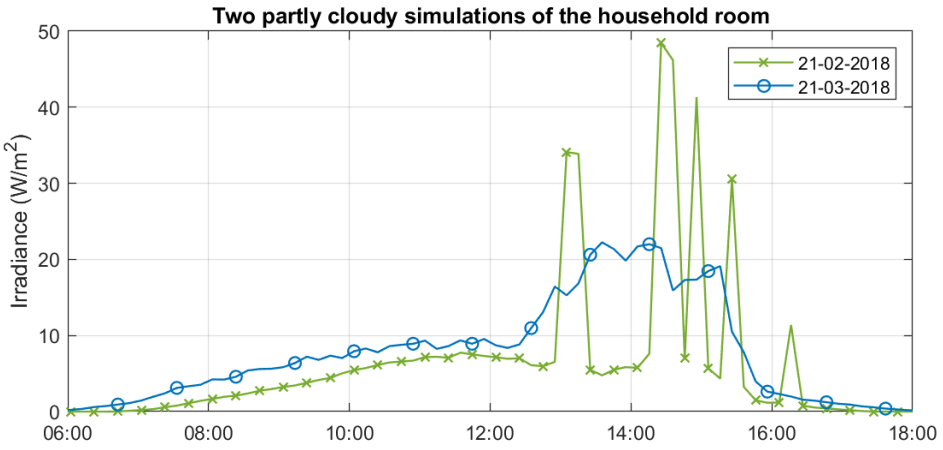

Figure 5.2: Simulation of the 21^{st} of February and March with partly cloudy sky settings for the full day.

It can be seen that for the regions where the irradiance changes gradually, the difference between the two months is generally smaller than 2 W/m^2. This means that over a 30 day period the irradiance for a certain time of the day changes roughly 0.07 W/m^2 per day, which is less then 2% for most of the day. For days that are furthest between the two dates, like the 5^{th} of March, the deviation can be up to 10% around noon in steady conditions. However, it can be assumed that the overestimations and underestimations cancel each other out over the year. The simulations are only unpredictable for the times when direct sunlight falls on the sensor and the irradiance becomes suddenly high. This can change more pronounced from day to day and these fluctuations are ignored in this method. But this is taken for granted as it means only 36 simulations are required instead of over 1000 to simulate a full year.

5.1.2 PV cell efficiency for indoor conditions

The previous step shows the calculation of the irradiance in W/m^2 for every hour of the year. Now the efficiency of the solar cells has to be considered to predict the electric energy yield from the module. Randall [10] investigated over twenty solar cell technologies and deducted the parameters a and b to calculate the efficiency in percentages. The model assumes a linear curve on the logarithmic scale for the efficiency below 100 W/m^2 and the relation between the parameters can be seen in Equation 5.1.

$$\eta(\%) = a \ln(G) + b \tag{5.1}$$

The values for the parameters a and b can be found in the Appendix C and G is the irradiance. Note that it is assumed here that the light source is a dimmed AM1.5 spectrum. This is of course not the case for each time of the day across the year. The spectrum of light depends on a lot of factors. Research has been done on the contribution of such factors, however, for now it was left out of the model for simplicity.

Selecting four PV cell technologies to investigate

Figure C.1 shows a list with details about all 21 investigated cells. Presenting results of this many different cell technologies would make the results unclear. Furthermore, some cells will outperform other cells in any case, so a selection has to be made of fewer cells. From the details in the list, it can be seen that eight cells were manufactured in a laboratory. These cells will be expensive and not commercially available, so they are excluded. Also, cells with a cell area smaller than 5 cm^2 have been excluded, because it is assumed that the smaller cells can have an exaggerated high performance, which will deteriorate when scaled up to normal sizes. Now, only four technological classes remain, namely mono- and polycrystalline silicon, polycrystalline thin films (CdTE and CIGS) and amorphous silicon. It has been decided to pick only the best performing cell from each class. Cells with a high a/b ratio are expected to perform best in low irradiance conditions, so they are picked. The four remaining cell technologies and their characteristics are shown in Table 5.1.

Code	Technology	Supplier	Active area [cm^2]	parameters	
				a	b
m-Si	moncrystalline silicon	BP Solar	9.36	1.71	2.58
p-Si	polycrystalline silicon	EFG, Tessag (RWE)	10.25	2.33	0.48
CdTe	cadmium telluride	Panasonic	5.80	0.38	3.30
a-Si	amorphous silicon	Tessag (RWE)	4.95	0.43	5.41

Table 5.1: Specifications of the four chosen solar cell technologies. Note, Tessag has had a name change to RWE.

Power obtained from solar cells

The model used to derive the efficiency inherently has losses, such as cable and connection losses, in the calculations. This is because the values for the parameters are obtained from real life measurements. The power P_{DC} can thus simply be calculated with

$$P_{\mathrm{DC}} = \frac{\eta(\%)}{100} G A_{\mathrm{cells}} \tag{5.2}$$

where G is again the irradiance in W/m^2 and A_cells is the active solar cell area. Note that this is the DC power before the rest of the system. Further losses can later be applied to account for DC-DC conversion losses.

5.2 Method to compare influence of room characteristics

This section describes how the simulations were used to get a the energy yield for a couple of cell technologies to compare which type performs best for different room characteristics. The investigated room characteristics are clarified below.

5.2.1 Multiple room orientations and sensor spots

For the purpose of getting a good overview which position in the room is best, it would be best to get an entire irradiance profile, like the one in Figure 2.9a, for the complete year and every surface. However, the programs used in this thesis did not allow for easy, large-scale simulations and the computation time would be unnecessary long. So instead it was chosen to only focus on the left adjacent wall of the main window and only at a comfortable working height of 1.8 m from the floor, which was discovered to be a suitable position with uniform light in Section 3.1.2. Along this wall, the three sky simulations were run for a distance of 1, 3 and 5 meters from the window.

In the same analysis, simulations are done for various global orientation angles of the two rooms. The same 3D models were used as described in Section 3.1.3, but now, the complete scene was rotated along the z-axis, see Figure 3.7. So instead of the real orientations as found in Section 3.1.1, the building is rotated so that the main window faces towards the four cardinal directions.

5.2.2 Simplifications for fast analysis

The simulations were done for both the household room and the office room, meaning that in total (3 skies x 3 wall distances x 4 cardinal directions x 2 rooms =) 72 yearly simulations are needed for the location and orientation analysis. Furthermore, a lot more simulations were also performed to analyse the module angle and in-depth seasonal influences, but these last simulation are outside of the scope of this research for now. Doing yearly simulations like explained in Section 5.1, takes approximately four hours and requires adjustments during this time. So now it becomes clear that the simulations need to be simplified further to save time.

Simulation of only one day in the year
It was found that the 21st of March is a very representative date to estimate the yield for the whole year, as will be discussed later in the chapter in Section 5.3. So for this very quick analysis, only three 24 hour base simulations of the three skies are simulated following the method explained in the previous chapters.

Using a fixed number of cloudy, sunny and partly cloudy sky days
Before, the weather data of every hour of the year was checked to determine the sky type at that hour. To further simplify, now historical data of the past 5 years is used to get an overview of how many hours of the day there are clouds, partly clouds or no clouds. Only the hours between sunrise and sunset are considered in this analysis. It can be seen that the majority of the hours the sky is cloudy in the Netherlands. In winter this is even more so. Overall, it can be seen that 40% of the time the sky is completely overcast and only 28% of the time is it clear. The remaining 32% is defined as partly cloudy. With these ratios the average curve can be calculated as the weighted sum of the three base curves.

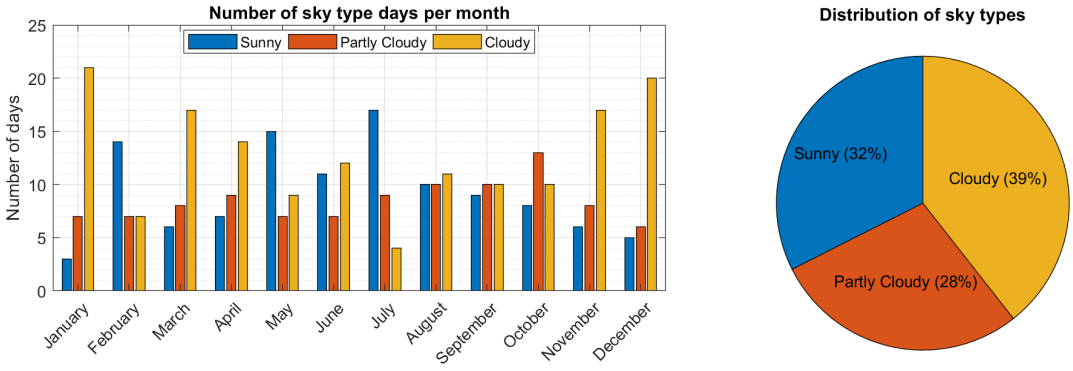

Figure 5.3: Number of hours of the three standard sky types.

5.3 Results and discussion

Here, the results from the yearly energy yield prediction are presented and discussed. The yearly insolation was calculated using the simulations as explained in Chapter 3 and 4. The cell efficiency was calculated with a model from Randal [10] for four different cell technologies, which are all commercially available and have a size of at least 5 cm^2.

5.3.1 Daily energy yield

With the method explained in the first section of this chapter, the irradiance was calculated for every hour of the year. This was done for both rooms with the 3D models as described in Section 3.1.3. A table or graph of all 365 days will not be presented here for obvious reasons, so instead the results include the graphs and tables of the simulation with monthly averages. The Figures 5.4 and 5.5 show the monthly average daily insolation and energy yield for a number of cell technologies. The Tables 5.2 and 5.3 support the figures with tabled data, which is needed to more easily see the difference in energy yield between the different solar cell technologies. Furthermore, it shows the important weather data used to determine the sky illumination settings for the simulation.

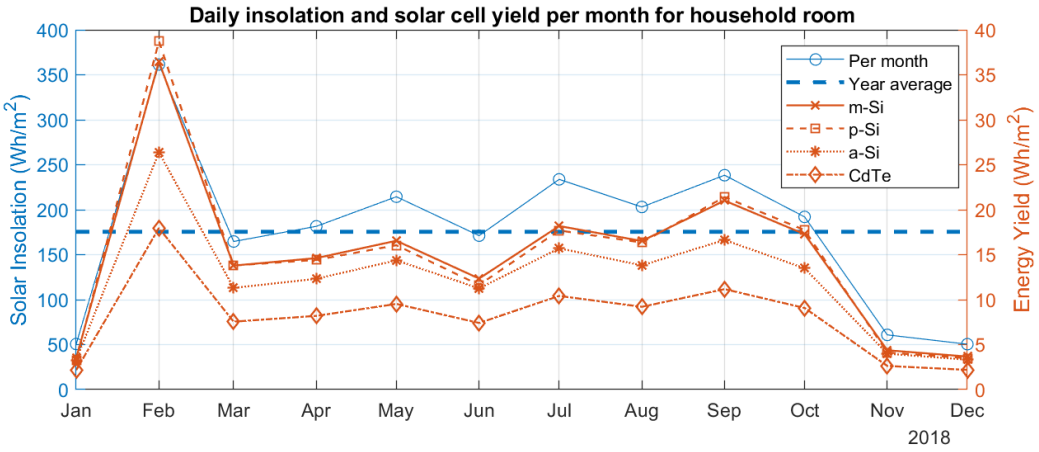

Figure 5.4: Average daily insolation for each month in the household room. The yearly average is also shown. The solar cell yield was calculated for four cell technologies

It can be seen that the difference are high. The insolation can be a factor 10 times larger during the long summer days, compared to the dark winter days. The spring and autumn months are right in between these values for the office room. But for the household room, in February the solar energy is noticeably higher. It was found that during these months, the solar position

Month	Mean cloud cover [okta]	Daily sun time [hh:mm]	Daily rain time [hh:mm]	Daily energy [Wh/m^2]				
				Solar Insolation	Solar cell yield *m-Si*	*p-Si*	*a-Si*	*CdTe*
January	7.0	01:33	00:42	50.7	3.5	3.3	3.3	2.2
February	4.3	06:01	00:27	361.4	36.5	38.7	26.4	18.0
March	7.0	03:56	01:25	164.6	13.8	13.8	11.3	7.6
April	6.7	05:56	01:01	181.5	14.6	14.4	12.3	8.2
May	4.6	08:52	00:35	214.4	16.5	16.1	14.4	9.5
June	5.4	07:53	00:18	171.2	12.3	11.6	11.3	7.4
July	3.9	11:08	00:06	233.7	18.2	17.7	15.7	10.4
August	5.7	06:35	00:38	203.0	16.5	16.4	13.8	9.2
September	5.9	06:09	00:51	238.4	21.0	21.4	16.6	11.2
October	6.3	05:30	00:42	192.0	17.3	17.7	13.5	9.1
November	6.5	03:02	00:47	60.8	4.4	4.1	4.0	2.6
December	6.9	01:46	01:00	50.1	3.6	3.4	3.3	2.2
Mean	**5.9**	**05:42**	**00:43**	**175.5**	**14.7**	**14.7**	**12.0**	**8.0**

Table 5.2: Monthly weather conditions and resulting mean daily solar insolation and energy yield for household room.

is very fortunate for the investigated area in the room. Furthermore, from the weather data, see Table 5.2 it was noticed that the weather was particularly good for that time of the year.

One important finding is that for both cases, the date around the March equinox has approximately the same daily insolation as an average day of the year. This means that for very rough estimations, the 21st of March can be used as a representative day to estimate the yearly yield. The same holds for the September equinox. This makes sense considering the solar position, as the zenith angle is right in the centre of its yearly trajectory. However, it should be noted that it could be coincidental that this time of the year is representative for the full year for both the rooms. It could be that for another room, this is not the case, so it is advised to always check this for every new scene. Nevertheless, for further simulations, the 21st has been used as a representative day, showing good results for this studied case.

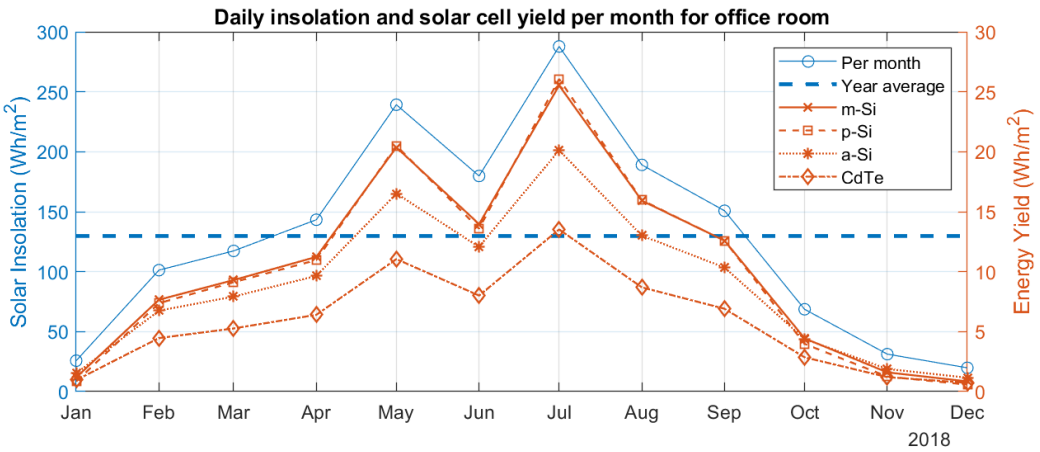

Figure 5.5: Average daily insolation for each month in the office room. The yearly average is also shown. The solar cell yield was calculated for four cell technologies.

Month	Mean cloud cover [okta]	Daily sun time [hh:mm]	Daily rain time [hh:mm]	Daily energy [Wh/m^2]				
				Solar Insolation	Solar cell yield *m-Si*	*p-Si*	*a-Si*	*CdTe*
January	7.0	01:33	00:42	25.8	1.2	0.8	1.5	1.0
February	4.3	06:01	00:27	101.3	7.7	7.4	6.7	4.5
March	7.0	03:56	01:25	117.3	9.3	9.1	7.9	5.3
April	6.7	05:56	01:01	143.3	11.2	11.0	9.6	6.4
May	4.6	08:52	00:35	239.2	20.4	20.5	16.5	11.0
June	5.4	07:53	00:18	179.8	14.0	13.6	12.1	8.0
July	3.9	11:08	00:06	287.8	25.5	26.1	20.1	13.5
August	5.7	06:35	00:38	189.1	15.9	16.0	13.0	8.7
September	5.9	06:09	00:51	150.8	12.6	12.6	10.3	6.9
October	6.3	05:30	00:42	68.6	4.4	4.0	4.4	2.9
November	6.5	03:02	00:47	31.2	1.6	1.3	1.9	1.2
December	6.9	01:46	01:00	19.8	0.8	0.6	1.2	0.7
Mean	**5.9**	**05:42**	**00:43**	**129.8**	**10.4**	**10.3**	**8.8**	**5.9**

Table 5.3: Monthly weather conditions and resulting mean daily solar insolation and energy yield for office room

5.3.2 Close up on winter months

From the previous part it can be noticed that the energy yield is very low in the winter months. Looking more closely at December, it becomes clear that on a daily basis the incident energy can become even lower. Figure 5.6 shows the mean daily insolation and yield for the office room, which is the worst room when a high irradiance is required, as can be seen from the Tables 5.2 and 5.3. Considering the worst-case scenario, an area of interest is 16-23 December. These days

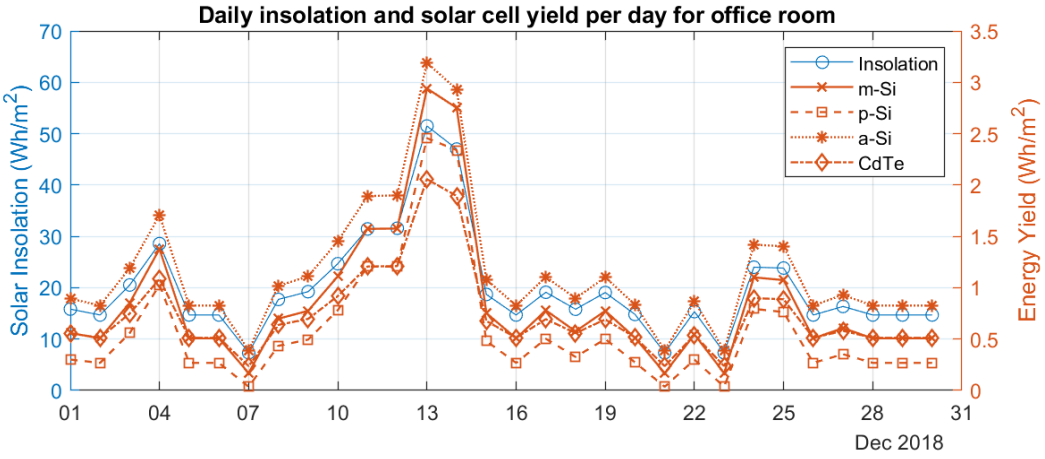

Figure 5.6: Mean daily insolation and solar cell yield during December for the office room. This is assumed to be the absolute worst-case scenario.

are complete overcast, with some precipitation during the day. It is interesting to see that at these irradiance levels amorphous silicon would actually outperform all other technologies, and more amazingly p-Si would be the worst performing one. So for devices that need to work in these conditions, a thin film technology could be the best option.

However, the insolation is lower than 20 Wh/m^2, resulting in an expected yield not much higher than 1 Wh/m^2. Building a device when focusing on these days could result in a very overdimensioned design for the remainder of the year. For example, a large battery could be implemented to cover for all of these dark days, and fill up during days with higher potential like the 13$^{\text{th}}$ and 14$^{\text{th}}$ of December in this case. This can be undesirable and thus, for devices that would have to work good for most of the year, it could be better to simply neglect these days

and have a loss of supply during these dark winter days.

5.3.3 Best PV cell technology for different room characteristics

With the method as explained in Section 5.2, an irradiance curve for the 21st of March is created as a representative day for the complete year, of the four cardinal orientations and three distances from the window. As a test, the results of the house 3D model at 1 meter from the window and south orientated main window are taken, as these characteristics suit the real investigated scene. The predicted daily insolation is 173 Wh/m^2, which is very close to the predicted mean daily insolation of 176 W/m^2 found in the previous section with the more complex analysis. The same can be done for the office room, which has an orientation closest to East. The predicted daily insolation for that scenario was 130 W/m^2, which is exactly the same as the predicted yield. However, it should be mentioned that the actual orientation is east-northeast, so the estimation here is actually a slight underestimation of the more accurate prediction.

Besides the daily solar insolation, the electric power conversion efficiency is determined of the four solar cells listed in Table 5.1. Note, it was first determined for all 21 cell technologies, as can be seen in Appendix D.4. For each of the data points, the best performing cell technology is determined as can be seen in Figure 5.7 for the household room. It can be seen that the insolation

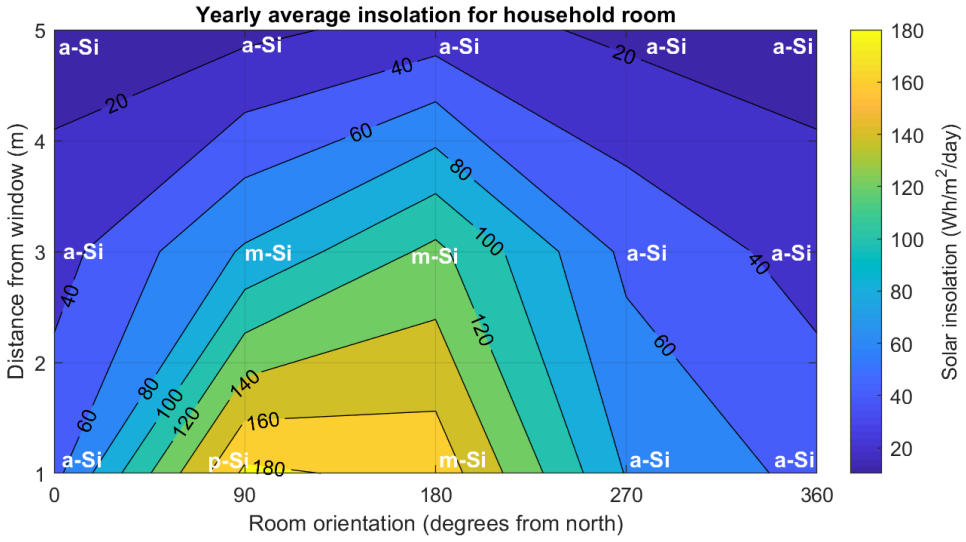

Figure 5.7: Average daily insolation for the 21st of March with best performing PV technology for the household room for different room characteristics. Zero and 360 degrees orientation means that the main window of the room is facing North, 90 degrees means it is facing East, 180 degrees for South and 270 for West. The colour scale indicates the daily solar insolation and the best performing PV cell technology is indicated for each data point.

is not much lower for the case that the house model is rotated towards the East. At first, this might look like something went wrong, but examining the rotated models more carefully, some interesting findings come to light. For one, when the window is facing south, the left wall beside the window is facing west. So if the module is to face north, the room should rotate towards the east. But turning the room fully towards the east would block light at noon from entering the room directly, so the optimal orientation is actually in between these directions. Another contributing factor could be that the height of the sun is not ideal at noon, so it could be better to focus on the light in the morning and/or evening. Note, that if the wall on the opposite side of the room is analysed, the angles reverse direction too, meaning a slight west orientation is preferred in that situation.

The same simulation and analysis is done for the office room. Note, that in this case the original global orientation is no longer relevant, as the values are calculated for each of the car-

dinal directions. The difference is the model of the room, so for the first time, the influence of building design can be analysed. Figure 5.8 shows the results with again the best perform cell technology. It can be seen that now the intensity of light is largely similar. The difference

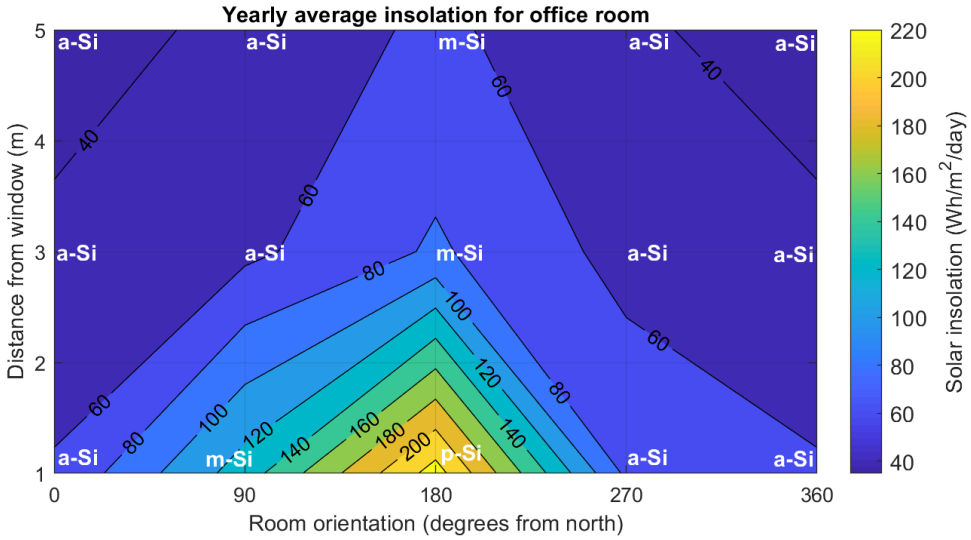

Figure 5.8: Average daily insolation for the 21st of March with best performing PV technology for the household room for different room characteristics. Zero and 360 degrees orientation means that the main window of the room is facing North, 90 degrees means it is facing East, 180 degrees for South and 270 for West. The colour scale indicates the daily solar insolation and the best performing PV cell technology is indicated for each data point.

in this case is that the irradiance values drop off more rapidly going deeper into the room and turning further from the ideal orientation. This is probably due to the wall in the centre of the household room, which can be seen in Figure 3.4a. This wall reflects a lot of light towards the wall and deeper into the room, especially when the building turns more towards the east. Also, the blinds in the rooms beside the investigated rooms are always down, as can be seen in figure 3.5b, meaning that the sun is more intensively blocked when changing the orientation.

Simulation right behind window

Somewhat later in the research, extra simulations were done for the position right behind the window, so no longer confined to the wall. The results showed that the insolation and PV yield can be more than twice as large as can be expected at 1 meter from the wall for a south orientated room. For a north orientated room this can even be three times as much. For the rest of the report a value of 2.5 will be considered as the factor of increase when going from 1 meter from the window to right behind the window. Note that for this case, the module angle is also changed to face the sun more. The result of this analysis will be used later in the design of the solar lamps.

5.3.4 Module angle influences

As mentioned briefly before in this chapter, additional analysis were made. Until now, only a plane parallel to the wall was considered, but with the fast simulation all possible orientations could be tested in a quick manner. For rotations around the horizontal axis, the irradiance increased only a few percentage. This was different for the change in module angle around the vertical axis, as can be seen in Figure D.1 in the Appendix. Applying this to the results gives a very rough view of how the energy yield can further increase up till 200% from the initial calculations in previous sections. Note, the simulations were only performed for cloudy weather days to eliminate the high influence the sun has on incident irradiance for a plane.

5.4 Conclusions and recommendations

The same simulation method as described in Chapter 3, and verified by Chapter 4, was used as a basis in this chapter to predict the irradiance for every hour of a whole year in the office and household room, with a computation time of 4 hours. The cell efficiencies of different PV technologies was calculated, using a model specifically designed for low-irradiance conditions, to also predict the PV energy yield. Furthermore, additional simplifications allowed for even faster simulations of 30 minutes to evaluate the influence of room orientation and position on the wall left of the main window. Figures 5.7 and 5.8 presented the most important outcome.

5.4.1 Only one day in the month needs to be simulated

Instead of doing the simulation for every day of the year, only one representative day in the month is chosen to do the simulations. In this case, only 36 simulations are required to perform the yearly calculations, instead of over 1000. So in total, a yearly simulation can take up to 4 hours to complete, instead of 5 full days. The decrease in accuracy is derived to be less than 10% on any random day, but over- and underestimations further from the 21st should cancel each other out over periods longer than a month. However, no full year simulation has been made, so there is no hard evidence to support this.

5.4.2 The PV energy yield in winter is four times lower than the yearly mean

One average, the daily insolation in the household room is 176 Wh/m^2 and 130 Wh/m^2 in the office room. Note, that this is on the wall 1 meter from the window. As expected the winter months yield much less power than all other months. The daily insolation then is 28% of the mean daily insolation over the year for the household and only 15% for the office room. For the office room the best performing month was July, which is as expected, and the daily solar insolation was over twice as much as the average. But February was the best month for the household room. This was a combination of fortunate solar position and abnormal good weather conditions. It should be noted that a change in environment has not been considered over the year simulation. For instance, it can be expected that after winter more vegetation will increase shading effects.

5.4.3 The March equinox is a representative date for the whole year

The complete scenes of the household and office room were rotated along the z-axis for the simulations of different room orientations. For each of the four cardinal directions, the sensor position was changed from 1 meter, to 3 and 5 meters. So in total, 24 yearly simulations were needed for both rooms combined, leading to the need of an even faster simulation method for this analysis. This was achieved by simulating only the 21st of March as a representative day of the year. The total computation time was reduce to 30 minutes, with a deviation not more than 2% compared to the more extensive approach explained above. This new method can be used well to quickly predict the average yearly insolation and PV energy yield, but important monthly data, such as the predicted yield in the winter months, is lost.

5.4.4 The optimal room orientation depends on room design and position

On the northern hemisphere, a south facing module orientation gives the highest PV energy yield. For the studied cases, this was also true for positions deeper than 2 meter in the rooms, where the average daily insolation is lower than 150 Wh/m^2. However, for the household room, the east orientation received the highest insolation of 200+ Wh/m^2 for positions closer than 1 meter from the window. This was not so for the office room, indicating the importance of

building design and surroundings. So close to the window, the optimal position is between south and east for the left wall, and due to symmetry, between south and west for the wall right of the main window.

5.4.5 Best cell technology depends on position

The cell efficiency was calculated with a model from Randal [10] for four different cell technologies, which are all commercially available and have a size of at least 5 cm^2. In the highest irradiance conditions, polycrystalline silicon is still the best option, but for very low irradiance sites, thin film technologies are competitive with both mono- and multicrystalline solar cells. For a module on the left wall beside a main window it was found that amorphous silicon outperforms the other solar cells when the window faces north or west, or when the position on the wall is further then 3 meters from the window. Polycrystalline is only the best performing cell, closer than one meter to the window when the room is facing at its optimal orientation. Everything in between and monocrystalline is the best cell technology.

Chapter 6

Designing and Building a IPV Lamp

The research part has now been concluded and the previous chapter provided the outcome of which photovoltaic cell technology is likely to produce the highest yield, for varying room characteristics. The final finding was that the best cell technology depends directly on the position in the room and also the environment the room is in. This means it is best to explore multiple positions in a room, and create three concept, corresponding to the three best performing cell technologies, before focusing on one to develop further. The gained knowledge on indoor light conditions will be of value to decide on shape and size of the product. Furthermore, a custom PV module will have be designed to use in the system, with a fitting electrical circuit to ensure very component functions well.

The purpose of this chapter is to describe the design thoughts and show the resulting product and its specifications. It stands as a basis for future indoor solar lamps and leaves plenty of room for improvements as future work. To start, a list of requirements is provided in Section 6.1, which should confine the operating space of the devices. In total, three designs were based on the results of the previous chapter and they are revealed in Section 6.2, along with there specifications. With the supervisors of this thesis, it was decided to prototype one of the concepts, and its development is described in Section 6.3. The remainder of the system is shown and explained in Section 6.4. Finally, the prototype can be build as it was designed, and the manufacturing procedures are put on paper in Section 6.5. Section 6.6 briefly talks about the testing of the prototype, which did not go as hoped. Figure 6.1 shows an overview of the content.

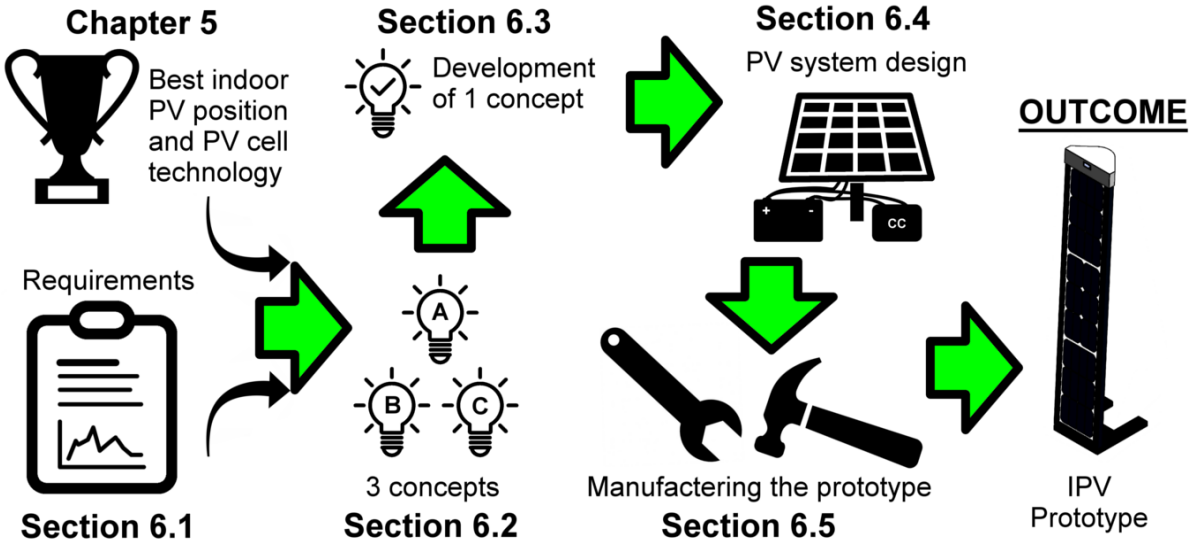

Figure 6.1: Visual representation of the content of Chapter 6. The section numbers can be found near the corresponding icons. The green arrows show the relation between the sections and outcome.

6.1 General requirements

Some general requirements for the considered IPV LED designs could be determined, even without extensive analysis. They arose from the very first analysis and discussions with the supervisors. First, they are listed here and below is given some further details and explanation on each of the points.

1. It should be easy-to-install on a wall at height of 1.8 meter.
2. The lamp will not be for main lighting purpose.
3. It should perform well without artificial light as a light source.
4. It should work almost any day of the year

1. Lightweight (<5 kg) and compact (<0.5 m^2)
The first requirement is not just about making the installation manual easy to follow, it is also there to make sure the system will not be sized out of proportion just to meet any other requirements. The main thought is that the design can handled easily and can be installed by a single person. This means it should not be bigger than 0.5 m^2, not heavier than 5 kg, and have an handle to pick up and replace easily.

2. Assistive light of 1-5 W
The second requirements is there to define the lighting specifications of the IPV LED system. From first analysis it was found that it will be hard to find a location indoors with irradiance values higher than 20 W/m^2 at a suitable location. In this case, assuming an optimistic 12 hours of light and 10% cell efficiency, the energy yield will be 24 Wh/day for a big module with a surface area of 1m^2. The suiting light-level in the living room of a home is approximately 150 lux (lumen/m^2) [12]. So lets consider a small room of 15 m^2, which would require 2400 lumen of artificial light during night time. With the most efficient LED lights of (100 lm/W) the required power is 24 W. This would mean that every day you could use the main light for a maximum of 1 hour, provided the you have had a sunny day. This is even a very high overestimation, so it can be concluded that indoor light at the moment cannot provide for the desired indoor conditions.

An assistive light is defined here as a lamp that can provide extra light in need, similar to a torch. From Section 2.3.2, it was found that the solar devices use a LED light around the 1 W. Considering these devices and other lamps available on the market it has been decided that the indoor solar lamp should be able to power a LED of 1-5 W.

3. Only sunlight as a source
The third requirement comes from the decision to neglect artificial light. The reasoning for this includes four points. First, the potential light from light sources is low compared to daylight in a room with an average sized day with average cloudiness. Secondly, most of the times, the rooms main light is aimed downwards. Focusing on that direction is unideal for harvesting daylight. Thirdly, the properties of artificial lights can vary a lot based on user preferences, meaning that the brightness and spectrum cannot be determined in a reliable manner. Finally, when relying on artificial light, the purpose of both light sources will be reduced. If the artificial light does become a significant source compared to daylight. The IPV system will charge as long as the lights are on (i.e. as long as someone needs light in the office). At the end of the day the batteries are charged, however, there is no need to use the IPV LEDs, as everybody will leave at the point the artificial light is turned off.

4. Ignore very overcast winter days
It was found out in Section 5.3 that during winter, the available energy can get so low, that it could result in an overdimensioned product for the remainder of the year. To prevent this it was decided not to focus on the absolute worst-case scenario, but rather on a slightly more lenient one. In this case three days of overcast days in Dutch winter months. During this period the expected insolation is approximately only 20 Wh/m^2 per day. This means that with an optimistic power conversion efficiency of 10%, only 2 W/m^2 is available. For a 2 W LED, this means either the module has to be very big (>0.5 m^2) or the usage time very short. So using the light more more than half an hour is not sustainable during this period. A period of 3 days of overcast weather can still be covered by one day of sun

6.2 Three product concepts

Based on the findings from Chapter 4 and the requirements described in the previous section, three concepts have been produced, corresponding to three separate room characteristics, for the three best performing cell technologies. They have been given suitable names for easier reference. The general specifications can be seen in Table 6.1.

	Window winner	**Defeating Darkness**	**Pocket Solar**
PV cell technology	monocrystalline silicon	amorphous silicon	multicrystalline silicon
Device dimensions [cm]	150x19x10	58x82x13	11x25x4
Active PV cell area [m^2]	0.2	0.45	0.1
Expected PV yield [Wh/day]	2-4	0.5-1	3-4
Light source [W]	2.5	0.75	2.5

Table 6.1: Table with concept specifications.

The design choices for each concept is explained in more detail in the subsections. It should be mentioned that the calculations performed here are very simplified back-of-the-envelop calculations to quickly determine requirements of the concept. For most calculation, yearly averages have been used, instead of worst case winter values, because the line of thought is that the product should not be overdimensioned for this case. Only for the second concept this can be argued as it is created to work reliably throughout the year. However, for the sake of equal comparison, its size has also been determined on yearly average values. The range of expected yield can be big due to the multiple different room characteristics that can determine the different light conditions.

6.2.1 Window Winner

Room position
The Window Winner (WW) has been designed to be placed on the wall for the average daily insolation of 100-170 W/m^2. It can be seen in Section 5.3 that for these values monocrystalline silicon is the best performing cell technology. The target group will be an ordinary household, so looking more closely at Figure 5.7, it can be seen that the direction of the main window should be between 60 and 240 degrees from north. Furthermore, only for houses with the main window in the optimal direction, the device can be placed further than one meter from the window. So it should be placed close to the window, hence, the name of this concept. The figure below shows some CAD model overview of the Window Winner.

Shape and size
From the Figures 2.8b and 2.9b it can be seen that there is only a narrow, elliptical shaped, area of uniform irradiance next to the window. This was the main reason to chose for the long, slim build of this concept. Considering that most windows in household rooms are generally as long

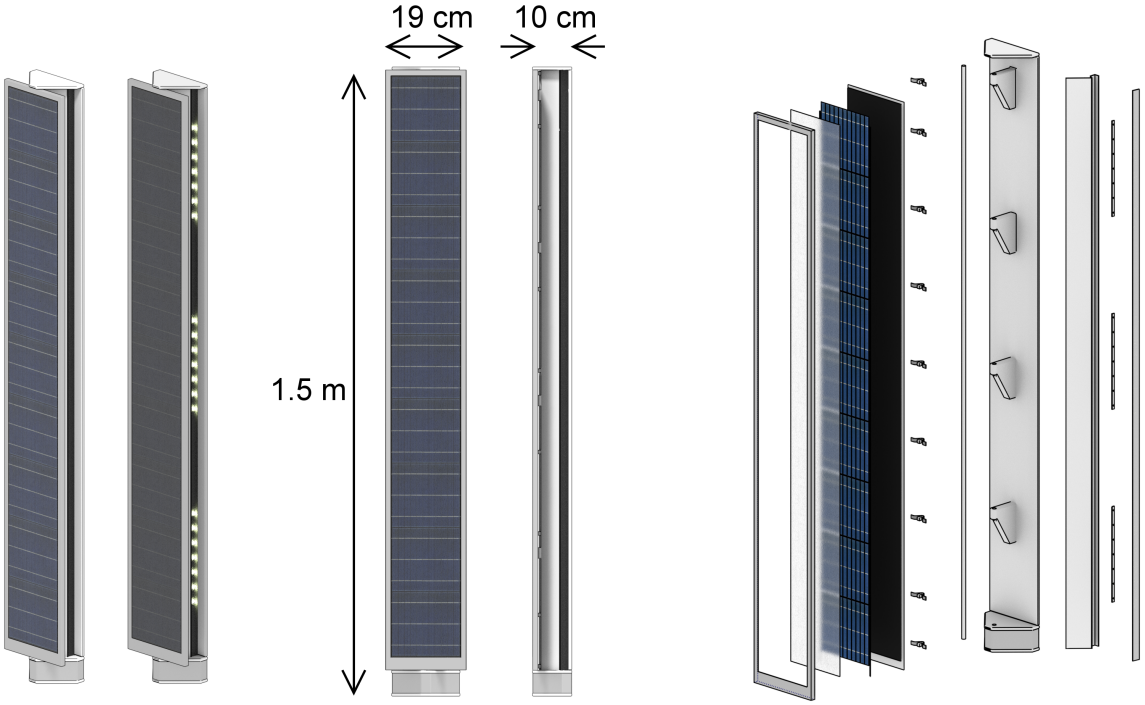

Figure 6.2: A 3D render of multiple angles of the Window Winner concept. A exploited view is included on the right-hand side and the centre shows the main dimensions of the design.

as 2 meters, so with an height of 1.5 meter, the PV module of this concept can be placed easily in this uniform area, and it will still be possible to carry if it can stay lightweight.

A long device, such as this one, can have an impact on room appearance. To prevent it from being highly noticeable, the thickness and distance it sticks from the wall is kept to a maximum of 10 cm. It has been chosen that it can be rotated 45 degrees either way, as an added functionality that could even be automated and to increase the PV energy yield. It also allows the lights to be aimed more towards a specific side, or even block it to prevent from looking directly into the light.

Predicted PV energy yield

From Table 5.2 it can be seen that inside the household at a position of 1 meter from the wall, the average predicted PV energy yield is calculated to be 14.7 Wh/m^2 per day for monocrystalline cell technology. Thus for an active area of 0.2 m^2, it is roughly 3 Wh/m^2. Using this same approach for the office room will lead to 2 Wh/m^2. With the possibility to turn the module, the PV yield can be increased up to 160% of the expected yield on a surface parallel to the wall. So for a south facing room, with turning the module towards the window, the maximum average yield is 4 Wh/m^2. More towards the east, without facing the window, it can be as low as 2 Wh/m^2.

Lighting requirements

The design has position constraints and has to be close to the window. Being in the corner of a room means it needs to have a sufficient brightness to have an impact on the room. It has already been calculated in Section 6.1 that the lamp will not be used to supply they main light requirement of 24 W. Instead it has been decide that it needs to have an illumination of 300 lumen to be competitive in the lamp market. With powerful LEDs (120 lm/W) this can be obtained with a power of 2.5 W. With a predicted yield of 2-4 Wh/m^2, the lights can be used from one to one and a half hour, including losses from the electrical components and surroundings of 25%.

6.2.2 Defeating Darkness

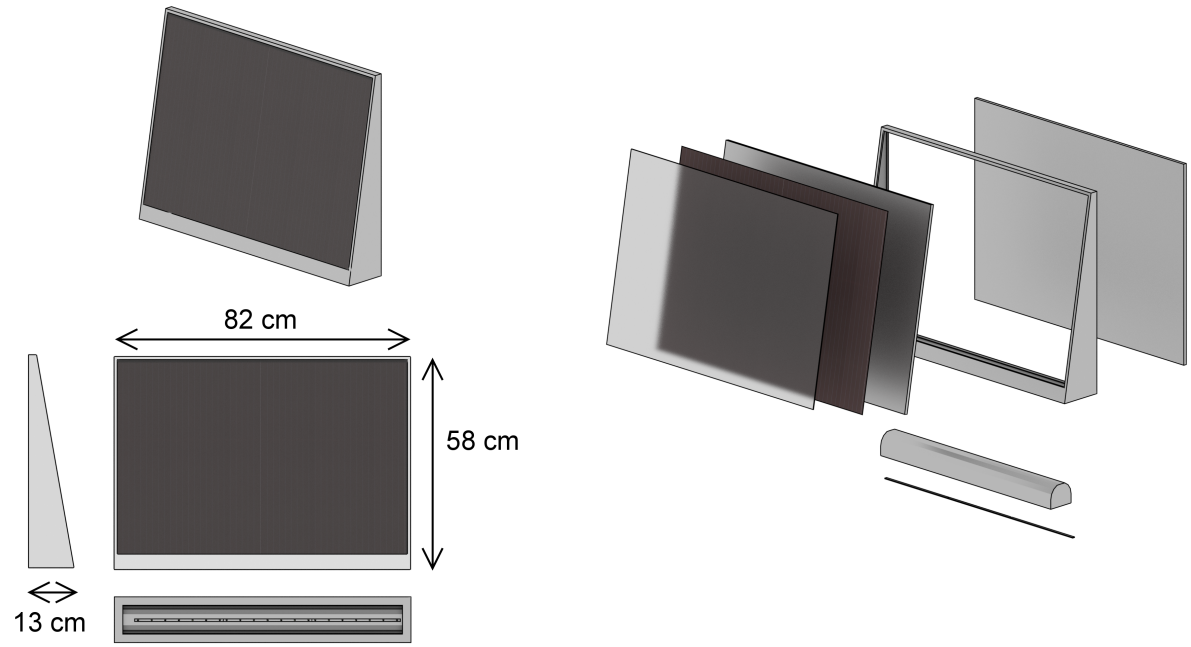

Figure 6.3: A 3D render of multiple angles of the Defeating Darkness concept. A exploited view is included on the right-hand side and the bottom left shows the main dimensions of the design.

Room position
The Defeating Darkness (DD) has been designed for a more constant and reliable incident irradiance. This is for households wall further than 3 meters from the window. It can be seen from Figure 5.7 that for these characteristics amorphous silicon is best for any orientation except east and south. After 3 meters amorphous silicon is always the best performing cell technology. The average daily insolation for this location is always smaller than 100 Wh/m^2, and for 5 meters into the room it can be as low as 20 Wh/m^2.

Lighting requirements
The lighting requirements will determine the required size of this concept. The DD will be used as a guidance lamp deeper into the room, used in complete darkness. For this purpose a light of 90 lumen will be sufficient, which is equivalent to a LED of 0.75 W, assuming a luminous efficacy of 120 lm/W. As a guidance lamp it can include a motion sensor to switch on the device when somebody passes by. This will save the precious energy for when needed. The lamp needs to be reliable, so it has to be able to give for at least 45 minutes continuously, or 9 times 5 minutes, without charging a day.

Required PV energy yield
With the LED of 0.75 W and on-time of 45 minutes, it can now be calculated that the required yield needs to be 0.56 Wh. As mentioned before, the average daily insolation can be as low as 20 Wh/m^2. Consulting Table 5.3 it can be seen that the same insolation in December, the power conversion efficiency of amorphous silicon is close to 6%, resulting in a daily energy yield of 1.2 Wh/m^2. This means the device needs an active cell area of 0.47 m^2.

Shape and size
This concept needs to support a thin film module of nearly 0.5 m^2. This means it is big and needs a solid frame to support it. To limit size the edges need to be as narrow as possible, and it must not come out from the wall too much. It has been chosen for this case to have the sizes

to form a normal sized rectangle of 58x82 cm, instead of a long device in one direction. This is because a wide solar module can experience a non uniform irradiance due to shading. Also it must not come down too low, to prevent shading of nearby objects in the room. The module is facing upwards to also harvest any artificial light, even though the focus is still on reflected sunlight. From quick simulations and measurements it could also be determined that having a slight upwards aiming orientation, the irradiance increases a few percentage. It also opens the possibility to have the lights fitted below, so they shine on the wall.

6.2.3 Pocket Solar

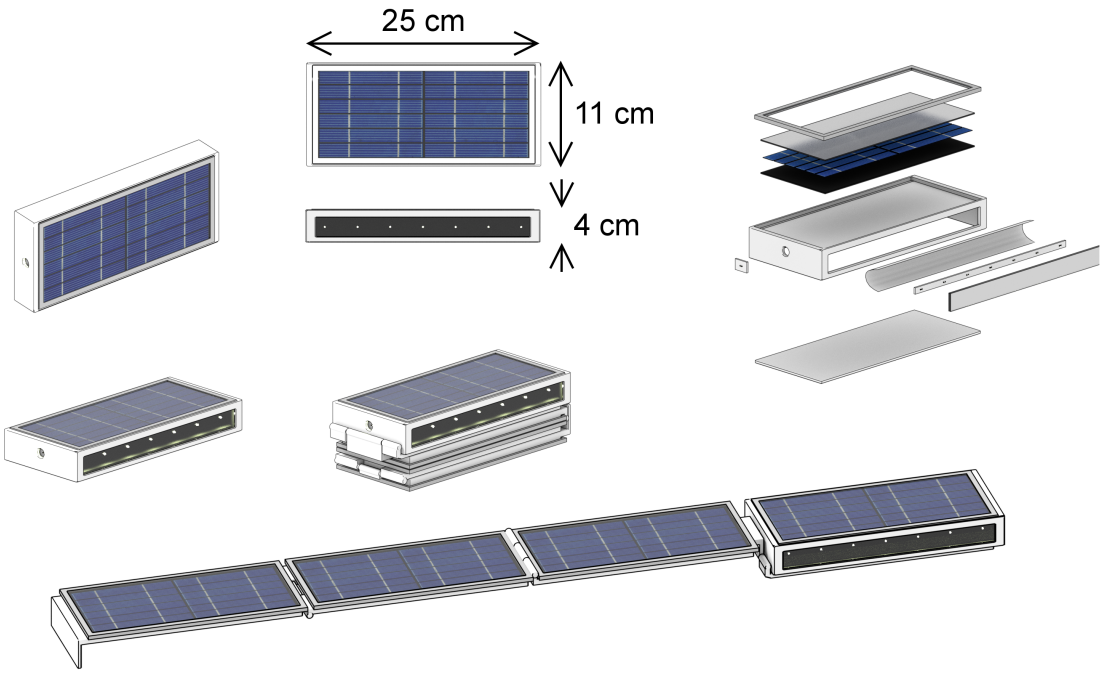

Figure 6.4: A 3D render of multiple angles of the Pocket Solar concept. A exploited view is included on the top right-hand side and the lower part shows an image with the full folded out solar module.

Room position

This concept has been designed to be as compact as possible and still have a lamp at least as bright as the first concept. Because it is easy to use, it can be placed anywhere in the room. The best charge point point is then as close to the window and preferably in direct sun. For most rooms this would mean it can be put on the windowsill right behind the window.

Shape and size

The ideal pocket size is not larger than the size of a small notebook. Having a module with this size would not yield sufficient electrical energy. Therefore there needs to be a extension of the module during charging. In this version it was chosen to design a foldable module, which can be detached while the light is in use, and reattached during charging. The size is 25x11 cm and with three extensions, the total active area is close to 0.1 m^2.

Predicted PV energy yield

Until now, the focus was on the walls of the room. But for this device a separate analysis was made directly in front of the window. It could be shown that insolation values where as much a 2.5 times as high as 1 meter from the window on the wall. This means between the office and

household room an average PV yield of 26-37 Wh/m^2 per day can be expected. With an active area of 0.1 m^2 the expected yield rounded up can be said to be 3-4 Wh/day, as it can be assumed the device has a slightly better power conversion efficiency in the higher irradiance conditions right behind the window.

Light requirements
The light used in this device can be manually changed between a spread out LED strip or one powerful LED used for flashlight purpose. Increasing the LED power will obviously shorten the available usage time. For this device, it has been chosen to use a light in the same order of magnitude of 2.5 W as the first design, and can thus be used up to one and a half hour. The flashlight function is brighter and can have a power of 4 W, but can then only be used for an hour.

6.3 Development of the Window Winner design

From discussions with the supervisors of this project, it has been decided to pick the Window Winner to develop further towards a functional prototype. It has been modified to suit a new set of requirements, and it can be found that the design has been developed more in the direction of a combination of the three concepts described in the previous section.

6.3.1 Design specific requirements

More specific design requirements followed from renewed discussions with the supervisors. These requirements listed here are all taken into account for the remainder of the design process and the reasoning for them is explained below the list.

1. The device should be mobile.
2. The main room window should face south ±45 degrees
3. The charging point should be within 2 meters from the window
4. The lights should be usable for at least 1 hour continuously per day.
5. The lights cannot be guaranteed to work in winter.
6. SunPower monocrystalline IBC cells will be used for improved aesthetics.
7. The system voltage should of 12 V is most suitable.
8. It should be able to remotely activate the lights during the night.

The starting point is the concept from Figure 6.2, but instead of limiting its use to the wall, it can be detached from it and placed in a foot so it can stand at any place in the room or even in front of the window to charge faster. Also, a tall standing module is much more convenient on the floor of household, reducing impact in the room appearance. But having the option to put it on the wall can be more convenient during long charging times and a more suitable lighting spot can be chosen deeper into the room.

As can be seen in Figures 5.7 and 5.8, the daily solar insolation can drop off quickly when the main window of the room faces more and more from the south towards the north. It would be too ambitious to design the lamp to suit any orientation and position, so a constraint of a minimum of 150 Wh/m^2 has been taken, which means that over the two rooms the rotation cannot be more than 45 degrees to the east. If the room is rotated within 45 degrees to the west, the right wall should be considered. Also, the charging point of the device should be within 2 meters from the window. This means that for further calculations, the household measurements and simulations can be taken into account.

The lights will be used as an assistive light, but can also be used as a guidance light in the

night when a motion detector is included to switch on the lights for a short time when somebody passes by. For continuous mode, it should on average work for 1 hour per day, but can be used more when the power is saved up in storage for some time. To achieve this in winter can be ambitious, as the lighting levels can be up to four times below the yearly average, as can be seen in Figure 5.2. The product will not be overdimensioned for this purpose, meaning conservative use of the lamp is required. Another option is to continuously charge the lamp right in front of the window, where the irradiance can be up to 2.5 times higher.

It was decide to use interdigitated back contact (IBC) monocrystalline solar cells from SunPower [40], as the general opinion is that the lack of front contacts makes it easier to look at. Especially with a dark back sheet will the cells almost disappear in a black coloured product.

Using a high system voltage will lower the current trough wires and components, hence, reduce resistive power losses to the square of the reduced current. On the other hand, the efficiency of DC/DC converters is less for larger voltage steps [41]. Thus, a 12 V system voltage has been chosen, largely also because of the wide availability of 12 V electrical components.

6.3.2 PV module design

There is no PV module on the market with such specific characteristics as required for this product. This means a module has to made specifically for this project. First, the design choices are explained here. Later, the steps required to actually build it will be described.

SunPower monocrystalline IBC cells specifications

The SunPower interdigitated back contact cells went into mass production in 2007 [42], and are flexible 5 inch cells with chamfered corners. The main specifications of the best performing cells under standard test conditions are a V_{OC} of 0.687 V, a I_{SC} of 6.28 A, a V_{MPP} of 0.582 V and a I_{MPP} of 5.93 A, taken from the datasheet [40]. This leads to a peak power P_{MPP} of 3.42 W and an efficiency η of 22.5%. The performance of the worst performing bin leads to a efficiency of 21.8%. No literature could be found on low-intensity performance of these cells, so for further calculations, the same model is used of the already investigated monocrystalline cell, assuming that the IBC performs at least as well in low-intensity conditions.

PV module of 36 series connected cells

As mentioned before, the design is build for an average daily insolation of 150 Wh/m^2 on the wall. The efficiency of monocrystalline cells in these conditions goes to 8%, as can be derived from Table 5.2, leading to a daily PV energy yield of 12 Wh/m^2. The total active cell area should be close to 0.2 m^2, to ensure a yield of 2.4 Wh/day, enough to power a 2.4 W LED strip for 1 hour. Now, approximating the area of the 5 inch IBC cells to a square of 125x125 mm, yields an area of 156.3 cm^2 per cell. So using 12.8 cells would be sufficient, but instead of make a module of 13 cells, 12 cells was found to be more convenient and allow for more configurations of cells. This means that the total active cell area will be 0.184 m^2.

If all cells would be connected in series, the maximum possible voltage would be only 7 V, where a higher than 12 V at least is preferred for the charge controller (see Section 6.4), meaning the cells need to be cut. It has been decided to cut the cells in three parts and have 36 cells in total, resulting in a module maximum power point voltage of approximately 21 V. This means that even a third of the three cells can be bypassed in shading conditions, and still the voltage would be sufficient for a 12 V circuit.

Cutting IBC cells in three pieces

The interdigitated back contact only allows for cuts in the direction of the contacts on the backside of the module, which can be seen in Figure 6.5b. Some wholesalers were found online selling IBC cells cut in even 6 parts [43], trying to cell them for triple the price of the original cells. For

a 5-inch cell with chamfered corners the exact total area is 153.3 cm^2, meaning the middle part needs to have a width of 40.88 mm and the sides a width of 42.06 mm, to make sure the parts are of equal surface area. With a caliper the parts were measured with the accuracy of a tenth of a millimetre.

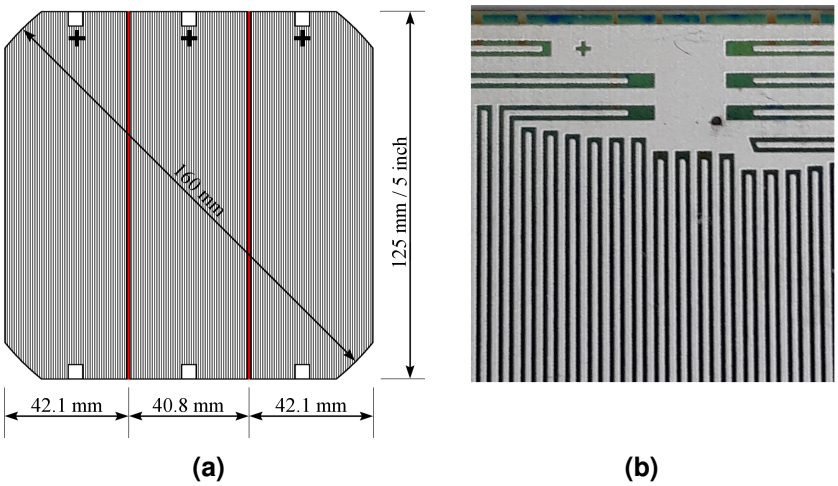

Figure 6.5: (a) A schematic image of the back size of the SunPower IBC cell with all important dimensions. The red lines indicate the place of the cuts. (b) A close up image on the back contacts of the IBC cell. The interdigitated pattern can clearly be seen and the little plus sign confirms it is the positive terminal of the cell.

Cell interconnection

The cells need to be interconnected in such a way to optimise power output, whilst maintaining aesthetics and minimise material use. This was done by connecting the cells in three groups of twelve pieces and add an Schottky bypass diode to benefit performance in shaded conditions, as can be seen in Figure 6.6. For a tall standing module, such as this one, the most likely shading condition it will encounter is a horizontal shade, coming from the knee-high wall part under most main windows (see Figure 3.5), crossing over the full bottom part of the module.

6.3.3 Warm LED lighting

As described in the main requirements in Section 6.1, the lighting will be used as assistive light and from testing out multiple LED lamps, it was found out that a LED strip of 2.4 W would be a suitable amount of light for this purpose. It has been decide, that for an average series of days, the lights should be usable for 1 hour at least. As mentioned at the start of this section, a 12 V system voltage is employed, so a 12 V, warm light, LED strip has been selected [44], which can be seen in Figure 6.7. The strip can be cut at any size the user demands. In this case, it will be cut to have a size over the full length of the module. The current will then have to be controlled by a current driver at 0.2 A to maintain a steady output of 2.4 W.

6.3.4 12 V Polymer lithium-ion battery pack

It has been estimated that the average PV energy yield is 2.4 Wh/day, which is equal to the daily demand from the LED source. This means that on average the start and end capacity of the battery will be the same after a full day. However, the battery should have sufficient capacity to account for a string of cloudy days. Furthermore, it should be able to charge fully during sunny days, without wasting produced energy when its full. It can be seen from Table 4.1 that a sunny day can have a insolation four times above average, and cloudy days roughly four times below average. This means that, if the battery can handle the peak from the sunny day, it can cover

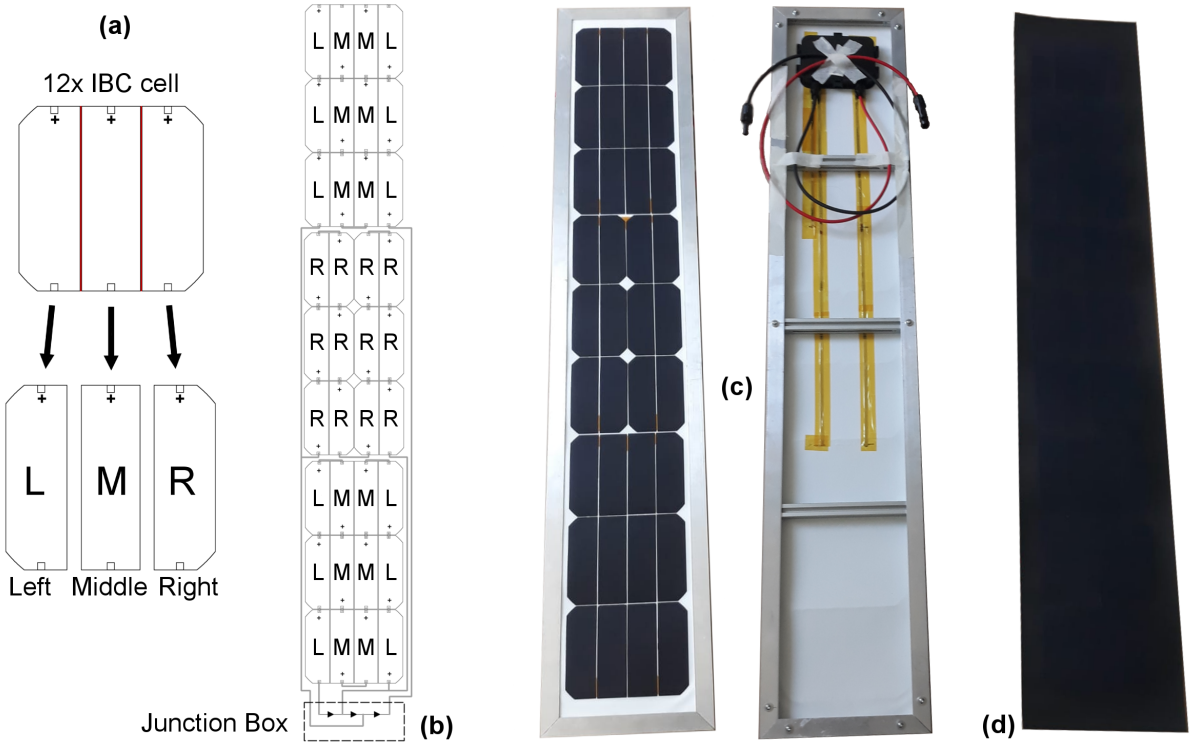

Figure 6.6: (a) The left side of the image shows the procedure of cell interconnection and how to efficiently use each part of 12 cut cells. Twelve IBC cell are cut in three pieces and are categorised by "Left", "Middle" and "Right". (b) Shows the cell interconnection, where the top part of the module includes 6 Left and 6 Middle pieces, the centre part of the module includes all 12 Right pieces, and the bottom part includes the remaining 6 Left and 6 Middle pieces. Each part is connected in parallel with a Schottky diode. The right side of the figure shows the two resulting modules, where (c) shows the front and back of the module with white back sheet in the aluminium frame and (d) with black back sheet without frame.

the four cloudy days, assuming average demand. So it has been decide that the battery should have a capacity of at least 9.6 Wh. Assuming 20% losses, and a maximum depth of discharge (DoD) of 70%, the nominal capacity should be 16.5 Wh. Note, with this capacity the lights can be used for 4 hours when the battery is fully charged.

It has been chosen to go for long-lasting polymer lithium-ion batteries [45] due to their high energy density. This will save weight and size. Using three 3.7 V lithium-ion batteries (see Figure 6.7), for a combined nominal voltage of 11.1 V, will be classified as a 12 V system voltage in most systems. But for further calculations, 11.1 V is a more accurate value to use. So considering a capacity of 16.5 Wh, a 11.1 V battery would need a capacity of 1.5 Ah. Note, in some images, it can be seen that a 12 V, 7 Ah Lead-Acid battery is being used, which was used only for testing purposes.

6.4 PV system design

The sizing and argumentation of the PV module, LED light source and battery have already been discussed in the previous section. In this section, the selection and function of the remaining elements in the PV system will be explained. All electrical components are combined in Figure 6.7. This is a simplified version of the interconnection, especially for the integrated sensor system, as will be shown later in this section.

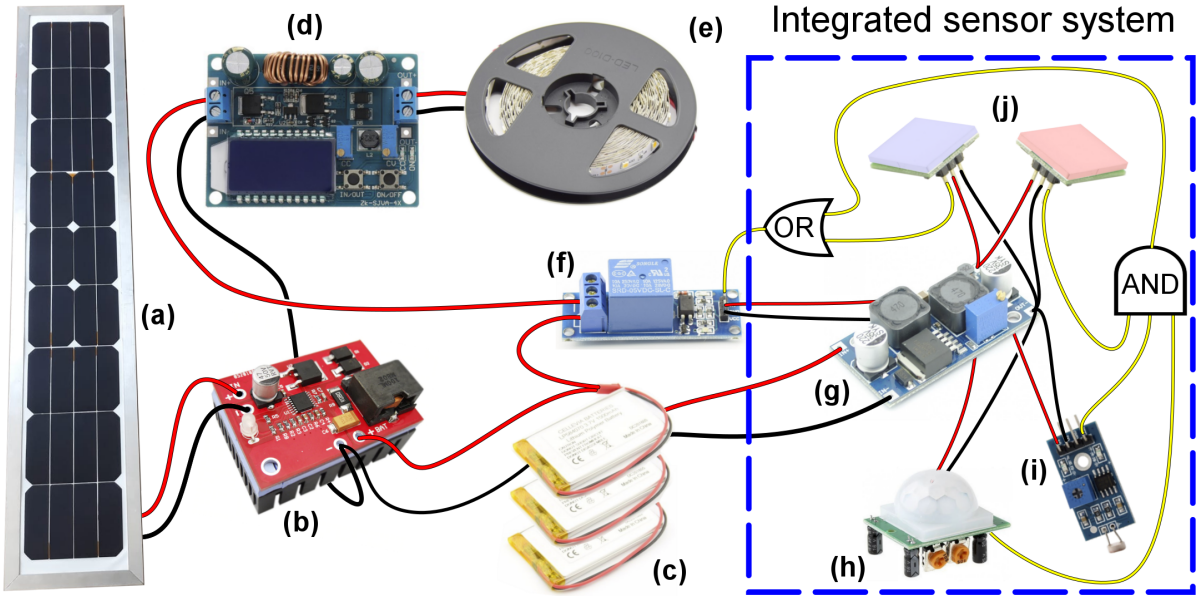

Figure 6.7: The figure shows a simplified representation of the interconnection between the main PV system components, where (a) is the tailor-made PV module, (b) is the 12 V MPPT charge controller [46], (c) is the 12 V polymer lithium battery pack [45], (d) is the constant current (CC) LED driver [47], (e) is the 12 V LED strip [44] and (f) is the 5 V relay [48] that opens or closes the line between the battery and CC driver. The blue dotted square encircles the integrated sensor circuit, responsible for switching the relay on/off, where (g) is a adjustable buck converter [49], (h) is pyroelectric infrared (PIR) motion sensor detector [50], (i) is light sensor module [51] and (j) are two 1-channel touch modules [52]. The red and black lines show the supply and ground cables, respectively. The yellow cables represent signal cables between the sensors, with an AND and OR gate to show the relation between the sensors.

6.4.1 Balance of System (BOS)

12 V MPPT charge controller

The PV module will need to charge the batteries during the whole day. Only when the batteries are full, will the module need to be disconnected to prevent overcharging. A charge controller can perform this task and can regulate the charge and discharge voltage to ensure a long battery lifetime [31]. The 12 V MPPT charge controller [46], includes a maximum power point tracking algorithm (MPPT) that using a switch mode DC-DC converter to find the operating point of maximum power from the PV module, for changing ambient conditions. The nominal output voltage is specially made for a string of three 3.7 V li-ion batteries. The maximum output current is 3 A, which is highly sufficient for the expected indoor PV performance. However, in standard test conditions, the peak power can be almost 36 V, meaning a output current of 3 A could be reached, for a output voltage of 12 V. This use should be discouraged, or a slightly more resilient charge controller should be found. Note, before using this charge controller, a constant current/voltage MPPT with display was used to manually set the PV module and charging voltage. It suited well with the Lead-Acid 12 V battery that was used before the lithium ion batteries.

Constant current LED driver

Any circuit power a LED load, must have constant current output controller [53]. In this case, a constant current LED driver [47] has been chosen with variable current and voltage settings. A display is incorporated on the printed circuit board (PCB), allowing the user to see the input or output voltage, as well as current in amperes or power in watts. The display shows two decimals for the voltage and power read, and three decimals for the current read. With small potentiometers on the PCB the output voltage and current can be regulated. The maximum output current is 3 A, which more than enough to supply 2.4 W of LEDs.

Relay

The relay opens or closes the loop with the LED driver when a 5 V signal is send to the IN pin. The switch can handle a maximum DC voltage of 110 V or AC voltage of 250 V. The maximum current is 10 A, meaning that the relay is can handle the load easily. There are convenient advantages of using a relay, instead of, for example, using a bipolar junction transistor as a switch. A relay is easy to use, with a binary operated signal of either 5 V, for which the circuit will be closed, or 0 V, for which the circuit stays open. It is also guaranteed that no power can flow from the battery anymore. The disadvantages are the big size compared to a small transistor, and a clearly audible switching "click".

6.4.2 Integrated sensor system

The LED lights should only turn on in the night, when there is motion and the user has pushed a button to enable the sensors being used, or when the user pressed another button to simply turn on the lights directly. The sensors are integrated in the control of the relay, which in turn can connect or disconnect the battery from the LED driver. This system is described in more detail below and the circuit can be seen in Figure 6.8. It can be seen that there is a main switch to completely disconnect the whole sensor system and LED circuit from the battery. The PV module is always connected, and the MPPT charge controller has protection build in to make sure the battery and PV module do not destroy each other when the product is not in use.

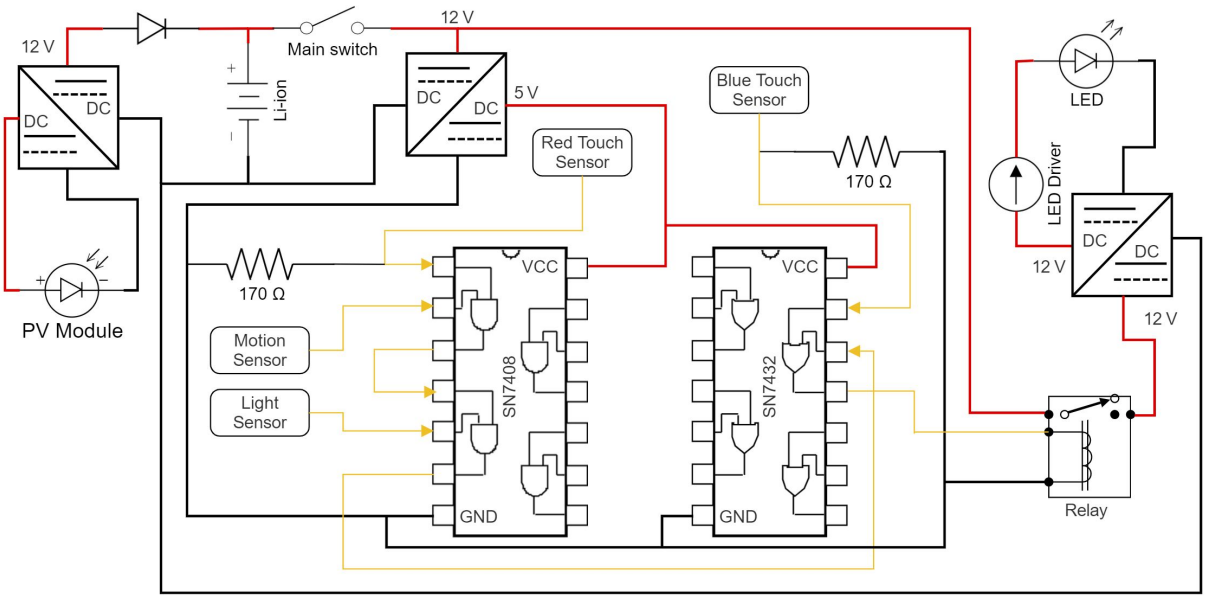

Figure 6.8: The circuit with integrated sensor system. The top left of the figure shows the PV module and MPPT charger controller, the far right shows the relay with LED driver and LED strip. In the middle is the integrated sensor system, with two integrated circuit logical gates SN7408 and SN7432. The orange arrows show the signal connection between the sensors, logical gates, and relay. The red and black lines indicate the positive and negative power supply lines, which can be either 5 or 12 V. In reality, power supply cables also go to the sensors, but for they have been neglected here for better overview.

DC-DC adjustable buck converter

The sensors need a steady 5 V power supply to function properly. In the first version of this circuit a 5 V voltage regulator, in combination with two capacitors, was used in favour of the more expensive and bigger buck converter [49], which was initially bought for testing purposes. However, after two regulators failed, it was chosen to go for the buck converter, as it isolates the input from the output, seemingly solving problems the voltage regulator could not cope with. The potentiometers can be turned to regulate the output voltage over a large range and the

rated output current is 4 A, where it was found that the overall consumption of all components together was in the order of 20 mA.

Capacitive touch sensor module (blue and red)
Apart from the main power switch, there are two capacitive touch sensors [52] in the circuit of Figure 6.8, that also function as a more sophisticated way of a manual switch. They can be touched through most materials, like wood and will indicate their on-status by shining either blue or red. The blue switch will bypass the rest of the sensors and immediately switch the relay and turn on the lights. The red touch sensor will make sure the rest of the sensors have a function. The modules work for an input voltage between the 2.7 and 6 V. In this system with the logical gates, they require a resistor to be connected with the ground to allow the IC gates to go to lower voltages.

Pyroelectric infrared (PIR) motion sensor detector
The PIR motion sensor [50] will detect infrared light changes and, based on the sensitivity setting, send a positive pulse between the 3 seconds and 5 minutes. Both the sensitivity and delay time can be adjusted using a little screwdriver. This is especially useful for prototype testing. In the lowest sensitivity setting the sensor can detect movement up to 3 meters, for the highest sensitivity this is roughly 7 meters.

LDR Light sensor module
Similar to the motion detector, a potentiometer can be turned to adjust the sensitivity of this light sensor module [51]. The module gives both a digital and analogue output. For the analogue output, the value is higher when the light intensity is lower and only when it drops beyond the set value will the digital output be high. The sensor works on a supply voltage of both 3.3 V and 5 V.

7400 series integrated circuit logic gates
Texas instruments has the whole 7400 series integrated circuits of logical gates, consisting of AND,OR, NAND, NOR and many more. In this way, sensors can be easily put together to work with the four logical ports per IC. As can be seen in Figure 6.8, not everything has to be connected to something, although it should be noted that, without anything connected, the voltage on a input is 1.7 V. This is above the border of detection, meaning that for logical gates, such as AND and OR, the output will be high, even when noting is connected. Also, if some connected sensors are isolated, there needs to be a way for the voltage to drop when the input is low. This can be done with a resistor of appropriate size, as is done with the touch sensor modules.

6.5 Manufacturing the main components

A separate section has been made on the manufacturing of some critical system parts. Each of the following parts was carefully designed in SolidWorks, and parts were even build during the design process, to speed up progression. In most cases, it was kept in mind that there should be room for adjustment, as the design was open for alterations deep in the building of the prototype process. Firstly, the module was created. After that, a frame needed to be made and the rest of the system came later. Figure 6.9 shows a engineering drawing of the modelled prototype. The drawing, much like the prototype, is incomplete, and lacks a finished of look.

6.5.1 Laser cutting 50 IBC cells

For this project the SunPower IBC cells needed to be cut in three pieces of equal area. This was done with a MT-F10/20/30/50 Fiber Laser Marking Machine [54] using EZCAD software to

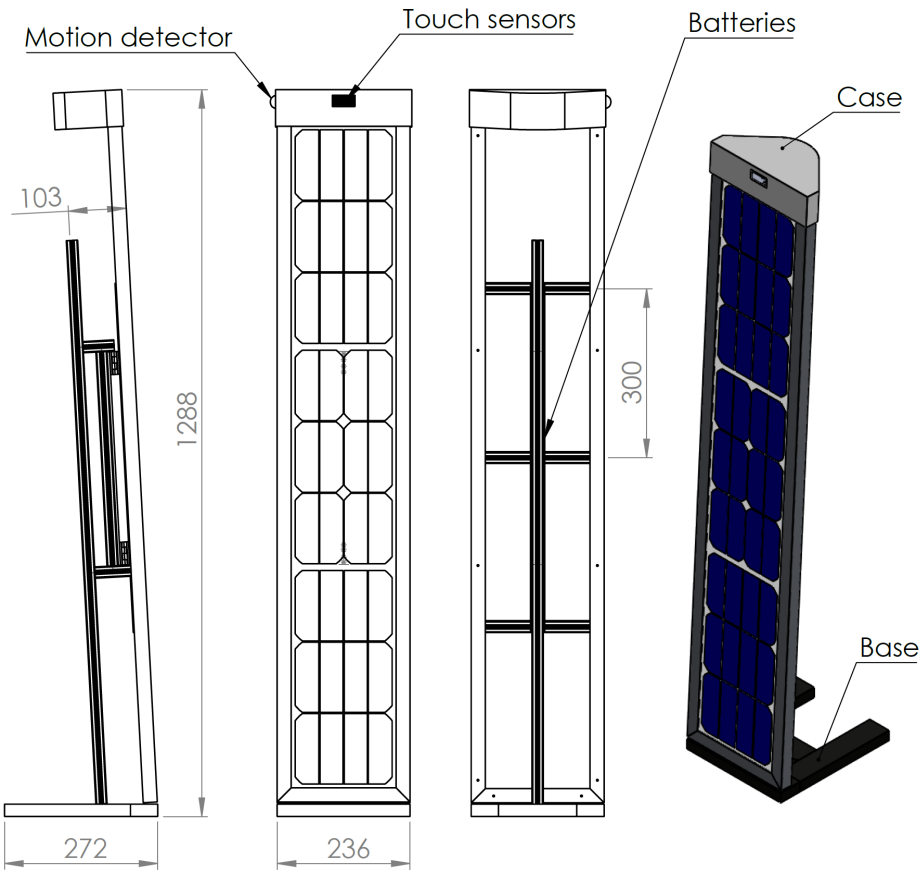

Figure 6.9: A engineering drawing of the indoor PV lamp. The main external components can be seen by the notes and only the most important dimensions are denoted. The motion detector is attached on the side and the touch sensor is on the front part of the casing.

control the laser. The cells were cut face down as can be seen in Figure 6.10a. The interdigitated back contact of the cells added some difficulty to the cutting process, meaning a trial-and-error method was needed to find the optimal cutting routine. Eventually, two laser operations were required to perform a successful cut. The first to cut through the reflective back contact with a lot of energy and the second to cut through the silicon below it, with a lot of low-energy fast cuts. After refining the procedure, the failure rate of the cutting process was approximately 20%. In these cases, the cells had either rough edges or a slight nick diagonally across the cell, as can be seen in Figure 6.10b. Both failures however, did not result in big losses of efficiency, only a decrease in aesthetics. IV-Measurements were done on all cells, showing an average efficiency of 21.2% meaning the cells had lost only 1% of efficiency during the cutting process. Further details and findings about the cutting process were used to set up a recipe for the cutting procedure of SunPower IBC cells.

6.5.2 Module lamination by WattLab

The available PVMD group module laminator is too small for a module of this size. So it was decided to let a company, with expertise in tailor made solar cells do the lamination process. From conversations with supervisors, Wattlab [55] came up as a trusted company with experience in foil-to-foil lamination of SunPower monocrystalline IBC cells. They are able to make, among others, thin (1 mm thick), lightweight (1 kg/m^2) flexible modules, with transparent, white or black back sheet. It was chosen to produce two modules in total, one with white back sheet and one with black, for comparison reasons.

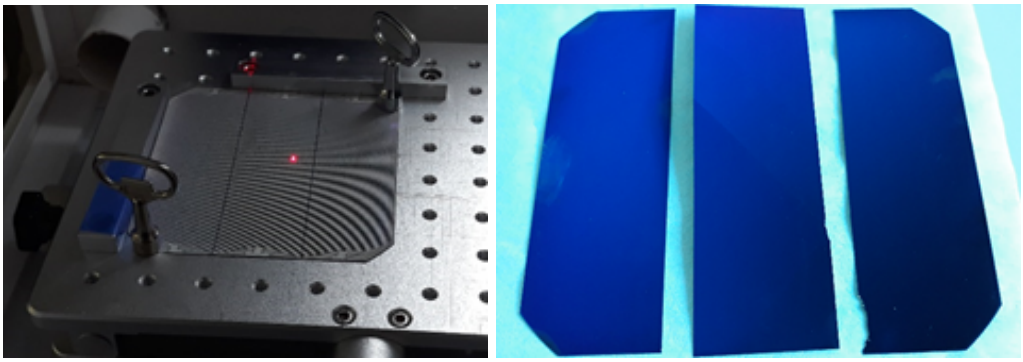

(a) (b)

Figure 6.10: (a) The cells were placed on the flatbed table in the cutting box and were pressed down by some weights on the sides, which were needed due to the curling up nature of the IBC cells. (b) Image of a IBC cell cut in three pieces in a poor way. The left piece has a stain on it, caused by uncareful handling. The middle piece is "nicked" in it and the right piece has a "rough edge", caused by an issue during breaking of the cells.

The cut cells were classified based on their performance and appearance. Poor looking cells, as in Figure 6.10b were left out. The best performing cells will be on the top part of the module, as it is expected that these will have to endure the least shadow and thus work the most. The cell were packed and send, in order from top left to right bottom, to Wattlab [55] for the lamination in foil-to-foil. One month later the modules were picked up and the results can be seen in Figure 6.6.

Junction Box

An option for the junction box was send to Wattlab to include during the production of the module. It already included the three sufficiently large Diotec (15SQ045) Schottky bypass diodes [56]. The box can be seen in Figure 6.6 on the back side of the module. It turned out that the size of the junction box was slightly bigger than expected, but it was still thin enough to fit inside the dimensions of the frame.

6.5.3 Aluminium 2020 profile frame

A aluminium frame was build from 20x20 mm extrusion profiles and U-profiles. This was done so the cross bars could be later adjusted and the flexible solar module could be easily replaced. The resulting module can be seen in Figure 6.6 and an engineering drawing can be seen in Figure 6.11. The close up shows that there is exactly a 1 mm space between the U-profile and 2020 profile. The PV module can be slid into this gap from below, when the bottom part of the aluminium U-profile is detached.

6.5.4 Base and casing

Figure 6.9 indicates the location of the base and case. The base is the foot of the IPV lamp and can be detached. The casing holds all electrical components. In the first version, both were made quickly out of wood, so they could be easily adapted.

6.6 Testing of the prototype

For the verification of the simulations from chapters 3 to 5, it would be useful to test the finished product at the same positions in the rooms as was done in the simulation and measurements. Sadly, too much time went into the final process of building the prototype. Also, the electrical circuit was constantly giving renewed issues, due to failure of components, such as the capacitors,

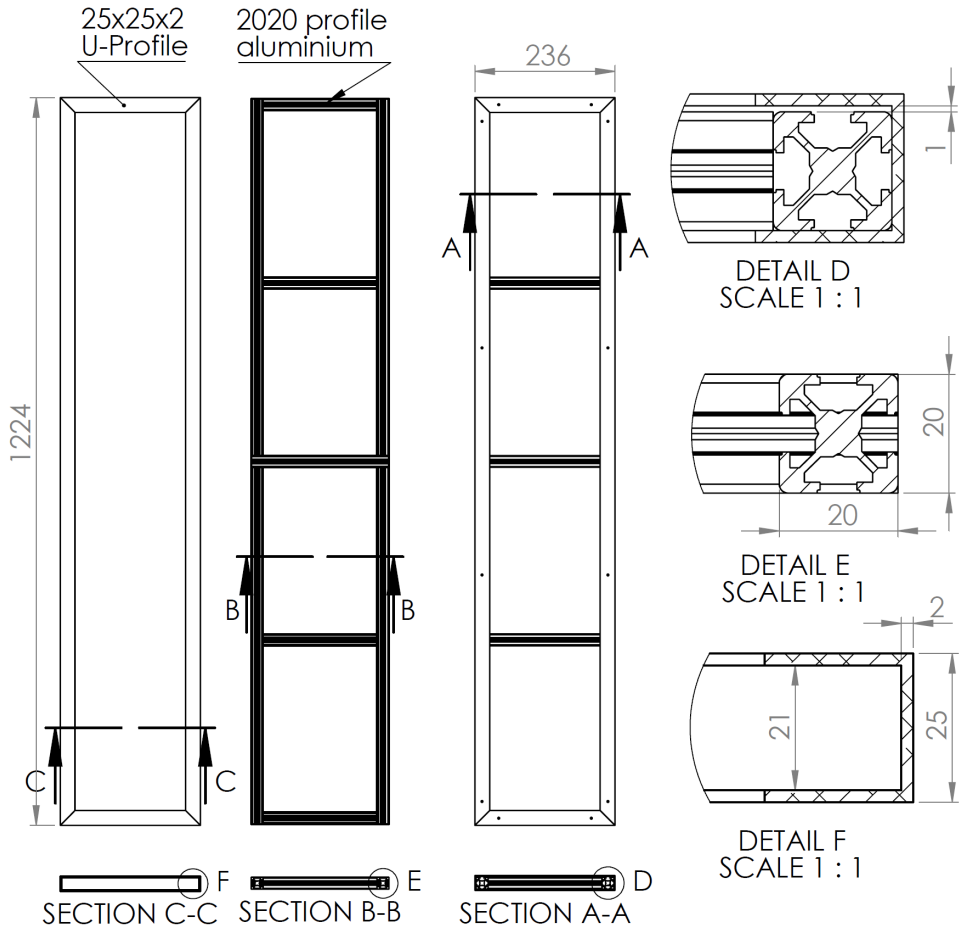

Figure 6.11: A engineering drawing of the frame of the module, consisting out of 2020 aluminium profiles and 25x25x2 aluminium U-profiles. Some detail close ups of the section cuts A, B and C can be seen on the right.

voltage regulators and buck converters. This means that no extensive testing has been performed at the time of writing. The only tests that have been performed are briefly described below.

6.6.1 Testing the module under a solar simulator

The module was placed in its frame, and before building the rest of the lamp, the IV characteristics were measured in standard test condition under a Large Area Solar Simulator (LASS) from Eternal Sun. The first module that was tested, was the module with white back sheet. The module was connected appropriately to the connectors and a temperature sensor was attached at the back of the module, after which the first IV measurement was performed. However, right after completion, the module was inspected and significant deformation of the cells had resulted in cracks and clear nicks of some of the IBC cells. It is thought that the cells could not handle the build up of stresses due to the cell wanting to curl up as a response to the heat coming from the LASS. In total five cut pieces of cell where slightly nicked, similar as can be seen in Figure 6.10b. It was chosen to not continue testing under the high irradiance of the solar simulator anymore. Luckily, the cracking of the cells did not seem to harm the output of the module too much and the curve from the sole IV measurement does reveal the main characteristics of the module under standard test conditions.

From the IV-curve, it can be determined that, at standard test conditions, the short-circuit current was 2.374 A, with an open-circuit voltage of 21.46 V. The voltage and current at the maximum power point are 17.25 V and 2.083 A, respectively, resulting in a maximum power of 35.94 W_p. The total irradiance was 963.2 W/m^2, and the total active cell area was determined

earlier to be 0.184 m^2, meaning the total power on the module was 177.2 W. This means the effective efficiency of the module is 20.3%. This means that, after everything that happened with the module, relatively, only 9% was lost of the initial efficiency of approximately 22.3%.

6.6.2 Testing indoors

No official indoor test were made. However, during the short time the complete products worked, some coincidental measurements were performed. Twice, the device was put in front of a window, facing outside, to check the charging of the battery. It was found to charge with a current around the 0.033 A. At 12 V, this means 0.4 W was generated. The "test" was performed late in the afternoon, and a guess based on experience is that the irradiance was close to 20 W/m^2. With a total area close to 0.2 m^2, this would mean the efficiency was still 10%, which would be good in those conditions. However, it must be stressed that this obviously will not be taken into account as a valid result. Or more strongly, well established tests are still pending with the current prototype.

6.7 Conclusions and recommendations

The research from the previous chapters has been used, together with a market research, to set up a list of general product requirements. Three concepts, corresponding to the best room position for monocrystalline, multicrystalline and amorphous silicon, were developed and 3D renders were presented. They were given names, fitting the position for which they were designed, being: (1) Window Winner, (2) Defeating Darkness and (3) Pocket Solar. The first one was further developed and a prototype was build. It contains of a custom-made, foil-laminated PV module, consisting of laser cut SunPower IBC cells. The module frame and casing were made to allow for easy modifications. The requirements of each electrical component was determined based on the expected PV energy yield and functional requirements of the product.

6.7.1 No big indoor solar lamps are currently on the market

The product research of Section 2.3 showed that there exist an variety of products on the market already using PV indoors. Now it is mainly to power small table lamps with LED light up to a power of only 1 W. Moreover, for indoor PV products it is still recommended to charge the module outside in clear sunlight. The market might not be ready for large IPV products, however, they can be slowly implemented in objects that are already big and spend most of the time in the sun, like a planter or a tall standing speaker.

6.7.2 A good functioning wall lamp needs to be close to the window to charge

The Window Winner was designed for the position of highest insolation per area on a wall, which is on the wall adjacent to the window within 0.5 and 1 meters of it. The expected yield is between the 2 and 4 Wh/m^2 for rooms with an orientation between east and southwest for the main window. Only right next to the window is a small patch of uniform light, where such a device can consistently charge and be used as a assistive light.

6.7.3 A reliable guidance lamp needs amorphous silicon solar cells

Defeating Darkness relies on more constant, reliable indoor irradiance, which can be found deeper than 3 meters in the room. For rooms not orientated perfectly to the south, the expected insolation is as low as 20 Wh/m^2/day. In these conditions, amorphous silicon outperforms the other cell technologies.

6.7.4 A compact, mobile IPV can be charged on the windowsill

The Pocket Solar is designed for easy mobility and carries high power LEDs to be used as a flashlight. It consist of a foldable PV module to keep it compact when being used, but sufficiently large during charging. For most household rooms in the Netherlands, the windowsill is a good option for charging and a good performance of the cells and product overall is more secure. However, it can be argued that the idea of a indoor PV lamp is somewhat overthrown, as the device can also be taken outside to charge faster.

6.7.5 Electrical components have high power ratings in case of full sun conditions

The nominal power and voltage ratings of the PV module are based on the performance in standard test conditions. The required input values for the charge controller are, in their turn, based on these nominal values of the PV module. This means that for the most part of its lifetime, the ratings will be much higher than the encountered power. It is only when the user decides to take the product outside, and places it directly in the sun, that the voltage and/or current ratings will be reached. It should be chosen if the system will be overdimensioned, leading to higher costs, or suitably designed, risking failure in improper use.

6.7.6 The PV module performed well, but was fragile

For the small amount of test that were performed, the prototype scored good results. But it was found that a foil-to-foil flexible laminated IBC cell module was very fragile. Before every replacement, extreme care was required to prevent the cell from getting nicked. Then, when it was tested in standard test conditions, did some cells ripple, expecting due to the sudden increase in module temperature. It has been determined that 9% of the initial cell efficiency In the future, a harder plastic should be considered to protect or stiffen the modules, for this purpose.

Chapter 7

Conclusions and Future Work

The goal of this thesis was to create a prototype of an indoor, easy-to-install solar powered LED lamp. Before the design was made, some research was performed to accurately determine the light conditions of the position where the device could operate. The research part of the thesis was separated in three steps, corresponding to Chapters 3, 4 and 5. The detailed conclusions for each of these steps can be found at the end of the chapter. Here, only the main findings are presented, using the three main research questions from the introduction in Section 7.1, 7.2 and 7.3. The subsections answer the subquestions and the header indicates the corresponding chapter number to find more detailed information in between brackets. Last, but not least, some recommendations for future work are listed in Section 7.4.

7.1 Research question 1: Ideal position for indoor PV

For a general household and office room in the Netherlands, what is the ideal position for an indoor PV installation?

The best position for highest yield is obviously near the main window in the room, but it needs to be determined what areas on the wall or ceiling are the best for a PV module, also considering artificial light. Two ordinary rooms were selected to perform the analysis and see what kind of room characteristics determine the outcome. The first room was a household living room with main window facing almost south and the second one a university office room facing east-northeast. The results are specific for these two rooms, but can also be applied to rooms of similar geometry along locations with similar latitude. From the scientific research it was found that there was a need to produce a light simulation specifically for the studied cases, because there are many contributing factors to the indoor light conditions. The results show that the wall adjacent to the main window contains a narrow strip of uniform high irradiance for most of the day, neglecting occasional direct sun entering the room. The highest yearly insolation on a wall left to the window is expected for a room with the main window orientated between south and east. Similarly, for the right wall, it is between south and west. On average, the daily insolation here is 200 Wh/m^2. Deeper into the the room, the daily insolation quickly drops of to almost half that near the window, but the irradiance is more constant and reliable here. Right behind the window, on the sill, the insolation is three times higher than the best location on the wall. Nevertheless, the wall is considered the best position, because an IPV product can hang uninterrupted there.

7.1.1 RADIANCE is the best tool for long indoor light simulations (C3)

A software review, lead to the combination of programs needed to perform the simulations. The rooms were recreated with the 3D modelling software program Blender and the validated lighting

simulation tool RADIANCE was used to perform indoor light calculations. An additional user-made code (add-on) was needed to translate the 3D model in Blender to the required input data for the RADIANCE calculations. Some user experience with Blender is required before hand, as it still contains difficulties that had to be overcome.

7.1.2 Centimetre accuracy is required in sunny conditions (C3 and C4)

From the scientific review it was found out that no detailed room furniture was needed for accurate simulations. Only main geometry is enough but this can mean that estimates are 5% higher compared to more detailed models, which contain objects that absorb light. The geometry of the rooms was measured and rebuild in 3D using Blender with centimetre accuracy. This level of detail is only required for comparing measurements with simulations, because a small misalignment can result in large deviations due to shading effects of window frames and nearby objects outside the window. For cloudy conditions this is less relevant, due to the overcast sky that more uniformly illuminates the room.

7.1.3 Ideal simulation settings depend on the sky type (C3)

The time interval and simulation accuracy were analysed and the ideal settings correspond to the different standard sky types. The CIE 110-1994 standard skies were used to define the sky illumination, for a sunny, cloudy and partly cloudy sky. A clear sky needs a short time interval, while a bright sky only needs a low accuracy setting. The opposite is true for a dark cloudy sky and a partly cloudy sky needs intermediate values.

7.1.4 Weather data is sensitive for sudden changes on a daily basis (C4)

Measurements were done with a pyranometer at the same position in the household and office room as in the simulations. For proper comparison with the measurements, weather data from the KNMI was used for every hour in the simulation to determine the sky conditions, based on cloud cover, sun hours and rain hours. On a daily basis, there can be an inaccuracy of 20%, due to inaccurate weather condition estimation. But over the full week, these deviations already cancel each other, showing an inaccuracy of only 5% between measurements and simulations. When direct sunlight enters the scene, the irradiance values becomes more unpredictable, due to occasional shading and reflections. This means the simulation is less accurate in these periods. For more constant irradiance values the method is very accurate, within a few percent.

7.1.5 Simplifications are needed for fast yearly simulations (C5)

The same simulation approach was used to predict the irradiance for every hour of a whole year. Only three standard sky simulations of one day in the month were used as a simulation for the other days, to speed up the simulations by 30 times, for an absolute inaccuracy increase up to 10% for the day furthest away from the simulated day. This is acceptable, especially since the inaccuracies cancel each other out over a full month. Furthermore, additional simplifications allowed for even faster simulations to evaluate the influence of room orientation and position on the wall left of the main window. Figures 5.7 and 5.8 presented the results in contour maps, also showing the best performing cell technology for the different room characteristics.

7.2 Research question 2: Indoor PV lamp design

How should the design of a indoor PV lamp look at the specified position, considering shape, size and PV technology used?

As is so often the case in engineering, there is not one ideal solution for any given situation. The design is dictated by the working environment of the product and the energy demand. Hence, three designs were made to suit positions in the room with different lighting properties. The first position is near the window on the wall. For this position the Window Winner (see Figure 6.2) was created. It has a narrow shape to fit the patch of uniform light that can be found 1 meter from the window. From Figures 5.7 and 5.8 it can be determined that monocrystalline is the best performing cell technology here. An active area of 0.2 m^2 is required to achieve a daily PV energy yield of 2-4 Wh/m^2. The second position is 3 to 5 meters deep into the room, where Defeating Darkness (see Figure 6.3) uses the more constant and reliable irradiance here as a source to power a guidance light. The light here is so dim that amorphous silicon outperforms the other technologies and the required module size needs to be as big as 0.4 Wh/m^2 to yield of 0.5 Wh/m^2 of electrical energy in the worst scenario. The third position is not on the wall but right behind the window, on the windowsill for example. For this area only a mobile IPV product is suitable and to achieve this a foldable PV module was designed for the Pocket Solar (see Figure 6.4). In the high irradiance values found here, a polycrystalline silicon solar cell of 0.1 m^2 in total, achieves an energy yield of 3-4 Wh/m^2.

7.2.1 The room design and orientation influence the optimal room position (C5)

Changing position of the main window determines the incoming irradiance in a room. When investigating the irradiance on a wall adjacent to the main window, a room with the window facing south is the best orientation for positions deeper than 2 meter in the rooms. However, for the household room, the east orientation received a higher insolation for positions close to the window. This was not so for the office room, indicating the importance of building design.

7.2.2 Best PV cell technology depends on the position in the room (C5)

The cell efficiency was calculated with a model from Randal [10] for four different cell technologies, which are all commercially available and have a size of at least 5 cm^2. In the highest irradiance conditions, polycrystalline silicon is still the best option, but for very low irradiance sites, amorphous silicon cells are competitive with both mono- and multicrystalline solar cells. For a module on the left wall beside a main window it was found that amorphous silicon outperforms the other solar cells when the window faces north or west, or when the position on the wall is further then 3 meters from the window. Polycrystalline is only the best performing cell, closer than one meter to the window when the room is facing at its optimal orientation. Everything in between and monocrystalline is the best cell technology. This shows that, for each position, the PV module can look different.

7.3 Research question 3: Design challenges

What are the challenges that come with the design and prototyping of a real indoor PV LED device?

A market review was performed, which exposed similar products that were already on the market. There are a wide variety of solar lamps for outdoor use. They are compact and powerful, but poor reviews indicate a poor performance and durability of the battery. Also, misinformation can lead to poor usage of the product, and the full potential is not extracted. There are also a lot of low power consumption indoor PV products, such as the famous pocket calculator, and small portable desk lights. But bigger medium consumption indoor PV products are scarce, due to the low potential of indoor light. Nevertheless, for the design of a IPV product, the knowledge about these smaller PV products can be used well for bigger devices with similar functionalities.

A challenge is that scaling up the PV module, will require the need for components with higher power ratings, even though most of the time, their potential is not being used. The main issue is that the price to produce a large custom PV module is much greater than the return of value of electricity it produces in its lifetime. But in this case, the main value of the PV cells is the added value of having a stand-alone source of power, but it can be argued if this out weights the costs already or in the nearby future.

7.3.1 It is no longer designed to cope with full sun conditions (C6)

All electrical components have been carefully designed to suit the expected performance of the PV module. This means the power will be not nearly as high in the indoor conditions of 10 W/m^2 as can be experienced outside in full sun conditions of 1000 W/m^2. The components have to be designed to handle a sudden increase in power, but cannot dissipate the power well enough to handle long periods in the full sun. A good example was the module itself, that could not handle the heat of a solar simulator and began to deform, casing cells to almost break. It needs to be made clear in user manuals of such products, as it can be tempting to fast-charge a device outside. A more advanced product could include more fail-safe options.

7.3.2 The sky is the limit

The biggest challenge for the future of IPV products is that a series of cloudy days can be detrimental for the performance and it is almost impossible to prevent a loss of load during winter months in the Netherlands. This means the product either has to be increased in size are the use needs to be limited. It is expected that closer to the equator, the concept of indoor PV can be much more profitable. Emerging PV technologies, like organic PV (Section 7.4.7) also open up a possibility for improved performance indoors.

7.4 Future work

As a researcher, the ultimate motivation is to create something useful meaningful. If that cannot be achieved, the it is necessary to . It is therefore justified that the standard thesis template saves the future work section for last, as indeed, this is the most important section of the entire research. And even in the case of this low-profile master thesis, an effort has been made to mention as much possibilities of how this research can be extended to further improve the knowledge on this topic.

7.4.1 Decrease of the simulation computation time

In this research, the simulation was validated for certain days. This meant that ideally, minutely data points were compared. However, to process the data for every investigated day for every minute at high accuracy can take unnecessarily long. There is the possibility to increase the computation speed up to ten times when it is known in advance when to expect sunny conditions and when not. The simulation setting could be adjusted to suit the recommended interval and accuracy for certain hours during the day, so that not a low interval and high accuracy is used throughout the day. This is for now out of the scope of this thesis, so another simplification is used to speed up the simulations.

7.4.2 Full week simulations to compare simulations with measurements

Using only one day simulation to simulate longer periods can have incidental errors. For example, only at a specific hour of the simulated day is the sun coincidentally blocked by a branch of a tree,

whilst for another day it is not. So having two days for a simulation can be enough to improve results during the moments when the sunlight comes in directly on the sensor. It needs to be investigated if this contributes significantly to the results over longer periods as well, keeping in mind that it will double the computation time.

7.4.3 More consistent year measurements indoors

At the start of this thesis, the focus was entirely on the performance during the worst months of the year. Also, measurements were done during the remainder of the week, but this was not done nearly as consistently as for the first investigated period. This meant the results were not trustworthy and are not featured in the results. Having a more consistent measurement approach will resolve this issue.

7.4.4 Full year simulation to verify the assumptions in the prediction method

Only one day in the month was simulated to predict the daily insolation and PV energy yield over the full month. This was done for every month in the year. Some efforts were made to estimate how much this had an impact on the results, and it was determined that this was not much on the long 30 day period. In this thesis, finding the exact accuracy of the yearly simulation was not found important enough to do a simulation over 100 hours. But this is definitely required to fully test the performance of the simulation method.

7.4.5 More room orientations to find the best direction

Staying on the subject of *more is better*, it would also be informative to make a contour map, such as the ones in Figure 5.7 and 5.8 with a higher resolution than 12 data points. This means that the simulation and calculation needs to be performed for more room orientations as well as for more room positions. However, it should be noted that the investigation is increased with the square of increasing either parameter. Doubling the resolution of each will require 48 simulations to be made, which could take up to 192 hours, not including all the little steps that need to be performed in between the simulations of each data point.

7.4.6 Investigating the spectrum of indoor light more carefully

In this work a simplified model was used to get to the efficiency of various solar cell technologies in low irradiance conditions. The AM1.5 spectrum was considered during every time of each day, but in reality the spectrum of light can vary a lot from the morning till evening. It has been decided to neglect the influence of artificial light on the spectrum, due to the small contribution it adds to the total irradiance during the day. However, during darker days and especially deeper into a room, the contribution can become significant. This is mainly true for rooms where artificial lights are on for most of the day anyways, as normally it would not make sense to have another light charging your indoor PV light when it is dark. So this is only really important for the design of products in office rooms or rooms alike. Also clouds change the spectrum of light. There is still discussion in the exact nature of the changes [57].

7.4.7 Explore organic PV possibilities

There are some interesting findings on the performance of organic photovoltaic (OPV) cells in low intensity indoor conditions. Organic PV is known for its cheap production cost and roll-to-roll printing methods [58]. The performance can be tweaked to suite indoor conditions and some high laboratory results, show some cells even producing efficiencies much higher than conventional PV [21]. This means it could become a dominant technology for future IPV systems.

7.4.8 Low-intensity light performance of SunPower IBC cells

Sadly, no literature could be found on low-intensity performance measurements could be found for the SunPower IBC cells. Also, there was no time to do the measurements on the cells beforehand, as already tight deadlines were made on the delivery of the cells. The results showed that the cells performed well on a modular level, but a big contribution to this research could be made if the individual cell performance was measured for different low-intensity light conditions.

7.4.9 Further development of IPV products

Some leftovers arose from working on the current version of the IPV lamp. The latest talks with the supervisors opened up possibilities in concealing the system components even more into the frame. Together, with a more advanced cell technology, made specific for indoor conditions could become a recognisable item in near future households. A very mobile IPV has always been desirable, so more care needs to be taken to make it lighter. In this case the IPV can be taken easily from charge point to use point, and can be even smaller. But it also needs to be impact strong, to allow for clumsy use, which is more than likely if it needs to placed to a charging place on a daily basis. Fibres could be introduced in the frame design, instead of the soft aluminium. It would also be beneficial if more modern application can be assigned to this product, like wireless phone charging, integrated speakers or even visuals effects like video player. The sky is the limit.

Appendix A

Dimensions of the two rooms

The dimensions of the rooms were obtained by measurements with a measurement tape. The values were rounded to the nearest centimetre, or half a centimetre in some cases. The figures below show a top view with the main room sizes and an overview shot to show the sizes of more detailed geometries like the windows.

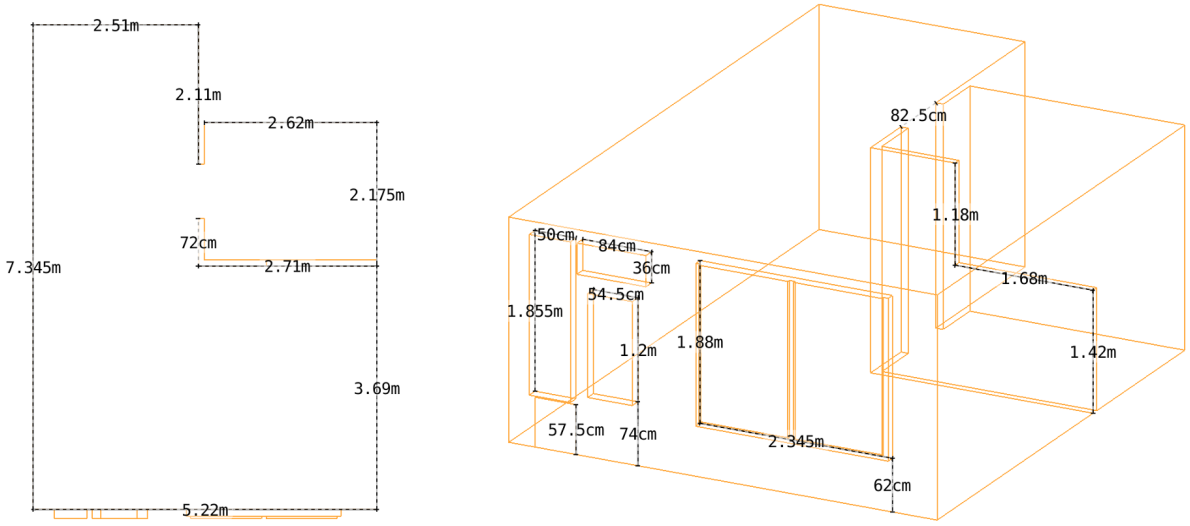

Figure A.1: Schematic figure of the household room with all relevant dimensions

The figure above shows the household room. Note that the main window is on the right side when standing outside the room. Looking at the top view image, the windows on the left side are there because there is a door there with windows in and beside it. In the top right of the room, there is a small block separated by a narrow wall with a 1.2x1.7m cut extruded from it, as can be seen in the right image. In reality, there is also a door on the backside of the room which allows some light in from the hallway. This light is not bright and no direct rays will enter the room, so it is neglected to increase computational speed.

The figures below shows the layout of the office room at the Delft University of Technology. The main window, on the bottom side of the top view image in Figure A.2. The room is surrounded by similar office rooms and in Figure A.3, a part of the building consisting of 5 adjacent rooms is shown. Also, the dimensions of the hallways and rest of the building can be seen in this figure.

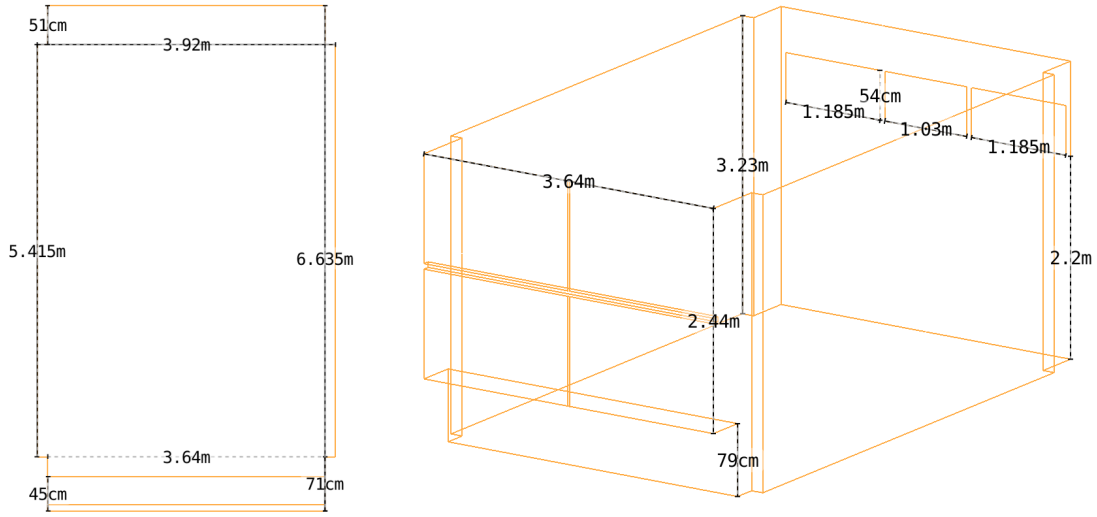

Figure A.2: Schematic figure of the office room with all relevant dimensions. Here the room is singled out from the rest of the building

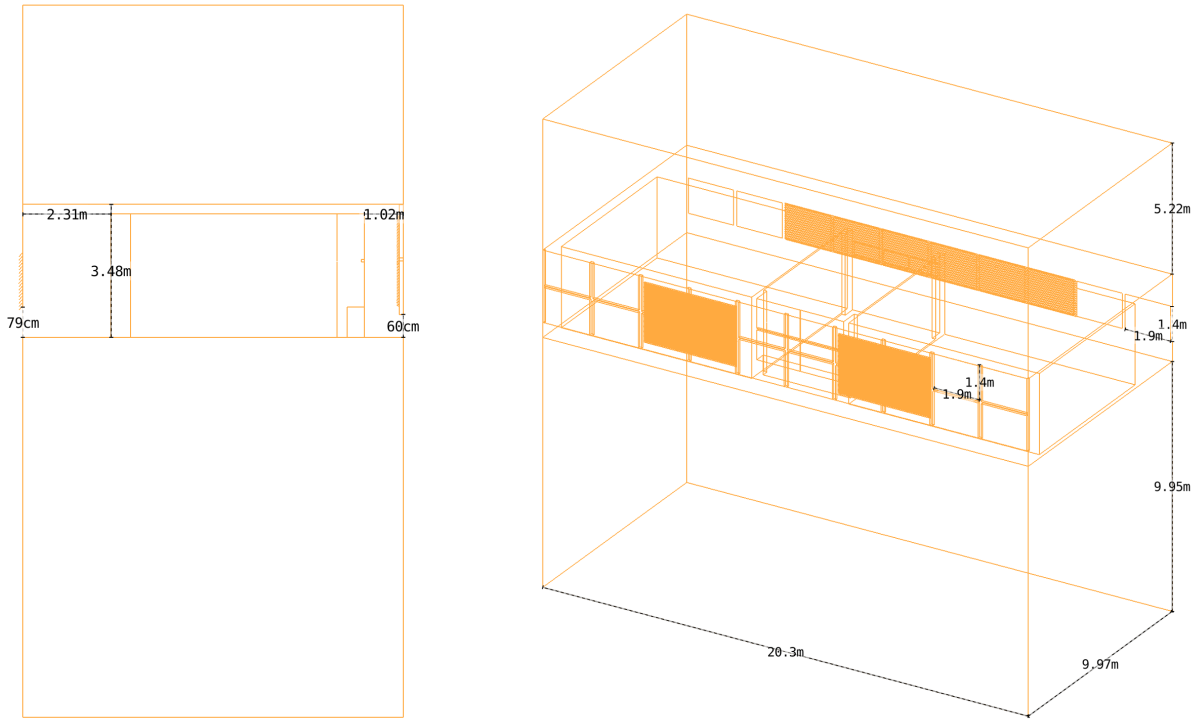

Figure A.3: Schematic figure of a part of the building in which the office room is placed.

Appendix B

Calculations for solar position

The position of the sun is calculated using the formulas from [31]. It uses the latitude ϕ_0 and longitude λ_0, date and time. The equation for the solar azimuth A_S and the solar altitude a_S are given in Equation B.1 and B.2, respectively.

$$\tan A_s = \frac{-\sin\theta_L \cos\lambda_S + \cos\theta_L \cos\varepsilon \sin\lambda_S}{-\sin\phi_0 \cos\theta_L \cos\lambda_S - (\sin\phi_0 \sin\theta_L \cos\varepsilon - \cos\phi_0 \sin\varepsilon)\sin\lambda_S} \tag{B.1}$$

$$\sin a_s = \cos\phi_0 \cos\theta_L \cos\lambda_S + (\cos\phi_0 \sin\theta_L \cos\varepsilon + \sin\phi_0 \sin\varepsilon)\sin\lambda_S \tag{B.2}$$

Here is the θ_L is the local mean sidereal time which is a function of the Greenwich mean sidereal time (GMST) and longitude [31], λ_S is the ecliptic longitude of the sun and depends on the mean longitude and mean anomaly of the sun. They are a function of the Julian date [31], which is the number of days since 1 January 4713 BC. Furthermore, ε is the axial tilt of the earth.

Appendix C

Model for PV cell efficiency in low intensity indoor light

Julian Randall proposed back a phenomenological model that relates the solar cell characteristics to a realistic solar cell efficiency in low-intensity light. This model is explained in detail in this appendix.

Testing 21 solar cell technologies
Randall performed measurements of 21 solar cell technologies, as can be seen in Figure C.1.

Table 5.1 Technologies and sources of the 21 types of solar cell/module that the author collected and tested, showing whether the manufacturer was a laboratory or industry, the active area and the number of cells in the module

Technological classification	Supplier or laboratory name	Cell code	Industrial = I Laboratory = L	Active area (cm^2)	Number of cells in module
Silicon (crystalline)	BP Solar (via IWS)	xSi-BP	I	9.36	1
Silicon (crystalline LGBC)	BP Solar, UK	xSi-LGBC	I	0.90	1
Silicon (crystalline)	Spacecells, Edmund Scientific, USA	xSi- EdSi	I	0.38	1
Silicon (crystalline)	Unknown (via distributor)	xSi-Dist	I	10.95	1
Silicon (polycrystalline)	MAIN, Tessag, Germany	pSi-MAIN	I	12.47	1
Silicon (polycrystalline)	EFG, Tessag, Germany	pSi-EFG	I	10.25	1
Silicon (polycrystalline)	Unknown (via distributor)	pSi-Dist	I	2.88	1
III–V cells (GaAs)	NREL, Golden, CO, USA	3-5-NREL	L	0.25	1
Polycrystalline thin film (CdTe)	Matsushita/Panasonic, Japan	CdTe-Mats	I	5.80	5
Polycrystalline thin film (CdTe)	Parma University, India	CdTe-Parm	L	0.79	1
Polycrystalline thin film (CIGS)	ZSW, Stuttgart University, Germany	CIGS-ZSW	L	0.46	1
Other (GaInP)	NREL, Golden, CO, USA	GIP-NREL	L	0.25	1
Amorphous silicon	Tessag, Putzbrunn, Germany	aSi-Tess	I	4.95	5
Amorphous silicon	Sanyo Electric, Hyogo, Japan	aSi-Sany	I	3.71	4
Amorphous silicon	Solems, Paris, France	aSi-Sole	I	1.76	3
Amorphous silicon	VHF Technologies, Le Locle, Switzerland	aSi-VHF	L	3.36	4
Amorphous silicon	Sinonar Corporation, Taipei, Taiwan	aSi- Sino	I	1.26	4
Amorphous silicon	Millenium, BP Solar	aSi-BP	I	0.20	1
Photochemical (nanocrystalline dye)	Greatcell SA, Yverdon, Switzerland	PC-GCSA	L	1.00	1
Photochemical (nanocrystalline dye)	EPFL ICP2, Lausanne, Switzerland	PC-ICP2	L	0.90	1
Multijunction cell (GaAs–GaInP tandem)	NREL, Golden, CO, USA	MJ-NREL	L	0.25	1

Figure C.1: Specifications of all investigated solar cell technologies by Randall [10]

It can be seen from the results in Figures C.2 and C.3 that the overall trend of the efficiency is constant down to 200 W/m^2 and a straight line on a logarithmic scale in the range 1-100 W/m^2.

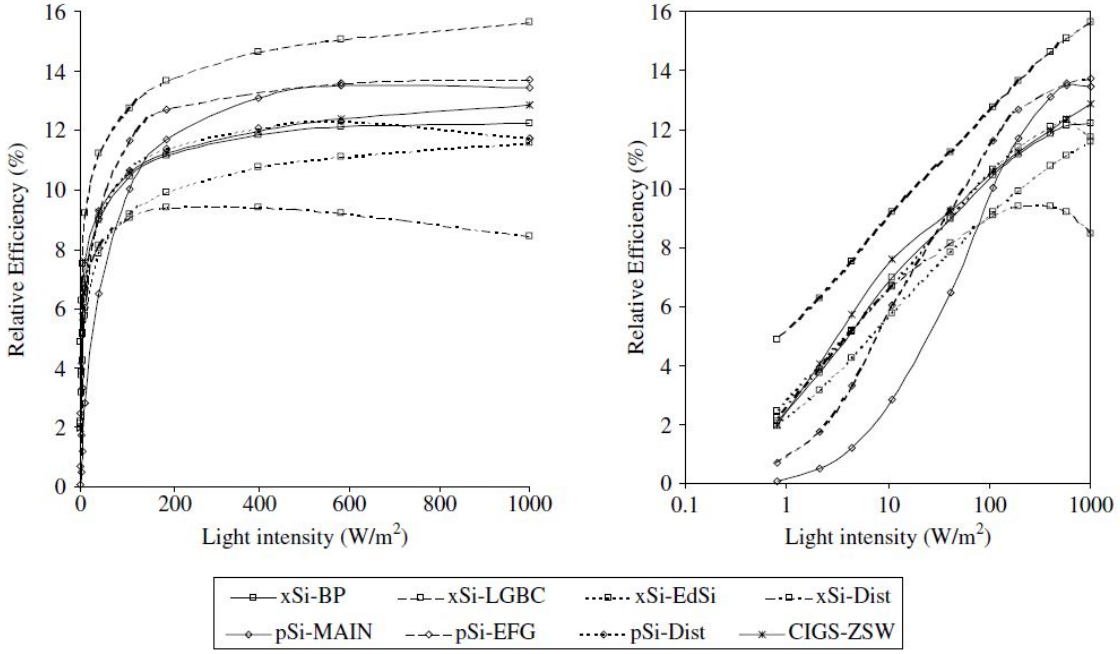

Figure C.2: Results from the measurements performed by Randall under a filtered AM1.5 light source [10]

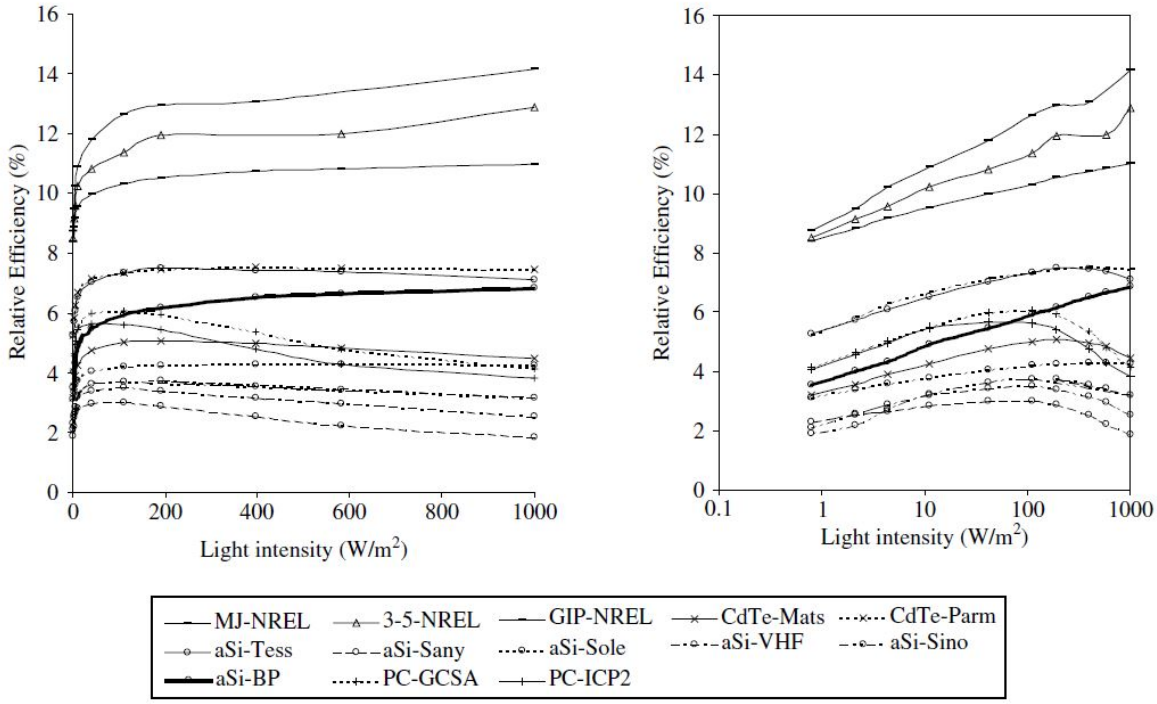

Figure C.3: Results from the measurements performed by Randall under a filtered AM1.5 light source [10]

Phenomenological Model

It was determined that the fill factor was approximately constant in the 1-100 W/m^2 region. Also, it is assumed that the short-circuit current I_{SC} is directly proportional to the irradiance G as

$$I_{\mathrm{SC}} = \alpha_f G \tag{C.1}$$

where α_f is a constant. For an ideal diode and with a light generated current that is much higher

than the dark current I_{S} the open circuit voltage V_{OC} can be described as

$$V_{\mathrm{OC}} = \frac{kT}{q} \ln \frac{I_{\mathrm{SC}}}{I_{\mathrm{S}}} \tag{C.2}$$

where k is the Boltzmann's constant, T the temperature and q the electronic charge. Now lets consider the solar cell efficiency formula

$$\eta = \frac{V_{\mathrm{OC}} I_{\mathrm{SC}} \mathrm{FF}}{P} \tag{C.3}$$

where P is the input power. Substituting Equation C.1 and C.2 in Equation C.3 gives:

$$\eta = \mathrm{FF}\alpha_f \frac{kT}{q} \left[\ln G + \ln \alpha_f - \ln I_{\mathrm{S}}\right] \tag{C.4}$$

with

$$I_{\mathrm{S}} = \beta_f \exp \frac{-E_g}{kT} \tag{C.5}$$

where E_g is the band gap and β_f is a constant of the form

$$\beta_f = eA_{\mathrm{CS}} N_{\mathrm{C}} N_{\mathrm{V}} \left(\frac{D_{\mathrm{n}} F_{\mathrm{p}}}{L_{\mathrm{n}} N_{\mathrm{A}}} + \frac{D_{\mathrm{p}} F_{\mathrm{n}}}{L_{\mathrm{p}} N_{\mathrm{D}}} \right) \tag{C.6}$$

where A_{CS} is the cross-sectional area, N_{C} and N_{V} are the effective densities of states in the conduction and valence bands, respectively, D_{n} and D_{p} are the electron and hole diffusion coefficients, L_{n} and L_{p} are the electron and hole diffusion lengths and N_{A} and N_{D} are the acceptor and donor densities. This can be filled in again in Equation C.4 to give

$$\eta = \mathrm{FF}\alpha_f \frac{kT}{q} \left[\ln G + \ln \alpha_f - \ln \beta_f + \frac{E_g}{kT}\right] \tag{C.7}$$

This can be rewritten in the form

$$\eta = a \ln (G) + b \tag{C.8}$$

and the parameters a and b are defined as

$$a = \mathrm{FF}\alpha_f \frac{kT}{q} \tag{C.9}$$

and

$$b = \mathrm{FF}\alpha_f \frac{kT}{q} \left[\ln \alpha_f + \ln \beta_f + \frac{E_g}{kT}\right] \tag{C.10}$$

With the results from the measurements, the parameters can now be determined for the investigated cell technologies.

Cell code	a_{AM}	b_{AM}	CC	a_{AM}/b_{AM}	$\sim E_g$
pSi-EFG	2.33	0.48	0.99	4.87	1.10
pSi-MAIN	2.05	(−)0.84	0.92	2.43	1.10
xSi-EdSi	1.50	2.16	1.00	0.69	1.10
xSi-BP	1.71	2.58	1.00	0.66	1.10
CIGS-ZSW	1.73	2.83	0.98	0.61	0.90
pSi-Dist	1.67	2.80	1.00	0.60	1.10
xSi-Dist	1.40	2.88	0.99	0.48	1.10
xSi-LGBC	1.62	5.18	1.00	0.31	1.10
aSi-Sino	0.40	2.06	0.95	0.19	1.70
aSi-VHF	0.33	2.30	0.96	0.14	1.70
aSi-BP	0.49	3.66	1.00	0.13	1.70
CdTe-Mats	0.38	3.30	1.00	0.11	1.40
PC-IPC2	0.42	4.25	0.95	0.10	—
PC-GCSA	0.40	4.37	0.96	0.09	—
MJ-NREL	0.74	9.02	0.99	0.08	—
aSi-Tess	0.43	5.41	0.99	0.08	1.70
CdTe-Parm	0.42	5.51	0.97	0.08	1.40
aSi-Sany	0.17	2.39	0.98	0.07	1.40
aSi-Sole	0.22	3.21	0.99	0.07	1.40
3–5-NREL	0.57	8.72	0.98	0.07	1.50
GIP-NREL	0.36	8.59	1.00	0.04	1.40

Note: a_{AM} and b_{AM} are values of a and b under AM1.5 source; cell codes are defined in Table 5.1; average CC for all 21 samples = 0.98

Figure C.4: Parameters a and b of all technologies [10]

Appendix D

Extra graphs

This appendix will be used to display plots that could be helpful in the analysis.

D.1 Module angle influence

The influence of module angle was derived, and the finding is fairly predictable. Turning the module more towards the window will increase yield. This is also true deep in the room. There it could even be beneficial to turn it completely to the wall. If there is a wall at this distance parallel to the window, then this is a very good IPV location.

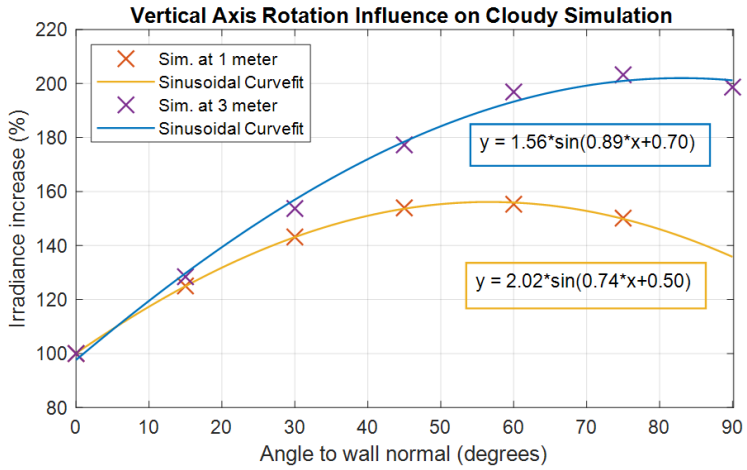

Figure D.1: Influence of module rotation around the vertical axis for two distances from the window, towards the main window for the household room. Zero degrees is parallel to the wall and 90 degrees is parallel to the window.

D.2 Three base simulations for a year

This section shows all used base simulations. They are dived per standard sky, and all 12 months are in one figure. This way it can only clearly be seen, that overall the irradiance does not change very much.

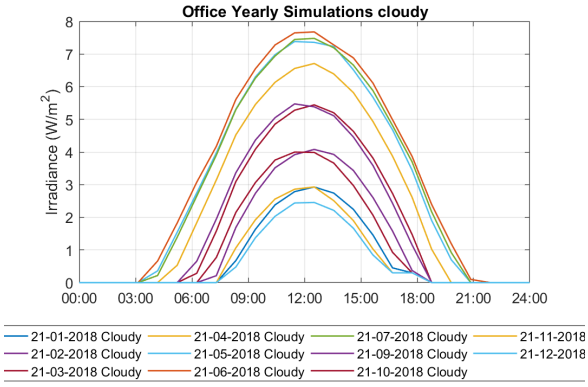

(a) Office at every month cloudy

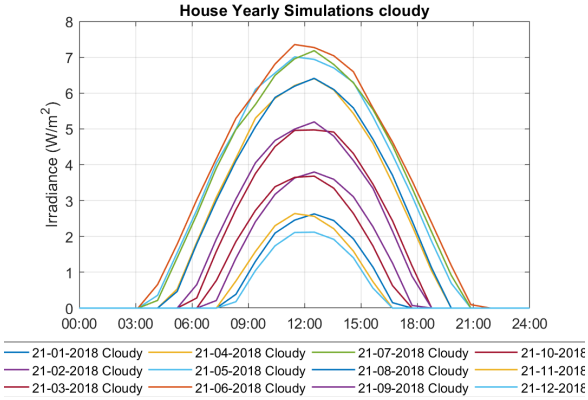

(b) House at every month cloudy

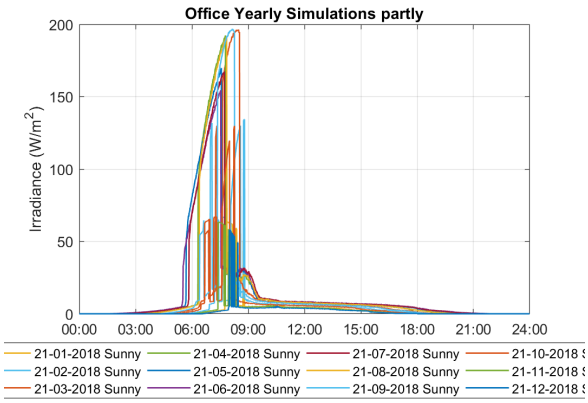

(c) Office at every month partly

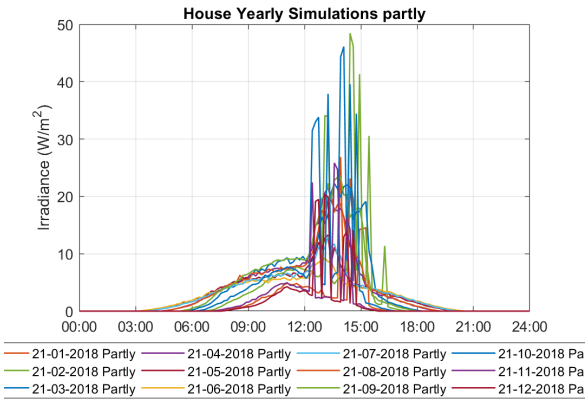

(d) House at every month partly

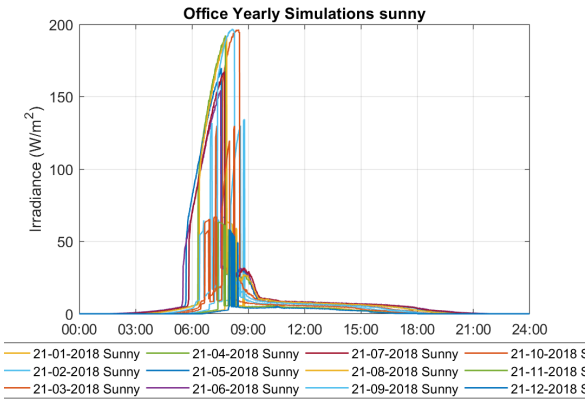

(e) Office at every month sunny

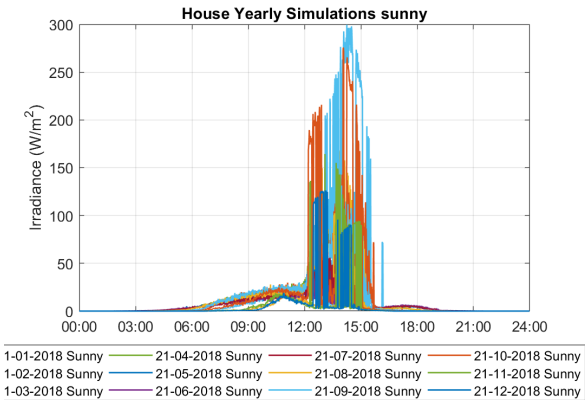

(f) House at every month sunny

Figure D.2: Base simulation of the three sky types for every month of the year for both rooms.

D.3 Measurements versus simulations per day

Here, the daily difference between measurements and simulations can be seen.

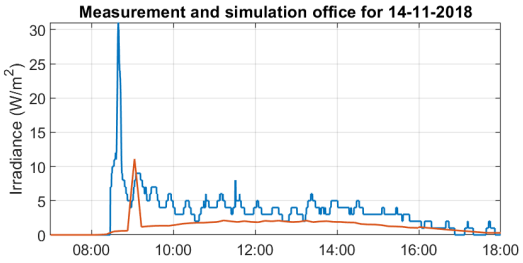

(a) Office at 14-11-2018

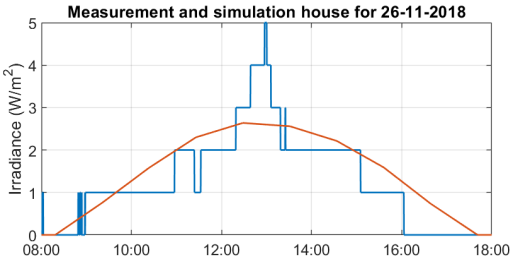

(b) House at 26-11-2018

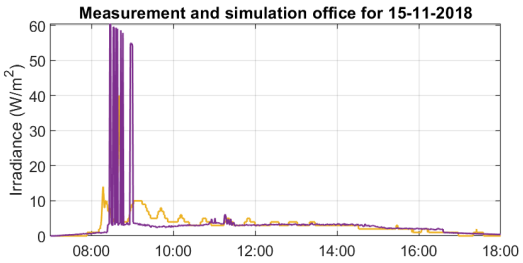

(c) Office at 15-11-2018

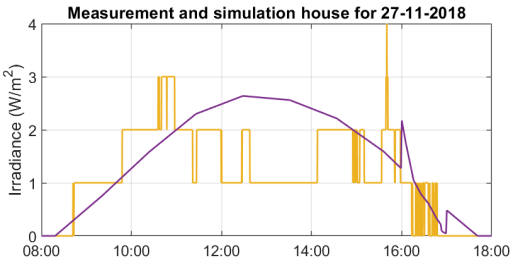

(d) House at 27-11-2018

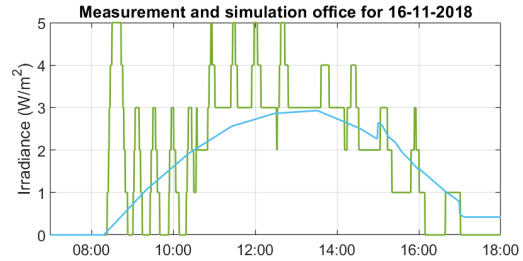

(e) Office at 16-11-2018

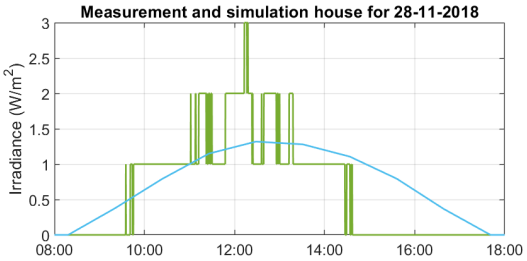

(f) House at 28-11-2018

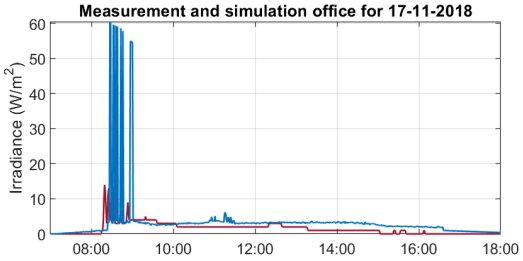

(g) Office at 17-11-2018

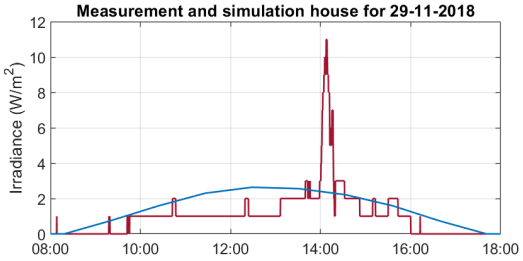

(h) House at 29-11-2018

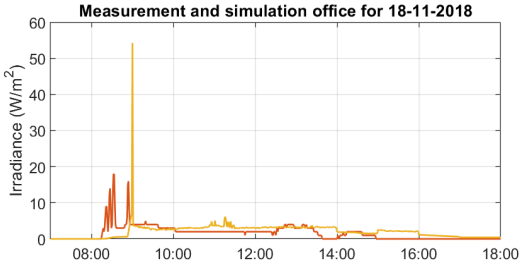

(i) Office at 18-11-2018

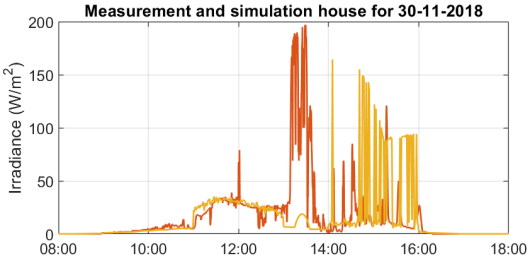

(j) House at 30-11-2018

Figure D.3: Measurements and simulations for each day of the five day period. It can be seen that most days are low and thus cloudy.

D.4 Contour plots with all cell technologies

The same contour plots as in Figure 5.7 and 5.8, only now with more solar cells in the pool.

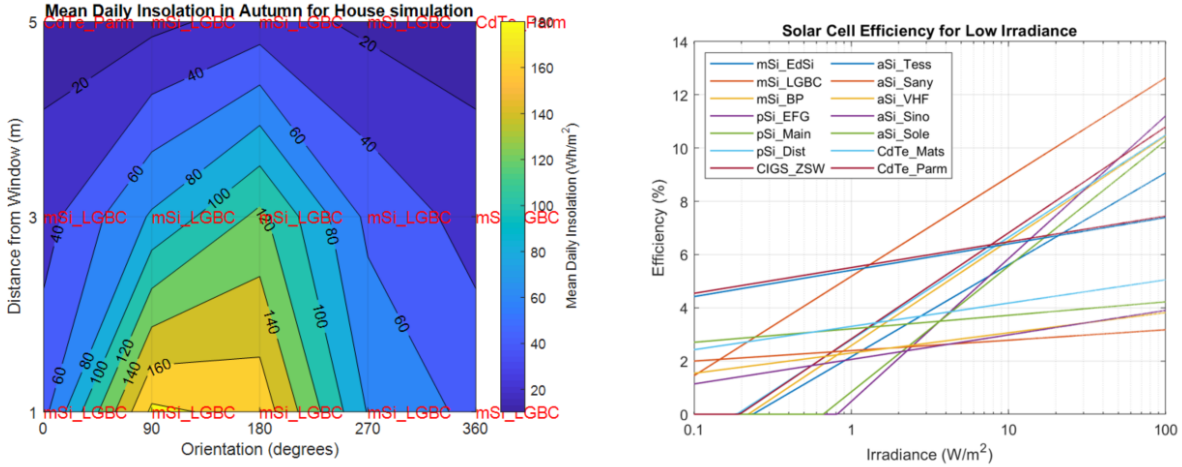

(a) Contour for all techs

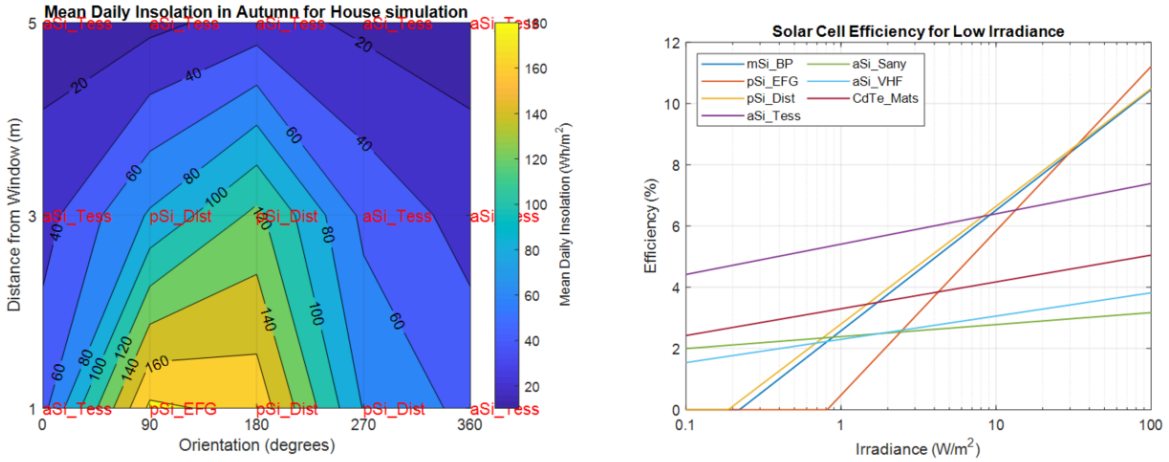

(b) Contour only commercial

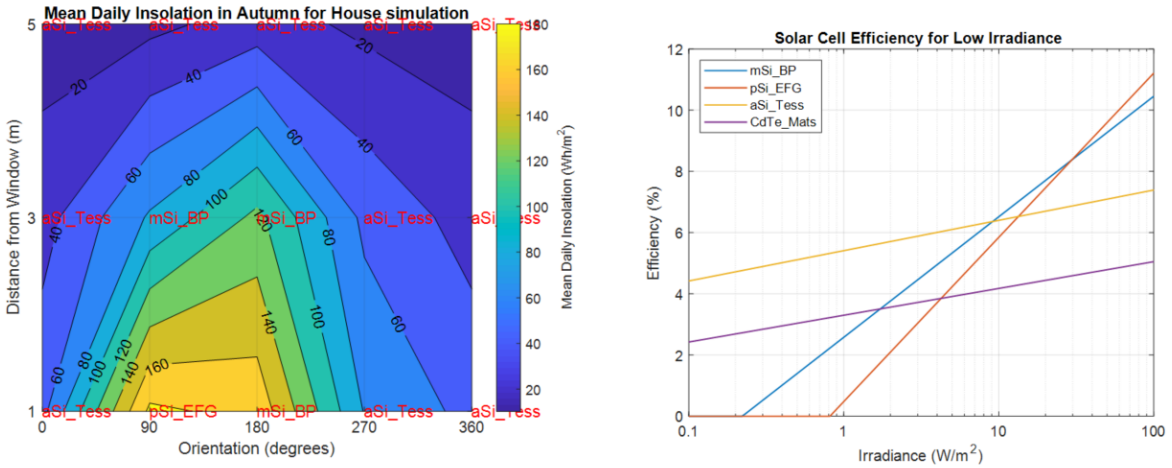

(c) Contour best technologies

Figure D.4: Contour plots with all cell technologies

Bibliography

[1] REN21, "Renewables 2019 Global Status Report," tech. rep., 2019.

[2] S. Strong, "Building Integrated Photovoltaics (BIPV)." `https://www.wbdg.org/resources/building-integrated-photovoltaics-bipv`, 2016. 2019-09-09.

[3] N. Tout, "The Pocket Calculator Race." `http://www.vintagecalculators.com/html/the_pocket_calculator_race.html`, 2000-2019. Accessed: 2019-09-09.

[4] E. Masanet and A. Horváth, "Single-use alkaline battery case study," 2012.

[5] J. Randall and J. Jacot, "Is AM1.5 applicable in practice? Modelling eight photovoltaic materials with respect to light intensity and two spectra," *Renewable Energy*, vol. 28, pp. 1851–1864, oct 2003.

[6] N. H. Reich, W. G. J. H. M. Van Sark, E. A. Alsema, S. Y. Kan, S. Silvester, A. S. H. Van Der Heide, R. W. Lof, and R. E. I. Schropp, "Weak light performance and spectral response of different solar cell types," in *Proceedings of the 20th EUPVSEC*, 2005.

[7] M. Hoffman, "Design of solar radiation and thermal capacity influence on the indoor climate of buildings," *Energy and Buildings*, vol. 4, no. 3, pp. 221 – 229, 1982.

[8] M. Luckiesh, "Simulating sunlight a new era of artificial lighting," *Transactions of the American Institute of Electrical Engineers*, vol. 49, pp. 511–516, April 1930.

[9] P. Vincent, S.-C. Shin, J. S. Goo, Y.-J. You, B. Cho, S. Lee, D.-W. Lee, S. R. Kwon, K.-B. Chung, J.-J. Lee, J.-H. Bae, J. W. Shim, and H. Kim, "Indoor-type photovoltaics with organic solar cells through optimal design," *Dyes and Pigments*, vol. 159, pp. 306 – 313, 2018.

[10] J. F. Randall, *Designing indoor solar products : photovoltaic technologies for AES*. J. Wiley & Sons, 2005.

[11] R. Vullers, R. van Schaijk, I. Doms, C. Van Hoof, and R. Mertens, "Micropower energy harvesting," *Solid-State Electronics*, vol. 53, pp. 684–693, jul 2009.

[12] Engineering ToolBox, "Illuminance - Recommended Light Level." `https://www.engineeringtoolbox.com/light-level-rooms-d_708.html`, 2004. Accessed: 2019-02-05.

[13] G. Apostolou, A. Reinders, and M. Verwaal, "Comparison of the indoor performance of 12 commercial PV products by a simple model," *Energy Science & Engineering*, vol. 4, pp. 69–85, jan 2016.

[14] UC Davis Academics, "Lecture 15: A Ray Tracing algorithm is described," 2014.

[15] A. Iversen, N. Roy, M. Hvass, M. Jørgensen, J. Christoffersen, W. Osterhaus, and K. Johnsen, *Daylight calculations in practice : an investigation of the ability of nine daylight simulation programs to calculate the daylight factor in five typical rooms.* Statens Byggeforskningsinstitut, 1 ed., 2013.

[16] N. Gatenby and T. Hewitt, "Radiosity in computer graphics: A proposed alternative to the hemi-cube algorithm," in *Photorealistic Rendering in Computer Graphics* (P. Brunet and F. W. Jansen, eds.), (Berlin, Heidelberg), pp. 104–111, Springer Berlin Heidelberg, 1994.

[17] C. Lu, A. Roetter, and A. Schultz, "Sophomore College Ray Tracing Site," 1997.

[18] M. Muller, J. Wienold, W. D. Walker, and L. M. Reindl, "Characterization of indoor photovoltaic devices and light," in *2009 34th IEEE Photovoltaic Specialists Conference (PVSC)*, pp. 738–743, IEEE, june 2009.

[19] Y. Afsar, J. Sarik, M. Gorlatova, G. Zussman, and I. Kymissis, "Evaluating photovoltaic performance indoors," in *2012 38th IEEE Photovoltaic Specialists Conference*, pp. 001948–001951, IEEE, jun 2012.

[20] F. De Rossi, T. Pontecorvo, and T. M. Brown, "Characterization of photovoltaic devices for indoor light harvesting and customization of flexible dye solar cells to deliver superior efficiency under artificial lighting," *Applied Energy*, vol. 156, pp. 413–422, oct 2015.

[21] C. L. Cutting, M. Bag, and D. Venkataraman, "Indoor light recycling: a new home for organic photovoltaics," *Journal of Materials Chemistry C*, vol. 4, pp. 10367–10370, nov 2016.

[22] P. Byrne, *Comparison Study of Four Popular Lighting Simulation Software Programs.* PhD thesis, Brunel University, 2014.

[23] DIALux, "Knowledge Base DIALux evo: Which weather model is used in the daylight calculation?." `http://evo.support-en.dial.de/support/solutions/articles/9000089634-which-weather-model-is-used-in-the-daylight-calculation-`, 2016. Accessed: 2018-09-14.

[24] CIE, "Spatial distribution of daylight - Luminance distributions of various reference skies." `https://www.techstreet.com/standards/cie-110-1994?product_id=1210128`, 1994. Accessed: 2018-09-17.

[25] R. Southall and F. Biljecki, "The VI-Suite: a set of environmental analysis tools with geospatial data applications," *Open Geospatial Data, Software and Standards*, vol. 2, p. 23, dec 2017.

[26] R. Compagnon, "RADIANCE: a simulation tool for daylighting systems," tech. rep., 1997.

[27] J.-J. Delaunay, J. Wienold, and W. Sprenger, "gendaylit - generates a RADIANCE description of the daylight sources using Perez models for direct and diffuse components," tech. rep., Radsite, 1994.

[28] S. Crone, *Radiance Users Manual: Integrated Lighting System Design and Visualisation*, 1992.

[29] G. Ward, "gensky - generate a RADIANCE description of the sky," tech. rep., Radsite, 1998.

[30] "All-weather model for sky luminance distribution—preliminary configuration and validation," *Solar Energy*, vol. 50, no. 3, pp. 235 – 245, 1993.

[31] A. Smets, K. Jäger, O. Isabella, R. van Swaaij, and M. Zeman, *Solar Energy: The Physics and Engineering of Photovoltaic Conversion Technologies and Systems*. UIT Cambridge, 2015.

[32] T. Hoffman, "Computation path of the sun." https://www.suncalc.org/, n.d. Accessed: 2018-11-15.

[33] DIALux, "Knowledge Base DIALux evo: Daylight." https://evo.support-en.dial.de/support/solutions/articles/9000121044-daylight, 2017. Accessed: 2018-09-14.

[34] H. Nakamura, M. Oki, and Y. Hayashi, "Luminance distributions of intermediate sky," *J. Light Vis. Env.*, vol. 9, no. 1, pp. 6–13, 1985.

[35] S. Darula and R. Kittler, "Cie general sky standard defining luminance distributions," 09 2002.

[36] D. H. W. Li, T. C. Chau, and K. K. W. Wan, "A review of the CIE general sky classification approaches," *Renewable and Sustainable Energy Reviews*, vol. 31, pp. 563–574, 2014.

[37] Kipp & Zonen, "CMP3 second class pyranometer." http://www.kippzonen.com/Product/11/CMP3-Pyranometer#.W7SKXWgzaHs. Accessed: 2018-10-03.

[38] Kipp & Zonen, "Adjustable Tilt Radiometer Mounting Kit." https://www.kippzonen.com/Product/195/Adjustable-Tilt-Radiometer-Mounting-Kit#.XSz2HegzaHs. Accessed: 2018-10-03.

[39] KNMI, "Daggegevens van het weer." https://www.knmi.nl/kennis-en-datacentrum/achtergrond/daggegevens-van-het-weer, 2019. Accessed: 2019-09-09.

[40] SUNPOWER, "C60 Solar Cell: Mono crystalline silicon," tech. rep., 2010.

[41] N. Mohan, T. M. Undeland, and W. P. Robbins, *Power Electronics: converters, applications, and design*. John Wiley & Sons, 3 ed., 2003.

[42] J. Svarc, "SunPower Solar Panels Review." https://www.cleanenergyreviews.info/blog/sunpower-solar-panels-review, 2019. Accessed: 2019-09-12.

[43] EBay, "0.5W 0.5V High Efficiency Back Contact DIY 1/6 Cut Sunpower Solar Cell 36pcs/lot." https://www.ebay.com/itm/291858971298, n.d. Accessed: 2019-05-19.

[44] TinyTronics, "Standaard 3528 Warm Witte LED Strip - 300 LEDs 5m - 12V." https://www.tinytronics.nl/shop/nl/verlichting/led-strips/standaard-3528-warm-witte-led-strip-300-leds-5m-12v, n.d. Accessed: 2019-06-10.

[45] TinyTronics, "Li-Po Accu 3.7v 1500mAh." https://www.tinytronics.nl/shop/nl/batterij-en-accu/li-po/li-po-accu-3.7v-1500mah, n.d. Accessed: 2019-06-22.

[46] AliExpress, "12 V MPPT Zonnepaneel Controller CN3722 3 S Lithium Li Ion 18650 Batterij Laadregelaar Module Opladen Board-in Zonnecellen van Consumentenelektronica." https://nl.aliexpress.com/item/32861049184.html, n.d. Accessed: 2019-06-10.

[47] Alexnld, "LCD Digital Display Buck-Boost Power Supply Module Board Constant Voltage Constant Current Crystal." https://alexnld.com/product/lcd-digital-display-buck-boost-power-supply-module-board-constant-voltage-constant-current-crystal/, n.d. Accessed: 2019-06-10.

[48] TinyTronics, "5V relais 1-channel hoog-actief." https://www.tinytronics.nl/shop/nl/diversen/relais/5v-relais-1-channel-hoog-actief, n.d. Accessed: 2019-06-12.

[49] TinyTronics, "DC-DC Verstelbare Step-up-down Buck-Boost Converter XL6009 4A." https://www.tinytronics.nl/shop/nl/spanning-converters/step-down/dc-dc-verstelbare-step-up-down-buck-boost-converter-xl6009-4a. Accessed: 2019-06-10.

[50] "IR Pyroelectrische Infrarood PIR Motion Sensor Detector Module - HC-SR501." https://www.tinytronics.nl/shop/nl/sensoren/optisch/ir-pyroelectrische-infrarood-pir-motion-sensor-detector-module. Accessed: 2019-06-10.

[51] TinyTronics, "Licht Sensor Module." https://www.tinytronics.nl/shop/nl/sensoren/optisch/licht-sensor-module-v3. Accessed: 2019-06-12.

[52] TinyTronics, "Touch Module 1-kanaals - Blauw - TOUCH1CHBLUE." https://www.tinytronics.nl/shop/nl/sensoren/touch/touch-module-1-kanaals-blauw, n.d. Accessed: 2019-09-13.

[53] X.-r. Li, S.-l. Wang, X.-q. Lai, and Y.-s. Li, "Design and implement of LED drive circuit chip with the controllable constant output current," *Optoelectronics Letters*, vol. 5, pp. 186–189, may 2009.

[54] Lasergraaf, "Q-switched fiber markeer laser "EMMA" full desk." https://lasergraaf.nl/product/20-30-watt-q-switched-fiber-laser-emma/, 2019. Accessed: 2019-04-25.

[55] WATTLAB, "Homepage." https://wattlab.nl/, 2019. Accessed: 2019-05-04.

[56] AliExpress, "Solar Junction Box voor Zonnepaneel 200 w 220 w 230 w 240 w 250 w sluit PV junction box solar kabel verbinding met Diodes-in Connectoren van Licht & verlichting." https://nl.aliexpress.com/item/32887332309.html, n.d. Accessed: 2019-04-02.

[57] S. Nann and C. Riordan, "Solar spectral irradiance under clear and cloudy skies: Measurements and a semiempirical model," *Journal of Applied Meteorology*, vol. 30, pp. 447–462, 03 1991.

[58] R. Steim, T. Ameri, P. Schilinsky, C. Waldauf, G. Dennler, M. Scharber, and C. J. Brabec, "Organic photovoltaics for low light applications," *Solar Energy Materials and Solar Cells*, vol. 95, no. 12, pp. 3256 – 3261, 2011.